# Dissertation

**submitted to the**
**Combined Faculty of Natural Sciences and Mathematics of**

## Heidelberg University, Germany

**for the degree of**
**Doctor of Natural Sciences**

**Put forward by**


## Michael J. Quin
**born in Portadown,**
**United Kingdom.**


**Oral examination: 18th October, 2023.**

# Classical Radiation Reaction and Collective Behaviour


| | |
|---|---|
| **Referee & Supervisor:** | **Prof. Dr. Antonino Di Piazza** |
| **Referee:** | **apl. Prof. Dr. John G. Kirk** |
| **Supervisor:** | **Dr. Matteo Tamburini** |

## Zusammenfassung

Geladene Teilchen emittieren elektromagnetische Strahlung, wenn sie beschleunigt werden. Die anschließende Auswirkung auf die Trajektorie muss durch die Energie- und Impulserhaltung in einer selbstkonsistenten Bewegungsgleichung, wie der Landau-Lifshitz-Gleichung (LL), berücksichtigt werden. Dieser Effekt, der als „radiation reaction“ (RR) bekannt ist, wird für relativistische Teilchen in Gegenwart von extrem starken elektromagnetischen Feldern, wie einem intensiven Laserpuls oder einer Pulsarmagnetosphäre, bedeutsam. Die LL-Gleichung wird in der Regel entweder analytisch gelöst, wobei jedes Teilchen unabhängig von den anderen Teilchen in einem externen Feld behandelt wird, oder numerisch, wobei ein mittleres Feld durch eine Ladungsverteilung zusätzlich zu einem externen Feld erzeugt wird, wie in „Particle-in-Cell“ (PIC)-Codes. Der erste Ansatz ist jedoch prinzipiell inkonsistent, während der zweite die punktförmige Natur der strahlenden Teilchen vernachlässigt. Wir erweitern die LL-Gleichung in ihrer reduzierten Form, um die Liénard-Wiechert-Felder von benachbarten Teilchen einzubeziehen, was unseres Wissens nach zum ersten Mal numerisch gelöst wird. Für die Kollision eines relativistischen Elektron-Positron-Bündels mit einem intensiven Laserpuls identifizieren wir ein Regime, in dem Mikrobündel durch die reflektierte Strahlung erzeugt werden, was zu kohärenter Emission über einen breiten Frequenzbereich im Röntgenbereich führt, in dem die RR eine bedeutende Rolle spielen kann. Eine ähnliche kohärent verstärkte RR wird auch in einem konstanten und einheitlichen Magnetfeld mit schwächeren Mikrobündeln beobachtet. In beiden Fällen fällt diese „kollektive RR“ mit einer Phasenraumerweiterung zusammen und ist daher vorübergehend.

## Abstract

Charged particles emit electromagnetic radiation when accelerated, and the subsequent impact on the trajectory must be accounted for by energy and momentum conservation in a self-consistent equation of motion, such as the Landau-Lifshitz (LL) equation. This effect, known as radiation reaction (RR), becomes significant for relativistic particles in the presence of extremely strong electromagnetic fields, such as an intense laser pulse or pulsar magnetosphere. The LL equation is typically solved either analytically, while treating each particle independently in an external field, or numerically, with a mean field generated by a charge distribution in addition to an external field, as in particle-in-cell (PIC) codes. Yet, the first approach is in principle inconsistent, while the latter neglects the point-like nature of particles which gives rise to RR. We extend the LL equation in its reduced form to include the Liénard-Wiechert fields from neighbouring particles, which is solved numerically for the first time, to our knowledge. For the collision of a relativistic electron-positron bunch with an intense laser pulse, we identify a regime in which micro-bunches are created by the reflected radiation, which leads to coherent emission across a broad range of frequencies in the X-ray domain, in which RR can play a significant role. A similar, coherently enhanced RR is also observed in a constant and uniform magnetic field, with a weaker form of micro-bunching. In both cases, this ‘collective RR’ coincides with a phase space expansion and is therefore transient.

Regarding the topic of this thesis, one article has been submitted to a peer reviewed journal:

- M. J. Quin, A. Di Piazza, C. H. Keitel and M. Tamburini
  *Interparticle-Fields Amplified Radiation Reaction*
  arXiv:2306.17832 [1]

While another article related to this thesis is in preparation:

- M. J. Quin and M. Tamburini
  *Collective Radiation Reaction in a Constant and Uniform Magnetic Field*

Outside the scope of this thesis, the following articles have been submitted to peer reviewed journals:

- S. Bohlen, Z. Gong, M. J. Quin, M. Tamburini and K. Põder
  *Colliding Pulse Injection of Polarized Electron Bunches in a Laser-Plasma Accelerator*
  arXiv:2304.02922 [2]

- Z. Gong, M. J. Quin, S. Bohlen, C. H. Keitel, K. Põder and M. Tamburini
  *Spin-polarized electron beam generation in the colliding-pulse injection scheme*
  arXiv:2303.16966 [3]

# Units and conventions

Throughout this thesis we will frequently consider relativistic bodies, such that it is convenient to set the reduced Planck constant $\hbar$ and speed of light in vacuum $c$ to unity

$$\hbar = c = 1.$$

Note that this convention applies even on graph axes. Following the classical literature on electromagnetism and radiation reaction we employ the so called 'natural' units

$$4\pi\epsilon_0 = 1.$$

This removes any dependence on the permittivity $\epsilon_0$ or permeability $\mu_0$ of free space. With these units, a factor of $4\pi$ does not appear in Coulomb's law. However, when defining a quantity with physical units we employ S.I. conventions, for example the critical magnetic field of Quantum Electrodynamics $B_{\rm cr} \approx 4.41\times10^9$ T is written in units of Tesla, as opposed to Gauss (or C.G.S units).

Four vectors are denoted by Greek indices $x^\mu$ while three vectors are written in bold typeface $\boldsymbol{x}$. We employ the Minkowski metric throughout

$$\eta^{\mu\nu} = \eta_{\mu\nu} = \begin{pmatrix} +1 & 0 & 0 & 0 \\ 0 & -1 & 0 & 0 \\ 0 & 0 & -1 & 0 \\ 0 & 0 & 0 & -1 \end{pmatrix},$$

and shorthand notation for Lorentz scalars $(ab) = a^\mu b_\mu = a_\mu b^\mu$ is used sparingly. The minus sign then appears on the covariant vector $x_\mu = (t, -\boldsymbol{x})$ as opposed to the contravariant vector $x^\mu = (t, \boldsymbol{x})$. Following this logic we can also write the four vector gradient in terms of its temporal and spatial derivatives:

$$\partial_\mu = \frac{\partial}{\partial x^\mu} = (\partial_t, \nabla_{\boldsymbol{x}}) \,, \qquad \partial^\mu = \frac{\partial}{\partial x_\mu} = (\partial_t, -\nabla_{\boldsymbol{x}}).$$

# Notation and abbreviations

Symbols $e$ and $m$ refer to the charge and mass of the particle in question, often either an electron $e = -|e|$ or positron $e = +|e|$ where $|e| \approx 1.6 \times 10^{-19}\,\mathrm{C}$ is the elementary unit of charge. Specifically for electrons and positrons ($e^-/e^+$), the term 'particle(s)' will often be used to refer to both species without distinction.

When considering many body problems, we tend to attach a Latin index to quantities pertaining to a specific particle, for example the $i$th particle's charge and velocity are $e_i$ and $u_i^\mu$ respectively.

We will often consider scenarios in which particles of various species are interacting. To that end, we define 'interparticle' as referring to interactions between particles of *any* species, and 'intraspecies' as referring to interactions between particles of the *same* species.

For brevity, we will also employ the following abbreviations:

| | |
|---|---|
| **RR** | Radiation Reaction |
| **LAD** | Lorentz-Abraham-Dirac |
| **LL** | Landau-Lifshitz |
| **QED** | Quantum Electrodynamics |
| **LW** | Liénard-Wiechert |
| **FWHM** | Full Width at Half Maximum |
| **RMS** | root-mean-squared |
| **adv** | advanced [field] |
| **ret** | retarded [field] |
| **ext** | external [field] |
| **sc** | synchrotron |
| **cv** | curvature |

# Contents

# Chapter 1

# Introduction

*"Nature never did betray the heart that loved her...*
*for she can so inform the mind that is within us,*
*so impress with quietness and beauty"*

— W. Wordsworth, *Tintern Abbey*

The discovery of the electron by J. J. Thomson profoundly altered our understanding and application of classical electromagnetism. At first, attempts were made to model the electron as a classical[1] object with an extended distribution in space; in particular, the charged sphere model of Lorentz and Abraham. Despite their inherent instability, these models could explain the electron mass entirely from an electromagnetic origin. Later, Einstein's energy-mass equivalency appeared to render this point obsolete. Physicists at the time were already aware of the conversion of mass into binding energy within Helium nuclei, although nucleons themselves were thought to be fundamental before the standard model was developed. The theory of *extended* electrons was then succeeded by *point* like electrons, which would provide an excellent approximation except at length scales where the concept of a localised electron breaks down and classical physics no longer applies; notice that the electron Compton wavelength $\lambda_e = 1/m \approx 2.4\times10^{-12}$ m is orders of magnitude above the classical electron radius $r_e = e^2/m \approx 2.8 \times 10^{-15}$ m.

Charged particles emit electromagnetic radiation when accelerated. Yet the Lorentz equation neglects this emission when describing the trajectory, thus violating energy and momentum conservation. The radiation reaction problem refers to how one should incorporate the particle's self-field to create a self-consistent equation of motion. This typically involves the inclusion of a self-force which intimately depends on the particle's structure. Abraham deduced the equation of motion for a small and rigid *charged sphere* [4], while Dirac derived the same equation in the limit of a *point* particle [5, 6]. The resulting, manifestly covariant equation of motion is then named the Lorentz-Abraham-Dirac (LAD) equation in their honour. Unfortunately, the LAD equation admits unphysical solutions, including indefinite acceleration in the absence of an external field, and acceleration from future fields, known as pre-acceleration [7]. These problems can be resolved by a perturbative expansion, by which one obtains the Landau-Lifshitz (LL) equation [8]. Following

[1] Here 'classical' pertains to relativistic mechanics but excludes quantum mechanics.

this logic we favour the LL equation, though a lively debate continues about the 'correct' equation of motion to this day. Suggestions have been made to discern between these equations with high intensity lasers, within the classical regime [9], but to our knowledge, this has not yet been achieved in the laboratory. The LL equation was derived assuming that the rest frame fields remain small compared to the classical critical value $F_c = m^2/e^3 \approx 1.8 \times 10^{20}\,\mathrm{V/m}$ and approximately constant over the classical length scale $r_e$. These conditions are automatically satisfied in the classical regime, providing the rest frame fields are small compared to the critical value of Quantum Electrodynamics (QED) $F_{\mathrm{cr}} = \alpha_f F_c$ and are approximately constant over the quantum length scale $\lambda_e$, where $\alpha_f = e^2/4\pi \approx 1/137$ is the fine structure constant.

In short, the radiation reaction phenomena arises when we derive an equation of motion which is *consistent* with the principle of energy and momentum conservation. In his original derivation, Abraham mentioned as a counter proof to his equation the example of $N$ electrons moving in a circle due to the influence of an external, electromagnetic field [4]. Under the limit $N \to \infty$, this system constitutes a steady current and emits no radiation, and as such there would be no radiation reaction effect. Yet, if one evaluated either the LAD or LL equations while treating each particle independently, that is only considering the external field, one might estimate the total energy radiated as a sum of the energies lost by all particles, which would be non-zero. This point was reviewed more recently by Gromes [10], who emphasised that the Poynting vector (and therefore self-force) vary quadratically with the fields; any approach which treats particles independently is then *inconsistent* with the principle of energy and momentum conservation. Both Dirac [5] and Rohrlich [6] provided generalisations of the LAD equation to many *point* particles, but to our knowledge this system of equations has never been solved for a given external field, perhaps due to the lack of closed form solutions. Following their approach, we suggest to evaluate the LL equation with the *total* electromagnetic field as seen by each particle, including the Liénard–Wiechert fields from neighbouring particles in addition to the external field.

Classical radiation reaction tends to become relevant when the rest frame field is a few orders of magnitude below the critical field of QED. Approaching the aforementioned field is challenging in the laboratory, and so experimental observation of radiation reaction remained a remote prospect during much of the 20$^{\mathrm{th}}$ century. Two innovations are responsible for changing this status quo. First, the production of GeV-energy electrons from conventional and later plasma-based particle accelerators. Second, the development of intense optical lasers ($I \gtrsim 10^{20}\,\mathrm{W/cm^2}$) following the advent of chirped pulse amplification [11]. A recent experimental campaign involving the collision of ultra-relativistic electrons with an intense laser pulse, has provided the first observations of radiation reaction with both classical and quantum characteristics [12, 13]. Another technique leverages the strong electromagnetic fields experienced as ultra-relativistic electrons propagate through aligned crystals, providing good agreement with the LL equation as a model for

the spectrum of emitted radiation [14–16]. We need not limit our search to the laboratory; radiation reaction is thought to be relevant in a variety of astrophysical contexts, for example as relativistic, charged particles propagate along the strong magnetic fields permeating the pulsar magnetosphere [17, 18].

We note that a few papers have suggested the possibility of a 'coherently enhanced radiation reaction' effect [19–21]. As the LAD self-force is proportional to the classical electron radius $r_e = e^2/m$, they argue a 'small bunch' of $N$ electrons could be approximated as a single *point* particle, which would experience a coherently enhanced self-force proportional to $(Ne)^2/Nm = Nr_e$. We refer to this as the 'model of effective electron radius $Nr_e$'. We interpret 'small' with respect to the characteristic wavelengths of radiation emitted in a predetermined external field. In short, the purpose of this thesis is to explore the interplay between coherent emission, collective behaviour and radiation reaction in a self-consistent manner, for a series of *point* particles. Specifically, we consider two cases: (i) the collision of an electron-positron ($e^-/e^+$) bunch with an intense laser pulse, as may be seen in the laboratory, and (ii) a cylindrical beam of $e^-/e^+$ in the presence of a constant and uniform magnetic field, with an interest towards astrophysical applications.

This thesis is then structured as follows; chapter 2 will describe the solution of Maxwell's equations for a point charge and their subsequent incorporation to create the self-consistent LAD and LL equations of motion. Their generalisation to systems of many point particles in the presence of an external electromagnetic field is demonstrated, and the leading order terms identified. Chapter 3 describes the development of our numerical code, which can numerically integrate the reduced LL equation for many point particles, and can evaluate the spectrum of emitted radiation. Chapter 4 then describes the application of this code to the collision of an $e^-/e^+$ bunch and laser pulse, modelled as a plane wave pulse. Here, we demonstrate a microscopic instability created by the reflected radiation, which is responsible for the broad, coherent amplification of the spectrum. Chapter 5 proceeds analogously with the previous chapter, instead considering a constant and uniform magnetic field. Here we observe a similar, weaker instability driven by the emission of low frequency radiation along the magnetic field lines, in the synchrotron regime.

# Chapter 2

## Classical dynamics of point particles and electromagnetic fields

> *"It is the classical theory of electromagnetic mass that is re-examined here. And why, after all these years, and in view of its apparent irrelevance to the real world? Quite simply, because it still isn't right."*
>
> — J. Schwinger [22]

The development of classical electromagnetism initially followed the same path as Newtonian gravity, with Coulomb's law bearing a striking resemblance to Newton's universal law of gravitation, both depending on the inverse square of the separation between two particles. From our point of view, the major distinction between gravity and electromagnetism remains the empirical observation that gravitational forces tend to be attractive, while electromagnetic forces can be either attractive or repulsive.

After gradual advances in theory and observation regarding electricity, magnetism and optics, spanning more than a century, a unified theory encompassing each was created by Maxwell in 1873. As with Newtonian mechanics, Maxwell's laws were initially applied to large scale, macroscopic bodies, with continuous charge and current distributions. These developments coincided with advent of atomic theory and the eventual discovery of the electron in 1897, the first known sub-atomic particle. It would require several years more before the concept of an extended electron was retired in favour of the point particle we are familiar with today.

This chapter then seeks to describe the classical dynamics of charged point particles. We begin by reviewing the solution of Maxwell's equations for a point like source, following the Green's function method of Jackson [23]. Then, we identify the Lorentz-Abraham-Dirac equation of motion which respects energy and momentum conservation, following the method of Dirac [5], which is compared with Teitelboim's approach of splitting the energy-momentum tensor [24–26]. A short explanation of the deficiencies of this equation is provided, which are resolved by the perturbative expansion of Landau and Lifshitz [8]. At this point we extend our discussion to many point particles, and highlight the importance of evaluating the radiation reaction equations of motion with the total electromagnetic field, particularly when coherent emission occurs.

## 2.1 Green's function solution to Maxwell's equations

Maxwell's equations describe the electromagnetic potential $A^\mu(x)$ from a source, four current density $J^\mu(x)$. These quantities, defined at position $x^\mu$ in Minkowski space, are related by a second order differential equation

$$\partial^2 A^\mu(x) = 4\pi J^\mu(x). \tag{2.1}$$

Where we have chosen to work in the Lorenz gauge $(\partial A(x)) = 0$. We seek to measure the response of this differential equation for a point like source, or in other words, we seek to solve with Green's functions

$$\partial^2 D(x) = \delta^{(4)}(x). \tag{2.2}$$

This procedure is carefully laid out by Jackson [23, Ch. 12.11], and as such we will review only the key steps here; that this is necessary reflects how regularly we refer to these fields throughout this thesis. Once the Green's functions are known, the potential from any source can be derived from the superposition of each current element at position $x'^\mu = (t', \boldsymbol{x}')$

$$A^\mu(x) = A_0^\mu + 4\pi \int_{-\infty}^{+\infty} D(x - x')\, J^\mu(x')\, d^4x'. \tag{2.3}$$

Here $A_0^\mu$ is a constant determined by the application of boundary conditions for the specific problem in question. By performing a Fourier transform

$$D(x) = \frac{1}{(2\pi)^4} \int_{-\infty}^{+\infty} \tilde{D}(k)\, e^{-i(kx)}\, d^4k, \tag{2.4}$$

we can move from a differential equation in space $x^\mu$ to an equation in frequency space $k^\mu = (k_0, \boldsymbol{k})$ which can be solved algebraically

$$\tilde{D}(k) = -\frac{1}{k^2}. \tag{2.5}$$

With the Green's function in frequency space now known, one can find the corresponding function in space by evaluating the Fourier transform. We divide this problem into integrals over the time like $k_0$ and space like $\boldsymbol{k}$ components

$$D(x - x') = -\frac{1}{(2\pi)^4} \int_{-\infty}^{+\infty} e^{i\boldsymbol{k}\cdot(\boldsymbol{x}-\boldsymbol{x}')} \int_{-\infty}^{+\infty} \frac{e^{-ik_0(t-t')}}{k_0^2 - \kappa^2}\, dk_0\, d^3\boldsymbol{k}, \tag{2.6}$$

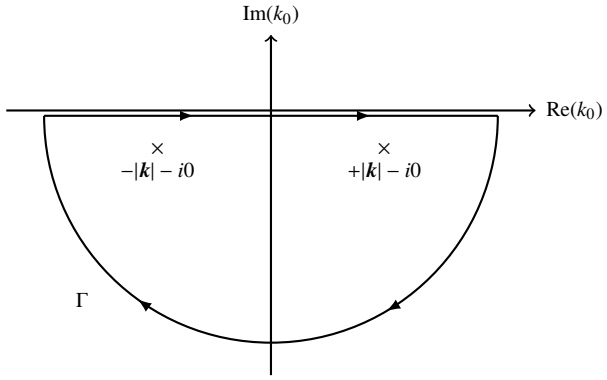


Figure 2.1: Contour of integration for the retarded Green's function in Eq. 2.7. As usual, the circular part of the contour Γ does not contribute as the radius tends to infinity, and one is simply left with an integral along the real axis.

we notice the presence of two poles on the real axis at $\pm\kappa$, where $\kappa = |\boldsymbol{k}|$ is the magnitude of the wave vector. First, consider the retarded case $D(x-x') = D_{\text{ret}}(x-x')$ for $t > t'$, where the signal propagates from the source at $t'$ to an observer at $t$. Here, the effect occurs after the cause. For $t > t'$, the time like integral converges in the lower half plane and can be solved by the residue theorem with contour Γ, as shown in Fig. 2.1

$$\int_{-\infty}^{+\infty} \frac{e^{-ik_0(t-t')}}{k_0^2 - \kappa^2}\, dk_0 = \oint_\Gamma \frac{e^{-iz(t-t')}}{z^2 - \kappa^2 + i0}\, dz = -\frac{2\pi}{\kappa} \sin\left(\kappa(t-t')\right). \tag{2.7}$$

While the remaining space like integral can be solved using spherical coordinates, to obtain the retarded Green's function

$$D_{\text{ret}}(x - x') = \frac{1}{4\pi R}\delta(t - t' - R), \tag{2.8}$$

where $R = |\boldsymbol{x} - \boldsymbol{x}'|$ is the separation of the observer and source, respectively. If we return momentarily to physical units, one can recognise the retarded condition $t = t' + R/c$ respects the finite speed of light in vacuum. This can be interpreted by inserting the retarded Green's function into our integral for the potential $A^\mu(x)$ in Eq. (2.3), which has the effect of localising the integral; only current elements which satisfy the retarded condition will contribute to the potential. Similarly, one can solve for the advanced case $D(x - x') = D_{\text{adv}}(x - x')$ for $t < t'$, by displacing the poles into a contour in the upper half plane

$$D_{\text{adv}}(x - x') = \frac{1}{4\pi R}\delta(t - t' + R). \tag{2.9}$$

As the advanced solution does not respect causality, it is said to be unphysical. One

could interpret the advanced case as describing the potential seen in the present, with an origin which lies in the future.

As will be discussed later in the section on the radiation reaction problem, one can add or subtract the retarded and advanced Green's functions; these auxiliary Green's functions have corresponding potentials, or fields, via Eq. (2.3). It is difficult to explain the physicality of these fields given that they do not respect causality. However, they are mathematically convenient when evaluating the self-field close to the world line, as shown by Dirac [5].

## 2.2 Liénard–Wiechert field

Having described the electromagnetic potential from a general charge and current distribution, we can specialise to a *point* charge. Consider then, a particle of charge $e$ and mass $m$ moving along a trajectory $z^\mu(\tau)$ with proper time $\tau$. A point charge is then defined as having a current density which is localised to its world line by a delta function

$$J^\mu(x) = e \int_{-\infty}^{+\infty} \delta^{(4)}(x - z(\tau))\, u^\mu(\tau)\, d\tau. \tag{2.10}$$

By substituting this current density into our equation for the four vector potential Eq. (2.3), along with the retarded Green's function (2.9), one can define the corresponding potential simply by using the elementary properties of the delta function [23]

$$\delta[f(x)] = \frac{\delta(x - x_0)}{|f'(x_0)|}, \tag{2.11}$$

where $f(x_0) = 0$ is a root of the function in question, which must be well behaved, i.e. real and analytic. In the retarded case, the appropriate root is the retarded proper time $\tau_{\text{ret}}$. Following this method, one can determine the retarded potential, though we will often refer to it as the Liénard–Wiechert (LW) potential for historical reasons

$$A^\mu_{\text{ret}}(x) = \left[\frac{e\, u^\mu}{(nu)R}\right]_{\tau_{\text{ret}}}. \tag{2.12}$$

This potential constitutes a solution to Maxwell's equations for a point charge, which respects causality.

Here we have defined a four vector $n^\mu = (1, \boldsymbol{n})$ which points from the particle to observer and satisfies the null condition $n^2 = 0$. Note that every quantity inside

the square brackets of Eq. (2.12) must be evaluated at the retarded proper time, except the charge and position of the observer $x^\mu$ which are treated as constant. This potential can be differentiated with respect to the observer's position to obtain the LW (or retarded) field in the usual way

$$F^{\mu\nu}_{\text{ret}}(x) = \partial^\mu A^\nu_{\text{ret}}(x) - \partial^\nu A^\mu_{\text{ret}}(x). \tag{2.13}$$

To explain the physical significance of this result, we separate the LW field into 'velocity' and 'acceleration' parts [24]

$$F^{\mu\nu}_{\text{ret}}(x) = F^{\mu\nu}_{\text{vel}}(x) + F^{\mu\nu}_{\text{acc}}(x), \tag{2.14}$$

$$F^{\mu\nu}_{\text{vel}}(x) = \left[\frac{e}{R^2}\,\frac{n^\mu u^\nu - n^\nu u^\mu}{(nu)^3}\right]_{\tau_{\text{ret}}}, \tag{2.15}$$

$$F^{\mu\nu}_{\text{acc}}(x) = \left[\frac{e}{R}\,\frac{n^\mu u^\nu - n^\nu u^\mu}{(nu)^2}(n\mathrm{a}) + \frac{e}{R}\,\frac{n^\mu \mathrm{a}^\nu - n^\nu \mathrm{a}^\mu}{(nu)^2}\right]_{\tau_{\text{ret}}}. \tag{2.16}$$

Where we have defined the acceleration four vector $\mathrm{a}^\mu = du^\mu/d\tau$. At first glance, the separation into velocity and acceleration fields seems artificial. However, an important physical distinction exists. The velocity fields represent energy and momentum bound to the charge. It is therefore nonsensical to talk of a potential, or velocity field irrespective of a source. This field depends on the inverse square of the separation from the source, and as such decays quickly with distance. If one boosts into the rest frame of the source, one can see the velocity field is simply a Coulomb field.

The acceleration fields represent the emission of electromagnetic radiation which propagates away freely, removing energy and momentum from the single particle system. Note that the particle only radiates when accelerated. As these fields decay slowly, with the inverse of the separation from the source, one often assumes the acceleration fields can be treated independently of their source. In a way, we can interpret the velocity and acceleration fields as asymptotic forms of the LW field, which dominate in the limit of small or large distances respectively. Note that, when the LW field from one particle is evaluated on the world line of another, distinct particle, we refer to it as an 'interparticle' field.

We point out that a near identical procedure can be carried out, utilising a point like current density with the advanced Green's function (2.9), to determine the advanced potential $A_{\text{adv}}$. The subsequent field $F^{\mu\nu}_{\text{adv}}$ changes little except for a global minus sign, and of course, it must be evaluated at the advanced proper time

$\tau_{\text{adv}}$. The fields in the retarded and advanced case, are found in the next section in Eq. (2.19).

## 2.3 The radiation reaction problem

Having established that a point particle radiates when accelerated it is natural to ask how we should describe its trajectory, in a way which conserves energy and momentum. Consider then, the electromagnetic energy-momentum tensor for a general field[1]

$$T^{\mu\nu} = \frac{1}{4\pi}\left[F^{\mu}{}_{\alpha}F^{\alpha\nu} + \frac{1}{4}\eta^{\mu\nu}F^{\alpha\beta}F_{\alpha\beta}\right]. \tag{2.17}$$

For brevity, we will omit the spatial dependence of the energy-momentum tensor $T^{\mu\nu} = T^{\mu\nu}(x)$, field tensor $F^{\mu\nu} = F^{\mu\nu}(x)$ and current density $J^{\mu} = J^{\mu}(x)$ here. Note the indentation which arises for tensors with mixed covariant and contravariant indices, defined by $F_{\mu}{}^{\nu} = \eta_{\mu\alpha}F^{\alpha\nu}$ and $F^{\mu}{}_{\nu} = F^{\mu\alpha}\eta_{\alpha\nu}$. By applying Maxwell's equations, one can relate the divergence of the energy-momentum tensor to the current density

$$\partial_{\mu}T^{\mu\nu} + F^{\nu\mu}J_{\mu} = 0. \tag{2.18}$$

In vacuum, the energy-momentum tensor is divergenceless, reflecting conservation of energy and momentum. As noted by Teitelboim [26], for a *continuous* distribution there is no distinction between the field at $x^{\mu}$ from all charges *excluding* the charge at $x^{\mu}$, and the field at $x^{\mu}$ from all charges *including* the charge at $x^{\mu}$, because the amount of charge at each *point* is zero. Only a volume will contain a non-zero amount of charge. For a *point* particle, however, the charge and current density are localised by a delta function, such that the stress energy-tensor is no longer divergenceless on the world line, although it is divergenceless everywhere else. By consistency with Eq. (2.18), one should then impose energy and momentum conservation on the world line of the particle. The 'radiation reaction problem' refers to how one should account for the divergence of the self-field on the world line, in particular the Coulomb-like field which is proportional to $1/R^2$ and diverges rapidly as $R \to 0$. This problem was first solved by Dirac [5], whose method we will follow here.

Consider then, a point particle in the presence of an external electromagnetic field. The solution of Maxwell's equations for such a particle were derived earlier, and are known as the retarded and advanced fields [6, Ch. 6.5]

[1] A derivation of the energy-momentum tensor can be found in any textbook on classical electromagnetism, including those by Jackson [23, Ch. 12.10] or Landau and Lifshitz [8, Sec. § 33-34].

$$F^{\mu\nu}_{\substack{\text{ret}\\\text{adv}}}(x) = \mp\left[\frac{2e}{(nu)R}\frac{d}{d\tau}\left(\frac{u^{[\mu}n^{\nu]}}{(nu)}\right)\right]_{\substack{\tau_{\text{ret}}\\\tau_{\text{adv}}}}. \tag{2.19}$$

Note that when square brackets appear around the Lorentz indices we take only the anti-symmetric part, $a^{[\mu}b^{\nu]} = \frac{1}{2}(a^\mu b^\nu - a^\nu b^\mu)$. Now, consider a frame of reference in which the particle is simultaneously at rest, at position $z^\mu(\tau_0)$ on the world line, when the field is seen by an observer at $x^\mu$. For brevity, we omit the dependence of the particle's position $z^\mu = z^\mu(\tau_0)$, velocity $u^\mu = u^\mu(\tau_0)$, acceleration $\mathrm{a} = \mathrm{a}(\tau_0)$ and its derivative when defined at this proper time, which we set to zero for convenience $\tau_0 = 0$. In this chapter, a dot denotes a derivative with respect to the proper time. The position of the particle at the retarded and advanced proper time(s) can be determined by an expansion up to $\tau \sim R$

$$z_{\substack{\text{ret}\\\text{adv}}} \equiv z(\mp\tau) = z^\mu \mp \tau u^\mu + \frac{\tau^2}{2}\mathrm{a}^\mu \mp \frac{\tau^3}{6}\dot{\mathrm{a}}^\mu + O(\tau^4). \tag{2.20}$$

One can then substitute the trajectory and its derivatives into our equations for the advanced and retarded field(s). The algebra involved is described in detail by both Dirac [5, Eqs. (55)-(60)] and Rohrlich [6, Ch. 6.5], and so will be omitted here. Following this procedure, we can describe the leading order terms of the fields close to the world line[2].

$$\begin{aligned} F^{\mu\nu}_{\substack{\text{ret}\\\text{adv}}}(x) = 2e\Bigg[ &-\frac{u^{[\mu}n^{\nu]}}{R^2} - \frac{\mathrm{a}^{[\mu}u^{\nu]} + (n\mathrm{a})u^{[\mu}n^{\nu]}}{2R} - \frac{3}{4}(n\mathrm{a})\mathrm{a}^{[\mu}u^{\nu]} \\ &+ \frac{\mathrm{a}^2}{8}u^{[\mu}n^{\nu]} + \frac{1}{2}\dot{\mathrm{a}}^{[\mu}n^{\nu]} \pm \frac{2}{3}\dot{\mathrm{a}}^{[\mu}u^{\nu]} + O(R)\Bigg]. \end{aligned} \tag{2.21}$$

Dirac noticed that the retarded and advanced fields differ only by the last term, and so it is convenient to construct the difference $F^{\mu\nu}_-$ as shown below. In the limit $R \to 0$ one can see this field remains finite on the world line, and vanishes everywhere as the source charge tends to zero. Conversely, the sum $F_+$ does not vanish in this limit, on the world line, and to leading order is simply the velocity field (2.15) in the rest frame, better known as the Coulomb field

$$F^{\mu\nu}_- = \frac{1}{2}\left(F^{\mu\nu}_{\text{ret}} - F^{\mu\nu}_{\text{adv}}\right) = \frac{4e}{3}\dot{\mathrm{a}}^{[\mu}u^{\nu]} + O(R), \tag{2.22a}$$

$$F^{\mu\nu}_+ = \frac{1}{2}\left(F^{\mu\nu}_{\text{ret}} + F^{\mu\nu}_{\text{adv}}\right) = \frac{2e}{R^2}n^{[\mu}u^{\nu]} + O(1/R). \tag{2.22b}$$

[2]Equation (2.21) was obtained by performing an expansion for small $R$ of Eq. (60) in Dirac's paper [5], both in the retarded and advanced cases. Note that we use the same metric signature (+,-,-,-) as Dirac, but both Rohrlich and Teitelboim use the (-,+,+,+) metric.

We seek to provide an interpretation for the auxiliary fields $F_{\pm}$ introduced above. The total field $F^{\mu\nu}$ can be written as the sum of the external field, and the retarded field produced by the particle (which respects causality)

$$F^{\mu\nu} = F^{\mu\nu}_{\text{ext}} + F^{\mu\nu}_{\text{ret}} = F^{\mu\nu}_{\text{ext}} + F^{\mu\nu}_{+} + F^{\mu\nu}_{-}. \tag{2.23}$$

Where we have decomposed the retarded field into a sum of the auxiliary fields $F_{\pm}$ introduced above. Due to its resemblance with the Coulomb field, one can interpret $F^{\mu\nu}_{+}$ as being associated with energy and momentum bound to the system. Following this logic, one can argue the total field can separated $F^{\mu\nu} = F^{\mu\nu}_{+} + f^{\mu\nu}$ into bound and unbound[3] parts, respectively. One then argues the unbound field includes both the external field, and a field associated with the 'radiation reaction' of the particle $f^{\mu\nu} - F^{\mu\nu}_{\text{ext}} = F^{\mu\nu}_{-}$.

Having evaluated the field(s) from the particle, as seen close to the world line (2.21), we would like to determine the electromagnetic energy and momentum leaving the system. This can be found by integrating the divergence of the energy-momentum tensor over a volume of Minkowski space, or with Gauss' theorem, by integrating over a closed surface with normal $n^{\mu}$

$$\int \partial_{\mu} T^{\mu\nu}\, d^4x = \oint T^{\mu\nu}\, n_{\mu}\, d^3\sigma. \tag{2.24}$$

A surface must be defined before this integral can be solved; Dirac employed a small tube in Minkowski space surrounding the world line. This corresponds to a three-dimensional surface $d^3\sigma$, which consists of a time-like element $d\tau'$ as measured at $x^{\mu}$ that can be related[4] to an element of proper time for the particle $d\tau$, and a two-dimensional surface $d^2\sigma = R^2 d\Omega$, where $d\Omega$ is a solid angle element. To solve, one should construct the energy-momentum tensor with the *total* field $F^{\mu\nu}$ according to Eq. (2.17). The algebra is lengthy, though greatly simplified by requiring only the component along $n^{\mu}$, and so we present only the final result as derived by Dirac [5, Eqs. (67)-(68)]

$$-\oint T^{\mu\nu}\, n_{\mu} d^3\sigma = \int \left( \frac{e^2}{2R} \mathrm{a}^{\mu} + eF^{\mu\nu}_{\text{ext}} u_{\nu} + eF^{\mu\nu}_{-} u_{\nu} \right) d\tau. \tag{2.25}$$

The integration limits on the right hand side are determined by the length of the tube, and the section of world line it encloses. One notices the first term under the

[3] The 'unbound' or 'free' field is $f^{\mu\nu}$ in Dirac's notation or equivalently $\overline{F}^{\mu\nu}$ in Rohrlich's notation [6]. In fact, both authors make use of a large number of auxiliary fields which we have attempted to eliminate in so far as this is possible, within our own interpretation of Dirac's work.

[4] To relate the proper time of the observer and particle, see Eq. (66) of Dirac's paper [5], or alternatively Eq. (3.9b) of Teitelboim's paper [24]; the geometry of this surface integral is particularly well illustrated in Fig. 3 of the latter paper.

integral is the electrostatic energy (outside the sphere) of a charged sphere at rest $m_C = e^2/2R$, which by energy-mass equivalency we refer to as the Coulomb mass $m_C$. This corresponds to the bound field $F_+^{\mu\nu}$ introduced earlier. The second and third terms are the force due to the external field and the self-force (due to radiation reaction), respectively. Now consider that this particle has a bare mass $m_b$, and a corresponding change in mechanical momentum $\int dp^\mu = m_b \int \mathrm{a}^\mu d\tau$. By energy and momentum conservation, this can be equated with the flux of electromagnetic momentum leaving the tube from Eq. (2.25)

$$(m_b - m_C)\,\mathrm{a}^\mu = eF^{\mu\nu}_{\text{ext}}u_\nu + eF^{\mu\nu}_{-}u_\nu + O(R). \tag{2.26}$$

Note that we have discarded the integral as this equation must be satisfied for an arbitrary set of limits. The meaning of the minus sign in Eq. (2.25) now becomes clear; as electromagnetic momentum leaves the tube it must correspond to a *loss* of mechanical energy by the particle. By contracting our definition of $F_-^{\mu\nu}$ in Eq. (2.22a) with the velocity, one can show

$$F^{\mu\nu}_{-}u_\nu = \frac{2}{3}e\left[\dot{\mathrm{a}}^\mu + \mathrm{a}^2 u^\mu\right], \tag{2.27}$$

where we have used both the on-shell condition $u^2 = 1$ and its second derivative $(\dot{\mathrm{a}}u) = -\mathrm{a}^2$. Finally, we are ready to write down an appropriate equation of motion for a *point* particle, which requires that we take the limit $R \to 0$. In this limit, the Coulomb mass will diverge $m_C \to +\infty$ and so we require the bare mass to diverge $m_b \to -\infty$ to compensate, such that the coefficient of the acceleration is the finite, experimentally measured electron mass. This is the somewhat infamous 'classical' mass renormalisation performed by Dirac [5], and as with renormalisation in quantum field theories it can only be justified by empirical observation and not by theory (to our knowledge). The Lorentz-Abraham-Dirac (LAD) equation of motion can then be written [5, Eq. (24)]

$$m\mathrm{a}^\mu = eF^{\mu\nu}_{\text{ext}}u_\nu + \frac{2}{3}e^2\left(\dot{\mathrm{a}}^\mu + \mathrm{a}^2 u^\mu\right). \tag{2.28}$$

While the LAD equation has been derived in a specific frame of reference, one argues that as this equation is manifestly covariant, it is in fact general. The method presented here closely follows that employed by Dirac in 1938, about eighty-five years ago at the time of writing. As such, a large body of literature has developed to review this important result; it seems prescient to mention their contributions here. First, one notices this derivation employs the advanced field which violates causality. It is commonly assumed this leads to the Schott force $\frac{2}{3}e^2\dot{\mathrm{a}}^\mu$, which allows for solutions of the LAD equation which violate causality themselves [7]. However, Teitelboim later demonstrated in 1970 that one can derive the LAD equation without reference to the advanced fields [24]. Teitelboim's approach involves

separating the energy-momentum tensor into bound and unbound parts which are treated independently. In particular, he shows that by assuming the particle posses a pure Coulomb field in the rest frame, which we identified with $F_+$, we are assuming it posses a straight world line in the *whole* of its history. Upon relaxing this condition, an additional term emerges which corresponds exactly to the Schott force.

Note that in the interest of avoiding a simple regurgitation of the literature we have omitted many important details. For example, we have conflated the radius of our particle with that of the tube (and its spherical surface) through which the energy-momentum flux passes. One should consider two tubes of identical length; a small tube which encloses the world line, enclosed within a large tube [24, see Fig. 3]. One evaluates the flux passing through the large tube, eventually taking the limit that its radius tends to infinity, while the radius of the small tube (and particle) tends to zero, and so the boundary problem is treated carefully before these limits are applied. We avoided a critical error due to this omission only because the energy-momentum tensor is divergenceless in the volume of Minkowski space between the tubes. There are more details besides on the origins of radiation reaction which have been glanced over here. To gain a more complete understanding we recommend the reader consult the original paper by Dirac [5] which was reviewed later by Erber [27] and Eliezer [28], the alternative derivation put forward by Teitelboim [24–26], as well as the book by Rohrlich [6] and references therein, which is perhaps the most comprehensive guide to radiation reaction yet written.

## 2.4 Deficiencies of the Lorentz-Abraham-Dirac equation

In the previous section, we described how the phenomena of radiation reaction arises when we demand conservation of energy and momentum on the world line of a *point particle*. This lead to the LAD equation of motion in the presence of an external electromagnetic field

$$m\mathrm{a}^\mu = eF^{\mu\nu}u_\nu + \frac{2}{3}e^2\left(\frac{d\mathrm{a}^\mu}{d\tau} + \mathrm{a}^2 u^\mu\right). \tag{2.29}$$

For now, we will continue with the consideration of only a single particle in the presence of an external field $F^{\mu\nu} = F^{\mu\nu}(x)$. The purpose of this section is to discuss the shortcomings of this equation. First, due to the presence of the Schott term, one can solve the LAD equation with an integrating factor to obtain solutions which are non-local in time, or in other words, which break causality [6, Ch. 6.6, Eq. 6-80]. This is clearly alarming at first glance. However, signals from the future are exponentially suppressed and only become relevant over time scales outside the classical regime, for which the LAD equation is no longer valid. The time scale in question is $\tau_e = 2e^2/3m$, which becomes $\tau_e = 2r_e/3 \approx 6.27 \times 10^{-24}\,\mathrm{s}$

for the charge and mass of the electron or positron. This problem could then be neglected as an excellent approximation.

Far more troublesome is the simple observation made by Rohrlich, that the acceleration is not identically zero for a null external field, violating Newton's first law [7]. To demonstrate why this is a critical failing, we can set the external field to zero $F^{\mu\nu} = 0$, and contract with the acceleration to identify the infamous 'run away' solution

$$\frac{d(\mathrm{a}^2)}{d\tau} = \frac{2}{\tau_e}\mathrm{a}^2, \tag{2.30a}$$

$$\mathrm{a}^2(\tau) = \mathrm{a}_0^2\, e^{2\tau/\tau_e}. \tag{2.30b}$$

Where the acceleration satisfies $\mathrm{a}^\mu(\tau = 0) = \mathrm{a}_0^\mu$ at the initial proper time. This solution suggests indefinite acceleration in the absence of an external field, and is therefore unphysical. Worse, this occurs rapidly within the classical regime, as the time scale $\tau_e$ is small. It is challenging to see how such a critical error can be overlooked, and in fact Rohrlich went as far as suggesting the LAD equation ought to be abandoned in light of its flaws [7].

## 2.5 Landau-Lifshitz equation of motion

As described above, the LAD equation admits unphysical solutions. We then seek to replace it with an alternative equation of motion, which does not admit unphysical behaviour. This problem was addressed by Landau and Lifshitz, who proceed by assuming a frame of reference exists in which the self-force (terms proportional to $e^2$ on the right hand side of the LAD equation (2.29)) is much smaller than the Lorentz force. One can then perform a perturbative expansion, by substituting $m\mathrm{a}^\mu = eF^{\mu\nu}u_\nu$ and its derivative into the self-force. The result is referred to as the Landau-Lifshitz (LL) equation, and can be written as follows [8, § 76, Eq. (76.3)]

$$\begin{aligned} m\mathrm{a}^\mu = eF^{\mu\nu}u_\nu + \frac{2}{3}e^2\Bigg[&\frac{e}{m}(\partial_\alpha F^{\mu\nu})u^\alpha u_\nu + \\ &\frac{e^2}{m^2}F^{\mu\nu}F_{\nu\alpha}u^\alpha + \frac{e^2}{m^2}(Fu)^2u^\mu\Bigg]. \end{aligned} \tag{2.31}$$

By setting the external field to zero one can see the acceleration will vanish identically, and so the LL equation avoids the critical flaw of the LAD equation. Following this argument, Rohrlich suggests the LAD equation should be replaced with that of LL [7], even going as far as suggesting the LL equation is the 'correct'

one. Yet, it is challenging to justify how one can obtain a 'correct' equation as an approximation to one which is apparently incorrect. To avoid unphysical solutions when solving the LAD equation, Dirac suggested the acceleration should vanish asymptotically $\mathrm{a}(\tau) \to 0$ under the limit $\tau \to +\infty$, in addition to the usual requirement that the initial position and velocity are known [5]. Spohn later demonstrated this condition restricts the solutions of the LAD equation to a critical surface, which can be determined perturbatively, such that the equation on this surface is the LL equation [29]. The perturbative expansion employed in deriving the LL equation can, of course, be extended to include second order corrections in terms of the small quantity $\tau_e$ [30]. However, it is difficult to see how these corrections could become experimentally relevant within the classical regime.

Alternatively, one can offer justification for utilising the LL equation from its agreement with experimental results. One approach involves leveraging the strong electromagnetic fields experienced by ultra-relativistic, charged particles as they penetrate aligned crystals [16, 31, 32]. Applying this method in the regime $\chi_0 \lesssim 0.05$, Nielsen et al [14, 15] demonstrate that a model based on the LL equation, with corrections for photon recoil and spin, provides excellent agreement with the spectrum of radiation emitted. Therefore, in this regime the classical approach can still provide at least the leading order corrections to the trajectories and spectrum of emitted radiation. Alternative schemes involve the collision of a relativistically strong laser pulse $a_0 \gtrsim 10$ with ultra-relativistic electrons $\gamma \gg 1$. With this method, Cole et al [13] consider electrons with $\gamma \approx 10^3$ which experience moderately strong rest frame fields $\chi_0 \sim 0.1$; they find the classical LL model provides reasonably good agreement with the spectrum of emitted radiation, though a description starting from QED provides better agreement. Poder et al [12] consider a similar setup with more energetic electrons $\gamma \approx 4{\times}10^3$ which experience a considerably stronger rest-frame field $\chi_0 \sim 0.25$ at which the classical model is expected to break down; they compare the spectrum of final particle energies with two models, one developed from strong field QED and another following a semi-classical approach based on the LL equation. As it happens, the semi-classical model was found to provide better agreement with the data.

Landau and Lifshitz note that their equation is only valid when the rest frame field is smaller than the classical critical value $F_c = m^2/e^3 \approx 1.8 \times 10^{20}\,\mathrm{V/m}$, and providing the field is approximately constant over distances comparable to the classical electron radius $r_e \sim 10^{-15}\,\mathrm{m}$ [8, 33]. However, it was later shown both theoretically [34, 35] and experimentally [36] that quantum effects already become important before this, when the rest frame field is an appreciable fraction of the critical field of QED $F_{\mathrm{cr}} = \alpha_f F_c$, where $\alpha_f \approx 1/137$ is the fine structure constant. By a similar argument, the relevant length scale over which the fields must remain constant is in fact the electron Compton wavelength $\lambda_e \sim 10^{-12}\,\mathrm{m}$.

## 2.6 Reduced Landau-Lifshitz equation of motion

The LL equation has been solved both analytically and numerically for one particle in a variety of electromagnetic fields, including: a plane wave [33, 37], focused laser [38] Coulomb potential [39], and a rotating magnetic dipole [17, 18]. When solving analytically, one often considers scenarios such as a constant electromagnetic field in which the derivatives of the fields vanish [40]. In fact this term is often neglected in general, as it is far smaller than the spin correction [41, 42], and therefore outside the regime of validity for the LL equation. This results in the so called 'reduced LL equation' which is commonly applied in numerical codes [43]

$$m\,\mathrm{a}^{\mu} = eF^{\mu\nu}u_{\nu} + \frac{2}{3}\frac{e^4}{m^2}\left[F^{\mu\nu}F_{\nu\alpha}u^{\alpha} + (Fu)^2 u^{\mu}\right]. \tag{2.32}$$

By contracting the LL and reduced LL equations with the velocity $u_{\mu}$, one can show both equations satisfy the on-shell condition. In the LL self-force, one can see the term $(Fu)^2 < 0$ is friction-like due to the anti-symmetric nature of the field tensor. As this term is proportional to $\gamma^3$, it tends to dominate when considering an ultra-relativistic particle. It is tempting then, to approximate the LL self-force with this friction-like term alone, however, such an equation of motion would no longer satisfy the on-shell condition.

We seek to summarise our discussion on the origin and applications of radiation reaction before proceeding. The LAD and LL equations are derived by imposing energy and momentum conservation on the world line of a point particle. The conceptual foundation of the radiation reaction phenomena is, therefore, strong. It is somewhat less clear, however, which equation of motion correctly incorporates this effect.

## 2.7 Generalisation to many point particles

Until now, our consideration of radiation reaction has been limited to a single *point* particle in an external, electromagnetic field. Indeed, most analytical solutions of these equations consider only one electron [33, 37, 44]. For many particle systems, one typically assumes the trajectory can be solved independently for each particle, considering only the external field. To challenge this approach, consider $N$ equally spaced particles moving in a circle due to the influence of an external field. Under the limit $N \to \infty$ this constitutes a steady current, and would emit no electromagnetic radiation. However, if one solved the LAD or LL equation for each particle independently, and found the total energy radiated by adding the energy lost by each particle, the result would be non-zero. This simple example was

originally developed as a counter proof to the LAD equation by Abraham[5], and has been reviewed more recently by Gromes [10]; their key argument being that each particle cannot be treated independently as the energy-momentum tensor and self-force vary *quadratically* with the *total* field.

This criticism does not necessarily imply the previous work, which treats particles independently, is inaccurate. Radiation reaction tends to become significant for relativistic particles propagating in strong electromagnetic fields, which often experience a non-negligible fraction of the critical field of QED in the rest frame. Yet, a relativistic beam of particles will often emit radiation at high frequencies (via the Doppler shift), which tend to be incoherent if the 'size' of the beam is larger than the typical wavelength emitted. These are exactly the scenarios which have been studied previously [12, 13], and indeed the analytical solutions for the energy lost, in which particles are treated independently, provide good agreement with the experimental data; in practice, we have little reason to doubt their validity. We conclude that *in principle*, one should evaluate the trajectory in terms of the total field, but *in practice* fields from neighbouring particles can be neglected as a good approximation in scenarios like the one outlined above.

It is interesting then, to consider scenarios in which the particles can no longer be treated independently. We suggest to look for situations in which coherent emission and subsequently strong collective behaviour occur. For this, we would need to generalise our equation of motion to systems of many *point* particles. Following the argument from previous sections, we begin from the reduced LL equation in an external field (2.32). We should now take care to define an external field, as one which is unperturbed by the presence of charges within the system. Given that the reduced LL equation is an appropriate equation of motion for one particle, we argue *by consistency* that for many particle systems it should be evaluated with the total field

$$F_i^{\mu\nu}(x_i) = F_{\text{ext}}^{\mu\nu}(x_i) + \sum_{\substack{j=1 \\ j\neq i}}^{N} F_{\text{ret}\,j}^{\mu\nu}(x_i). \tag{2.33}$$

In the case of one particle $N = 1$, this will reduce to the previous equation (2.32). Here we have defined the total field $F_i^{\mu\nu} = F_i^{\mu\nu}(x_i)$ acting on particle $i$ at position $x_i^\mu$ on the world line, as the sum of an external field $F_{\text{ext}}^{\mu\nu} = F_{\text{ext}}^{\mu\nu}(x_i)$ and LW fields from all other particles in the system $F_{\text{ret}\,j}^{\mu\nu} = F_{\text{ret}\,j}^{\mu\nu}(x_i)$, excluding itself $i \neq j$. The LW field from particle $j$ is evaluated with the historical trajectory $\{x_j^\mu, u_j^\mu, \mathrm{a}_j^\mu\}$ at the retarded time from Eq. (2.14). In general, the charge $e_i$ and mass $m_i$ of the particle in question are not necessarily the same as the particle which produces the LW field, which has charge $e_j$ and mass $m_j$. For completeness, we can write the full

[5] Abraham's current loop counter-proof to the LAD equation can be found in Ch. 2 §15 pp. 134-135 of his book [4].

equation of motion for $i$ by substituting the total field (2.33) into the reduced LL equation (2.32)

$$
\begin{aligned}
m_i \mathrm{a}_i^\mu = \Bigg\{ & e_i F^{\mu\nu}_{\mathrm{ext}} u_{i,\nu} + e_i \sum_{\substack{j=1 \\ j\neq i}}^{N} \left( F^{\mu\nu}_{\mathrm{ret}\,j} u_{i,\nu} \right) \\
& + \frac{2}{3}\frac{e_i^4}{m_i^2} \left[ F^{\mu\nu}_{\mathrm{ext}} F_{\mathrm{ext},\nu\alpha} u_i^\alpha + (F_{\mathrm{ext}} u_i)^2 u_i^\mu \right] \\
& + \frac{2}{3}\frac{e_i^4}{m_i^2} \sum_{\substack{j=1 \\ j\neq i}}^{N} \left( F^{\mu\nu}_{\mathrm{ext}} F_{\mathrm{ret}\,j,\nu\alpha} u_i^\alpha + F^{\mu\nu}_{\mathrm{ret}\,j} F_{\mathrm{ext},\nu\alpha} u_i^\alpha \right. \\
& \qquad \left. + F^{\nu\alpha}_{\mathrm{ext}} u_{i,\alpha} F_{\mathrm{ret}\,j,\nu\sigma} u_i^\sigma u_i^\mu + F^{\nu\alpha}_{\mathrm{ret}\,j} u_{i,\alpha} F_{\mathrm{ext},\nu\sigma} u_i^\sigma u_i^\mu \right) \\
& + \frac{2}{3}\frac{e_i^4}{m_i^2} \sum_{\substack{j,k=1 \\ j,k\neq i}}^{N} \left( F^{\mu\nu}_{\mathrm{ret}\,j} F_{\mathrm{ret}\,k,\nu\alpha} u_i^\alpha + F^{\nu\alpha}_{\mathrm{ret}\,j} u_{i,\alpha} F_{\mathrm{ret}\,k,\nu\sigma} u_i^\sigma u_i^\mu \right) \Bigg\}.
\end{aligned}
\tag{2.34}
$$

The terms have been grouped together in order of decreasing significance, assuming the external field dominates the motion. The first line is simply the Lorentz force including interparticle fields, while the second line refers to the self-force due to the external field only. The third and fourth lines contain cross terms within the self-force, in which we see the contraction of the external and interparticle fields. Finally, the fifth line is the self-force evaluated with contractions of the interparticle fields (this includes a double sum over both particle indices $j$ and $k$). The full, quadratic dependence on the fields is now apparent. In short, the central problem of this thesis involves evaluating the above equation of motion, which to our knowledge has not been solved previously for $N > 1$.

It is worth investigating why our replacement of the external with total field as shown in Eq. (2.33) is valid. The radiation reaction problem arose because of the divergence of the self-field on the world line. We argue the derivation for a system of many *point* particles should be virtually identical to that of a single particle, as the interparticle fields do not diverge providing the world lines of all particles *never* cross, so that the interparticle fields can be treated in the same way as the external field. Or in other words, recall that the divergence of the energy-momentum tensor is non-zero only on the world line of the particle; one can always construct an infinitesimally small tube in Minkowski space around the world line of each particle independently providing they do not cross. Finally, we note that both Dirac [5, Eq. (41)] and Rohrlich [6, Ch. 7.1, Eq. (7-12)] considered the generalisation of the LAD equation to many particles. Their approach is more lengthy, starting instead from first principles by considering an action for many particles. From our understanding of their derivations, we have applied a similar logic to the reduced LL

equation here.

Finally, we note that as the interparticle fields are not simultaneously defined[6] a closed form solution to Eq. (2.34) seems unlikely. Instead, we will solve for the trajectories numerically, as seen in the next chapter. In fact, a wide variety of particle-in-cell (PIC) codes [43, 45, 46] already solve variants of the LAD and LL equations of motion in the presence of an external field and *mean field* generated by the charge distribution. However, PIC codes utilise macroparticles, each of which represents many real particles occupying a region of phase space [47, 48]. From our perspective, it is not clear why the radiation reaction equations of motion can be applied to any charge distribution other than *point* particles, unless further assumptions are made, which need to be clarified. Perhaps this requires neglecting the impact of coherent emission as seen 'inside' the macroparticle. We opted instead to proceed from first principles, evaluating the LW fields by interpolating the historical trajectories, instead of solving Maxwell's equations on a discrete grid as with PIC codes [47, 48].

## 2.8 Limitations of classical radiation reaction

Before proceeding to the next chapter, note that our classical description will break down when quantum mechanical behaviour becomes important. For example, consider two oppositely charged particles for which a common rest frame exists; we expect quantum effects to emerge as their separation tends to the Bohr radius, such as the formation of bound states. It may well be that a sufficiently strong external electromagnetic field is present which would ionise any bound system, but one cannot safely say that quantum mechanical behaviour is irrelevant in such a scenario. In addition, the classical approach will of course break down if the rest frame field is sufficiently close to the critical field of QED [49–51]; the quantum regime can be defined as $\chi \gtrsim 1$, in terms of the quantum parameter

$$\chi = \frac{\sqrt{\left|(Fu)^2\right|}}{F_{\mathrm{cr}}}. \tag{2.35}$$

Here $\chi$ is written for a particle of velocity $u^\mu$ and field tensor $F^{\mu\nu}$. A modulus is required as the inner product of the field and velocity constitutes a space like four vector, because the field tensor is anti-symmetric. This parameter governs a variety of QED effects which have been neglected here, including recoil from emission of a photon, and electron-positron pair production. Strictly speaking, $\chi$ should be evaluated in terms of the total field. However, we will often assume the external

[6] The LW field from each particle is defined at the respective, retarded (proper) time as seen in Eq. (2.14).

field dominates the scenario under consideration when calculating $\chi$, which can be confirmed later with the simulation results.

# Chapter 3

# Numerical code

Previously, we described the application of the LL equation to many particle systems, where one should seek to evaluate the equation of motion with the total electromagnetic field. Starting from first principles, we constructed the total field from an external field and LW fields from every other particle in the system, each evaluated at their respective retarded time. As the fields are no longer simultaneously defined, a closed form solution for the trajectory seems unlikely. Instead, one can solve numerically.

This chapter describes the development of our numerical code, which calculates the trajectories of *point* particles in a self-consistent manner. Here we describe how the LW fields can be evaluated by interpolation at the respective retarded time(s), providing the historical trajectories are stored in the memory at discrete, evenly spaced intervals. When the total field is known, one can then numerically integrate the equation of motion. With the complete trajectories known, the physical system in question can be understood completely, and the spectrum of electromagnetic radiation emitted can be evaluated to ensure consistency.

## 3.1 Calculation of the fields

Consider a distribution of $N$ particles occupying a volume of phase space at time $t^n$. The position $\boldsymbol{x}$, velocity $\boldsymbol{u}$ and acceleration $\dot{\boldsymbol{u}} = d\boldsymbol{u}/dt$ of all particles $i \in [1, N]$ are determined simultaneously at discrete intervals $t^n = t^0 + n\Delta t$ in the past, as shown in Tab. 3.1, starting from an initial time $t^0$. Note that $t^0$ is not necessarily the beginning of the simulation, but rather the earliest time we can store in the random access memory (RAM), as determined by the time step $\Delta t$, number of particles and available memory of the system.

To advance the trajectory to time $t^{n+1} = t^n + \Delta t$, we need to numerically integrate an appropriate equation of motion with the total electromagnetic field, as seen by each particle. For point particles, this requires evaluating the LW fields at the retarded time (2.14). To that end, we define a function which relates the propagation of a light signal seen by an observer at position $\boldsymbol{x}$ and time $t$, from a particle $j$ at position $\boldsymbol{x}_j(t_j)$ and time $t_j$

| Historical trajectory of $i$th particle | | | |
|---|---|---|---|
| $t^0$ , | $t^1$ , | ... | $t^n$ |
| $\boldsymbol{x}_i^0$ , | $\boldsymbol{x}_i^1$ , | ... | $\boldsymbol{x}_i^n$ |
| $\boldsymbol{u}_i^0$ , | $\boldsymbol{u}_i^1$ , | ... | $\boldsymbol{u}_i^n$ |
| $\dot{\boldsymbol{u}}_i^0$ , | $\dot{\boldsymbol{u}}_i^1$ , | ... | $\dot{\boldsymbol{u}}_i^n$ |

Table 3.1: Schematic showing the $i$th particle's position, velocity and acceleration at discrete time steps. This data is stored in the RAM for all particles, from an initial time $t^0$ to the current time $t^n$.

$$\mathcal{T}_j(t_j) = t - t_j - R_j(t_j),, \tag{3.1a}$$

$$R_j(t_j) = |\boldsymbol{x} - \boldsymbol{x}_j(t_j)|. \tag{3.1b}$$

It should be clear that our intention is to evaluate this function on the world line of another, distinct particle, i.e. our observer becomes a particle $i$ at the current time $t = t^n$ with position $\boldsymbol{x} = \boldsymbol{x}_i^n$. For now, however, we will consider a general observer at $t = t^n$ to avoid overcomplicating the notation, otherwise we would need to attach another Latin index $i$ to every quantity.

Our goal is to find the root of this function $\mathcal{T}_j(t_{\text{ret}\,j}) = 0$, which is known as the retarded time. The cost of this operation scales quadratically $O(N^2)$ for many particles $N \gg 1$. To alleviate this, each interaction is computed in parallel on a GPU. The cost could be further reduced to $O(N \ln N)$ with the Barnes-Hut algorithm; this requires dividing the particles into cells in space, treating interactions with nearby particles individually, and approximating the position of distant particles with the cell centre [52]. While increasing performance, this requires discarding information, and as such we have not implemented this technique so far.

For a particle at the current time $t_j = t^n$, the function $\mathcal{T}_j(t^n) = -R_j(t^n) < 0$ is strictly negative. However, at the initial time there are two possible cases; either the retarded time is outside (i) or inside (ii) the historical trajectory retained in the memory, as shown in Tab. 3.1. For (i), that is $\mathcal{T}_j(t^0) < 0$, one must extrapolate the trajectory backwards in time. For example one could assume the motion is ballistic for $t < t^0$, the retarded time can then be determined from the quadratic equation (only one solution will respect causality). Yet, this is completely inaccurate if the initial acceleration is non-zero. Alternatively, as the external field is defined at all times (unlike the interparticle fields), one could numerically integrate the trajectory backwards in time using only the external field. This introduces a discontinuity in the fields at $t^0$, and effectively requires the assumption that interparticle fields are perturbatively small compared to the external field. We have rejected this procedure due to the high cost and circular logic; this would require integrating backwards in

time, to evaluate the fields at the retarded time, to integrate forward at the current time.

In practice, to address (i) we simply set the field from $j$ to zero. That is, if two particles are sufficiently far apart that we cannot accurately determine the retarded time, then we assume this field is small and can be neglected. Clearly this is not ideal, so we record each instance and check *a posteriori* that the percentage of interactions that cannot be resolved lies below a predefined threshold [0.5%, of $N(N-1)$ total interactions] throughout the simulation. The number of particles $N$ and time step $\Delta t$ should be restricted to meet this requirement, otherwise the results cannot be considered reliable.

For (ii), that is $\mathcal{T}_j(t^0) \geq 0$, the retarded time lies within the historical trajectory, in the memory. We search the array to find the step before $\mathcal{T}_j(t^k) > 0$ and after $\mathcal{T}_j(t^{k+1}) < 0$ the retarded time, which can be determined approximately by linear interpolation

$$\mathcal{M} = \frac{\Delta t}{\mathcal{T}_j(t^{k+1}) - \mathcal{T}_j(t^k)}, \tag{3.2a}$$

$$t_{\mathrm{ret}\,j} \approx t^k - \mathcal{M}\mathcal{T}_j(t^k). \tag{3.2b}$$

Where $\mathcal{M}$ is the gradient, and the approximation indicates that terms of second order and above have been neglected. This procedure is only possible as $\mathcal{T}_j(t_j)$ decreases monotonically due to the finite speed of light, such that the retarded time is uniquely determined. One can similarly perform a linear interpolation for the position $\boldsymbol{x}_j(t_j)$ between time $t^k$ and $t^{k+1}$, which can be evaluated at the retarded time $\boldsymbol{x}_{\mathrm{ret}\,j} = \boldsymbol{x}_j(t_{\mathrm{ret}\,j})$

$$\boldsymbol{m}_{\boldsymbol{x}} = \frac{\boldsymbol{x}_j^{k+1} - \boldsymbol{x}_j^k}{\Delta t}, \tag{3.3a}$$

$$\boldsymbol{c}_{\boldsymbol{x}} = \boldsymbol{x}_j^k - \boldsymbol{m}_{\boldsymbol{x}} t^k, \tag{3.3b}$$

$$\boldsymbol{x}_{\mathrm{ret}\,j} \approx \boldsymbol{m}_{\boldsymbol{x}} t_{\mathrm{ret}\,j} + \boldsymbol{c}_{\boldsymbol{x}}. \tag{3.3c}$$

Where $\boldsymbol{m}_{\boldsymbol{x}}$ and $\boldsymbol{c}_{\boldsymbol{x}}$ are the three vector gradient and intercept respectively.

This interpolation procedure can similarly be applied to determine the velocity $\boldsymbol{u}_{\mathrm{ret}\,j} = \boldsymbol{u}_j(t_j)$ and acceleration $\dot{\boldsymbol{u}}_{\mathrm{ret}\,j} = \dot{\boldsymbol{u}}_j(t_{\mathrm{ret}\,j})$ at the retarded time, from which we can evaluate the LW field from particle $j$

$$\boldsymbol{E}_{\mathrm{vel}\,j}(t,\boldsymbol{x}) = \left[\frac{e_j(\gamma_j\boldsymbol{n}_j - \boldsymbol{u}_j)}{(\gamma_j - \boldsymbol{n}_j\cdot\boldsymbol{u}_j)^3 R_j^2}\right]_{t_{\mathrm{ret}\,j}}, \tag{3.4a}$$

$$\boldsymbol{E}_{\mathrm{acc}\,j}(t,\boldsymbol{x}) = \left[\frac{e_j\boldsymbol{n}_j\times\left(\boldsymbol{n}_j\times[\gamma_j^2\dot{\boldsymbol{u}}_j - (\boldsymbol{u}_j\cdot\dot{\boldsymbol{u}}_j)\boldsymbol{u}_j] + \gamma_j\dot{\boldsymbol{u}}_j\times\boldsymbol{u}_j\right)}{(\gamma_j - \boldsymbol{n}_j\cdot\boldsymbol{u}_j)^3 R_j}\right]_{t_{\mathrm{ret}\,j}}, \tag{3.4b}$$

$$\boldsymbol{E}_{\mathrm{ret}\,j}(t,\boldsymbol{x}) = \boldsymbol{E}_{\mathrm{vel}\,j}(t,\boldsymbol{x}) + \boldsymbol{E}_{\mathrm{acc}\,j}(t,\boldsymbol{x}) \tag{3.4c}$$

Which we have separated into acceleration and velocity components as described in Eqs. (2.16) and (2.15). As before, $R_j(t_j) = |\boldsymbol{x} - \boldsymbol{x}_j(t_j)|$ is the separation of the source and observer in the direction defined by unit vector $\boldsymbol{n}_j(t_j) = [\boldsymbol{x} - \boldsymbol{x}_j(t_j)]/R_j(t_j)$. The transverse magnetic field can be constructed in a similar way

$$\boldsymbol{B}_{\mathrm{ret}\,j}(t,\boldsymbol{x}) = \boldsymbol{n}_j(t_{\mathrm{ret}\,j})\times\boldsymbol{E}_{\mathrm{ret}\,j}(t,\boldsymbol{x}). \tag{3.5}$$

In summary, providing the historical trajectories are known, we can evaluate the LW fields seen by a general observer from each particle. When evaluating the LW fields on the world line of other particles within the system, we refer to them as 'interparticle' fields. In addition, we can artificially 'switch off' the interaction between particles of different species; we refer to this case as 'intraspecies fields'.

We can then construct the total electric field $\boldsymbol{E}_i$ observed by particle $i$ at time $t_i$ and position $\boldsymbol{x}_i$, as the superposition of an external field $\boldsymbol{E}_{\mathrm{ext}}$ and LW fields from all other particles excluding itself

$$\boldsymbol{E}_i(t_i,\boldsymbol{x}_i) = \boldsymbol{E}_{\mathrm{ext}}(t_i,\boldsymbol{x}_i) + \sum_{\substack{j=1\\ i\neq j}}^{N}\boldsymbol{E}_{\mathrm{ret}\,j}(t_i,\boldsymbol{x}_i), \tag{3.6a}$$

$$\boldsymbol{B}_i(t_i,\boldsymbol{x}_i) = \boldsymbol{B}_{\mathrm{ext}}(t_i,\boldsymbol{x}_i) + \sum_{\substack{j=1\\ i\neq j}}^{N}\boldsymbol{B}_{\mathrm{ret}\,j}(t_i,\boldsymbol{x}_i). \tag{3.6b}$$

Where an identical superposition has been carried out for the magnetic field. We assume the external field is defined everywhere, unlike the interparticle fields which must be evaluated by interpolation. Specifically, we wish to determine the total field at the current time step $t^n$ of the simulation, that is $\boldsymbol{E}_i^n = \boldsymbol{E}_i(t^n,\boldsymbol{x}_i^n)$ and $\boldsymbol{B}_i^n = \boldsymbol{B}_i(t^n,\boldsymbol{x}_i^n)$, such that we can advance the trajectory.

## 3.2 Integrating the equation of motion

In the previous section, we explained how the total field observed by a particle can be constructed, providing the historical trajectories are known at discrete time steps. With the total field known, the equation of motion can be integrated numerically.

### 3.2.1 Lorentz integrator

First consider the Lorentz equation below, which describes the trajectory of particle $i$, and can be discretised according to a second order leapfrog scheme

$$m_i \frac{d\boldsymbol{u}_i}{dt} = e_i \left( \boldsymbol{E}_i + \frac{\boldsymbol{u}_i}{\gamma_i} \times \boldsymbol{B}_i \right), \tag{3.7a}$$

$$m_i \frac{\boldsymbol{u}_i^{n+1/2} - \boldsymbol{u}_i^{n-1/2}}{\Delta t} = e_i \left( \boldsymbol{E}_i^n + \frac{\boldsymbol{u}_i^n}{\gamma_i^n} \times \boldsymbol{B}_i^n \right) + O(\Delta t^2). \tag{3.7b}$$

Where the position and fields are defined at integer steps, and the velocity at half integer steps. The discretised Lorentz equation is commonly solved with the Boris algorithm [53][47, Ch. 15-4], which assumes the velocity at the midpoint $\boldsymbol{u}^n$ on the right hand side of Eq. (3.7b), can be approximated by the average

$$\boldsymbol{u}_i^n = \frac{\boldsymbol{u}_i^{n+1/2} + \boldsymbol{u}_i^{n-1/2}}{2}. \tag{3.8}$$

This step introduces a symmetry which can be exploited; first, the velocity is translated by the electric field

$$\boldsymbol{u}^+ = \boldsymbol{u}_i^{n+1/2} - \frac{e_i \Delta t}{2 m_i} \boldsymbol{E}_i^n, \tag{3.9a}$$

$$\boldsymbol{u}^- = \boldsymbol{u}_i^{n-1/2} + \frac{e_i \Delta t}{2 m_i} \boldsymbol{E}_i^n. \tag{3.9b}$$

Then, the discretised Lorentz equation reduces to a rotation around the magnetic field $\boldsymbol{b} = e_i \Delta t \boldsymbol{B}_i^n / 2 m_i \gamma_i^n$, written here in normalised units,

$$\boldsymbol{u}^+ - \boldsymbol{u}^- = (\boldsymbol{u}^+ + \boldsymbol{u}^-) \times \boldsymbol{b}. \tag{3.10}$$

By taking the scalar product with $(\boldsymbol{u}^+ + \boldsymbol{u}^-)$, one can show the Lorentz factor is invariant under the rotation $\gamma_i^n = \sqrt{1 + (\boldsymbol{u}^-)^2} = \sqrt{1 + (\boldsymbol{u}^+)^2}$ around the magnetic

field. Instead of evaluating the Lorentz factor at the midpoint $\boldsymbol{u}^n$, one *assumes* it can be evaluated from the known quantity $\boldsymbol{u}^-$. Note that this approximation can break down for ultra-relativistic particles, as the force due to the magnetic field is of the same magnitude as that of the electric field; as such we will consider only mildly relativistic particles. By taking the cross product with $\boldsymbol{b}$, one can solve algebraically for the unknown velocity $\boldsymbol{u}^+$

$$\boldsymbol{u}^+ = \boldsymbol{u}^- + 2\left(\boldsymbol{u}^- + \boldsymbol{u}^- \times \boldsymbol{b}\right) \times \frac{\boldsymbol{b}}{1+\boldsymbol{b}^2}. \tag{3.11}$$

Finally, the velocity at the next half integer time step $\boldsymbol{u}^{n+1/2}$ can be found by another translation with the electric field, seen by rearranging Eq. (3.9a)

$$\boldsymbol{u}_i^{n+1/2} = \boldsymbol{u}^+ + \frac{e_i \Delta t}{2m_i}\boldsymbol{E}_i^n + O(\Delta t^3), \tag{3.12}$$

from which the Lorentz factor is evaluated $\gamma^{n+1/2} = \sqrt{1+(\boldsymbol{u}^{n+1/2})^2}$. One can see we have re-inserted the error term, omitted in previous steps for brevity. While this method is locally accurate to third order, for a simulation of duration $T_{\text{sim}}$ which requires $T_{\text{sim}}/\Delta t$ steps, we expect the accumulated (or global) error to be second order $T_{\text{sim}}O(\Delta t^3)/\Delta t = T_{\text{sim}}O(\Delta t^2)$. Due to its simple implementation and low computational cost, the Boris approach is the de-factor standard in PIC codes [45, 46]. As it preserves the structure of the Lorentz equation, it leaves the on-shell condition intact. Further, the Boris algorithm conserves the volume of phase space occupied by our particles (independent of the time step chosen), which leads to excellent long term stability compared to explicit Runge-Kutta integrators [54].

### 3.2.2 Landau-Lifshitz integrator

We seek to apply a similar leapfrog scheme to the LL equation, which includes radiation reaction. Consider an equation of motion for particle $i$

$$m_i \frac{d\boldsymbol{u}_i}{dt} = \boldsymbol{f}_L + \boldsymbol{f}_R, \tag{3.13}$$

which includes the Lorentz force $\boldsymbol{f}_{L,i} = \boldsymbol{f}_{L,i}(\boldsymbol{E}_i, \boldsymbol{B}_i, \boldsymbol{u}_i)$ acting on $i$, written as a function of the total fields and velocity

$$\boldsymbol{f}_{L,i} = e_i\left(\boldsymbol{E}_i + \frac{\boldsymbol{u}_i}{\gamma_i} \times \boldsymbol{B}_i\right). \tag{3.14}$$

In addition, we incorporate another force $\boldsymbol{f}_{R,i} = \boldsymbol{f}_{R,i}(\boldsymbol{E}_i, \boldsymbol{B}_i, \boldsymbol{u}_i)$ which includes the radiation reaction effect

$$\begin{aligned} \boldsymbol{f}_{R,i} = \frac{2e_i^4}{3m_i^3}\Bigg\{ &\left(\boldsymbol{E}_i + \frac{\boldsymbol{u}_i}{\gamma_i} \times \boldsymbol{B}_i\right) \times \boldsymbol{B}_i + \left(\frac{\boldsymbol{u}_i}{\gamma_i} \cdot \boldsymbol{E}_i\right) \boldsymbol{E}_i \\ &- \gamma_i \left( \left[ \boldsymbol{E}_i + \frac{\boldsymbol{u}_i}{\gamma_i} \times \boldsymbol{B}_i \right]^2 - \left[ \frac{\boldsymbol{u}_i}{\gamma_i} \cdot \boldsymbol{E}_i \right]^2 \right) \boldsymbol{u}_i \Bigg\}. \end{aligned} \tag{3.15}$$

This is known as the reduced LL equation, so called as we have neglected terms involving derivatives of the fields, arguing that they are smaller than spin corrections and therefore negligible in a classical theory [42]. This assumption is widely applied in a number of PIC codes [43, 45]. As with the Lorentz equation, we discretise this equation with a second order leapfrog scheme

$$m_i \frac{\boldsymbol{u}_i^{n+1/2} - \boldsymbol{u}_i^{n-1/2}}{\Delta t} = \boldsymbol{f}_{L,i}^n + \boldsymbol{f}_{R,i}^n + O(\Delta t^3), \tag{3.16}$$

Here the respective forces $\boldsymbol{f}_{L,i}^n = \boldsymbol{f}_{L,i}(\boldsymbol{E}_i^n, \boldsymbol{B}_i^n, \boldsymbol{u}_i^n)$ and $\boldsymbol{f}_{R,i}^n = \boldsymbol{f}_{L,i}(\boldsymbol{E}_i^n, \boldsymbol{B}_i^n, \boldsymbol{u}_i^n)$ are evaluated at integer time steps. As before, the key problem involves the presence of the velocity $\boldsymbol{u}_i^n$ on the right hand side of our equation.

It is challenging to see how such an equation can be solved algebraically, as the force $\boldsymbol{f}_R$ breaks the symmetry of the equation; we can no longer solve by translating with the electric field and rotating around the magnetic field, as we did with only the Lorentz force. Instead, we follow the perturbative approach of Tamburini et al [41]. First, we advance the velocity according to the Lorentz equation alone using the Boris algorithm to find $\boldsymbol{u}_{L,i}^{n+1/2} \equiv \boldsymbol{u}_i^{n+1/2}$ from Eq. (3.12). Then we apply the Boris assumption to determine the velocity at the midpoint

$$\boldsymbol{u}_i^n \approx \frac{\boldsymbol{u}_{L,i}^{n+1/2} + \boldsymbol{u}_i^{n-1/2}}{2}. \tag{3.17}$$

As before, the Lorentz factor $\gamma_i^n = \sqrt{1 + (\boldsymbol{u}_i^n)^2}$ is determined via the on shell condition. After evaluating the respective forces $\boldsymbol{f}_{L,i}^n$ and $\boldsymbol{f}_{R,i}^n$ with the velocity at the midpoint, we can directly advance to the next time step

$$\boldsymbol{u}_i^{n+1/2} = \boldsymbol{u}_i^{n-1/2} + \frac{\Delta t}{m_i}\left(\boldsymbol{f}_{L,i}^n + \boldsymbol{f}_{R,i}^n\right) + O(\Delta t^3). \tag{3.18}$$

This approach is expected to be accurate providing the Lorentz force dominates the motion $\boldsymbol{f}_{L,i}^n \gg \boldsymbol{f}_{R,i}^n$, a requirement which is usually satisfied in the classical regime, providing we are not in the radiation dominated regime [55, 56]. Regardless of the equation of motion chosen, advancing the position of particle $i$ with a leapfrog scheme is trivial once the velocity is known

$$\frac{d\boldsymbol{x}}{dt} = \frac{\boldsymbol{u}}{\gamma}, \tag{3.19a}$$

$$\frac{\boldsymbol{x}^{n+1} - \boldsymbol{x}^n}{\Delta t} = \frac{\boldsymbol{u}^{n+1/2}}{\gamma^{n+1/2}} + O(\Delta t^3). \tag{3.19b}$$

Following the scheme laid out in this section, the complete trajectories of all *point* particles can be determined in a self-consistent manner. A careful reader will notice that when evaluating the interparticle fields we assumed the historical trajectory was determined at integer time steps $\{t^n, \boldsymbol{x}^n, \boldsymbol{u}^n, \dot{\boldsymbol{u}}^n\}$, as seen in Tab. 3.1, yet the integrator above defines the velocity at half integer steps. At the end of each step both the previous $\boldsymbol{u}^{n-1/2}$ and new $\boldsymbol{u}^{n+1/2}$ velocity are known, from which one can estimate the average $\boldsymbol{u}^n$ according to Eq. (3.8). This interpolation should be reasonably accurate providing the time step is small enough to properly resolve the trajectory. With the fields and velocity simultaneously known at each step, one can simply evaluate the equation of motion to recover the acceleration $\dot{\boldsymbol{u}}^n$, which is necessary to calculate the radiation part of the LW fields (2.16).

We note here the limitations of this approach. We are, of course, restricted to the classical regime $\chi \ll 1$ for the LL equation to be valid, and in principle one should evaluate the quantum parameter $\chi$ with the total field as opposed to the external field, for each particle. However, as the number of particles we can consider is severely limited by the available memory and computational cost, the external field is expected to dominate over interparticle fields in practice. A more pressing requirement arises from the $1/R^2$ dependence of the velocity field in (3.4a), which diverges as $R \to 0$. The world lines of two particles can *never* cross if the code is to be valid. Further, the distance between any two particles (in their common rest frame, assuming that one exists) should be large enough such that quantum mechanics can be safely ignored; in particular, for two oppositely charged species the distance between electrons and positrons (or ions) should be large enough such that we can ignore the creation of bound states.

### 3.2.3 Test LL integrator with a constant, uniform magnetic field

Our code now includes a numerical integrator for the reduced LL equation, which relies on the assumption that radiation reaction is perturbatively small compared to the Lorentz force. A test is now in order to probe the validity of this assumption. Consider then, an electron moving in a constant magnetic field. The exact analytical solutions for the velocity, and the leading order solution for the position are shown in Eqs. (5.10) and (5.14), in a later chapter. However, our code utilises a common coordinate time, as opposed to the proper time which is distinct for each particle. To provide a fair comparison, we demonstrate here the relationship be-

tween the proper and coordinate time such that the analytical equations can easily be evaluated.

An electron with Lorentz factor $\gamma_0$ in the presence of a constant magnetic field will lose energy on the scale of the damping frequency $\omega_d = \omega_B^2 \tau_e$ [see Eq. (5.3)]

$$\frac{d\gamma}{dt} = -\omega_d \left( \frac{\gamma^2}{\gamma_{0,\parallel}^2} - 1 \right). \tag{3.20}$$

Where $\omega_B = eB/m$ is the frequency associated with the magnetic field, while the conserved Lorentz factor of the longitudinal velocity is $\gamma_{0,\parallel} = 1/\sqrt{1 - v_{0,\parallel}^2}$. This differential equation can be solved by separation

$$\gamma(t) = \gamma_{0,\parallel} \coth\left( \frac{\omega_d}{\gamma_{0,\parallel}} t + C \right), \tag{3.21a}$$

$$C = \frac{1}{2} \ln\left( \frac{\gamma_0 + \gamma_{0,\parallel}}{\gamma_0 - \gamma_{0,\parallel}} \right). \tag{3.21b}$$

Which satisfies the initial condition $\gamma(t = 0) = \gamma_0$ and exhibits the expected asymptotic behaviour $\gamma(t) \to \gamma_{0,\parallel}$ in the limit $t \to +\infty$. This happens to be a generalisation of a result previously obtained by M. Tamburini for non-zero longitudinal velocity [42]. Recalling the definition of the velocity $u^\mu = dx^\mu/d\tau$, particularly the time-like component $\gamma = dt/d\tau$, we can solve the following standard integral to find the proper time as a function of the coordinate time

$$\int_0^\tau d\tau' = \frac{1}{\gamma_{0,\parallel}} \int_0^t \tanh\left( \frac{\omega_d}{\gamma_{0,\parallel}} t' + C \right) dt', \tag{3.22a}$$

$$\tau(t) = \frac{1}{\omega_d} \ln\left[ \cosh\left( \frac{\omega_d}{\gamma_{0,\parallel}} t \right) + \frac{\gamma_{0,\parallel}}{\gamma_0} \sinh\left( \frac{\omega_d}{\gamma_{0,\parallel}} t \right) \right]. \tag{3.22b}$$

Where we have made use of the identity $\tanh(C) = \gamma_{0,\parallel}/\gamma_0$. One can now move freely from coordinate to proper time, which allows for a direct comparison between our numerical and analytical solutions, which are derived in a later chapter [see Eqs. (5.10) and (5.14)].

Consider then, a relativistic electron with $\gamma_0 = 10$ moving in the $xy$-plane transverse to a constant magnetic field $\boldsymbol{B} = B\hat{\boldsymbol{z}}$. The initial velocity lies entirely along the $y$-axis $\boldsymbol{u}_{0,\perp} = u_{0,y}$ with no longitudinal component $\gamma_{0,\parallel} = 1$. If we ignore radiative emission, one would expect a circular orbit with radius $R_0 = |\boldsymbol{u}_{0,\perp}/\omega_B|$

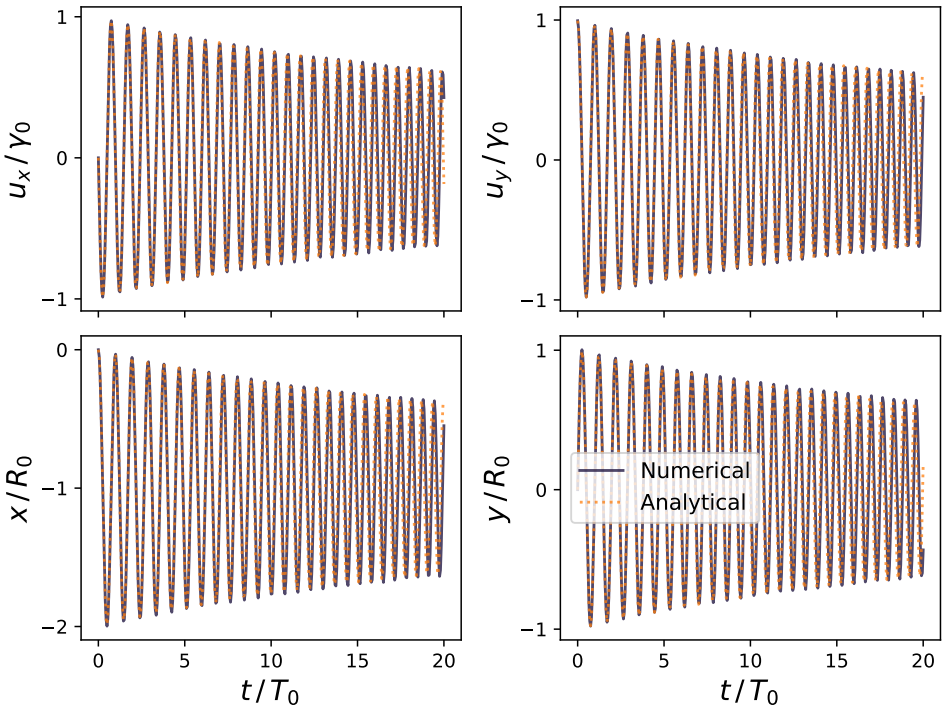


Figure 3.1: Test of the numerical integrator for the reduced LL equation against analytical solutions in a constant and uniform magnetic field. Analytical solutions are exact for the velocity (5.10) and approximate for the position (5.14).

and period $T_0 = 2\pi\gamma_0/|\omega_B|$. We wish to 'break' our perturbative numerical approach by considering a strong field. To that end, we choose a quantum parameter $\chi = |\boldsymbol{u}_{0,\perp}|B/B_{\mathrm{cr}} = 0.1$, or equivalently a magnetic field $B = 4.4 \times 10^8$ T, at which the classical theory should provide the leading order behaviour and QED effects can be accounted for perturbatively. This is approaching the regime at which the LL equation can no longer be considered valid, and should therefore provide a sufficiently strenuous test. Finally, we run our code for 20 oscillations with a relatively large time step $\Delta t = T_0/20$.

The comparison of numerical and analytical solutions can be seen in Fig. 3.1. One can observe the impact of radiation reaction from the decaying amplitude of the oscillations. While the agreement is excellent initially in all cases, the accumulated error becomes significant as we approach $t = 20\,T_0$ for step size $\Delta t = T_0/20$. Around this time and beyond, our approach can no longer be considered accurate (for the time step chosen here).

## 3.3 Integrating the spectrum of emitted radiation

Providing the trajectories are known, one can evaluate the spectrum of energy radiated via the LW fields. Consider then, an observer far away from the volume of space occupied by the complete trajectories of our particles. In this case, the unit vector which defines our observer $\boldsymbol{n}$ becomes approximately constant, both in time and for each particle. We write the spectrum of energy radiated at frequency $\omega$ per unit solid angle, as a Fourier transform of the acceleration field [23, Ch. 14.5]

$$\frac{d\varepsilon}{d\omega d\Omega} = \frac{1}{4\pi^2}\left|\int_{-\infty}^{+\infty} e^{i\omega t}\sum_{i=1}^{N} e_i \boldsymbol{A}(\boldsymbol{x}_i, \boldsymbol{u}_i, \dot{\boldsymbol{u}}_i)\, dt\right|^2, \tag{3.23a}$$

$$\boldsymbol{A}(\boldsymbol{x}, \boldsymbol{u}, \dot{\boldsymbol{u}}) = \frac{\boldsymbol{n}\times\left(\boldsymbol{n}\times[\gamma^2\dot{\boldsymbol{u}} - (\boldsymbol{u}\cdot\dot{\boldsymbol{u}})\boldsymbol{u}] + \gamma\dot{\boldsymbol{u}}\times\boldsymbol{u}\right)}{\gamma(\gamma - \boldsymbol{n}\cdot\boldsymbol{u})^2} e^{-i\omega\boldsymbol{n}\cdot\boldsymbol{x}}. \tag{3.23b}$$

Where the position $\boldsymbol{x} = \boldsymbol{x}(t)$, velocity $\boldsymbol{u} = \boldsymbol{u}(t)$ and acceleration $\dot{\boldsymbol{u}} = \dot{\boldsymbol{u}}(t)$ of a generic particle, are defined as a function of the coordinate time $t$ common to all $N$ particles. To evaluate the Fourier transform, first define the light cone coordinate $x_{i,-}(t) = t - \boldsymbol{n}\cdot\boldsymbol{x}_i(t)$ which appears in the exponent. The trajectories are determined at uniform intervals in time $t^n$ but non-uniform intervals in the coordinate $x^n_{-,i} \equiv x_{-,i}(t^n) = t^n - \boldsymbol{n}\cdot\boldsymbol{x}^n_i$. Yet uniformity is a condition for applying the Cooley-Tukey algorithm for fast Fourier transforms (FFT) [57], the standard method for numerically solving integrals of this type. Typically one would interpolate the (non-oscillatory part of the) integrand $\boldsymbol{A}/e^{-i\omega\boldsymbol{n}\cdot\boldsymbol{x}}$ onto a uniform grid in $\boldsymbol{x}_{-,i}$ (in each dimension), before applying the FFT.

Our approach is slightly different. We utilise the NFFT3 library to represent the integrand with a series of 'window' functions, which are chosen to be Gaussian in shape [58]. Once this approximation of the integrand is known, it can be evaluated on a uniform grid. Note that the frequency $\omega$ is constant for all particles, such that the argument of the oscillatory function can be restricted to a single period $\omega x_{-,i} \in [0, 2\pi]$ without loss of information; one can then evaluate the integrand of each particle on a uniform grid which is common to all particles. Then, we can superpose the integrand from each particle, before applying the FFT algorithm once. This greatly reduces the cost compared to carrying out a separate FFT for each particle. Following this, one can integrate the spectrum over a solid angle interval on the unit sphere, as desired.

By expanding the square modulus in Eq. (3.23a) we will obtain a double sum, and by considering only the diagonal terms which pertain to the same particle one can define the incoherent energy radiated

$$\left.\frac{d\varepsilon}{d\omega d\Omega}\right|_{\text{incoh}} = \frac{1}{4\pi^2}\sum_{i=1}^{N}\left|\int_{-\infty}^{+\infty} e_i \boldsymbol{A}(\boldsymbol{x}_i, \boldsymbol{u}_i, \dot{\boldsymbol{u}}_i)\, e^{i\omega t}\, dt\right|^2. \tag{3.24}$$

Where the diagonal, interference terms between different particles are neglected. If the particles' trajectories differ only by a constant phase in the observation direction $\omega \boldsymbol{n} \cdot (\boldsymbol{x}_i - \boldsymbol{x}_j) = 2\pi l$, where $l$ is an integer, the energy radiated will be coherent at a given frequency (that is, proportional to $N^2$). In practice, the limits of integration are truncated to a finite interval. This poses no physical problem providing the acceleration is zero everywhere except during this interval.

# Chapter 4

# Electron-positron bunch and laser collision

*"When God said 'Let there be light', he surely must have meant 'perfectly coherent light' "*

— Charles H. Townes

At the time of writing, tightly focused optical lasers are among the most intense sources of electromagnetic radiation available in the laboratory, and are therefore essential if we wish to observe strong field behaviour such as radiation reaction. Petawatt lasers of this kind have been instrumental in generating relativistic plasmas in the laboratory [59–64], and testing the validity of the LL equation in collisions of ultra relativistic particles with a counter propagating laser pulse [12, 13]. In previous chapters, we have discussed the generalisation of the reduced LL equation to many point particles in Eq. (2.34), and we developed a numerical method to solve this equation in Ch. 3. Our goal is to find regimes in which the usual approximation of solving the LL equation analytically with only an external field, or in other words, treating each particle independently of one another, no longer applies. To that end, we seek to observe strong collective behaviour and radiation reaction in the presence of a laser field.

In this chapter, we describe the trajectory and spectrum of electromagnetic radiation emitted from a single charged particle colliding with a counter-propagating laser pulse, which we model as a plane wave pulse. From the single particle spectrum, we identify the conditions required for a bunch of particles, specifically electrons and positrons ($e^-/e^+$), to emit coherently. We expect strong collective behaviour to be induced under these conditions. The collision of an $e^-/e^+$ bunch with a counter-propagating laser pulse is then simulated with the code described in Ch. 3. A brief study of the experimental feasibility of this scenario is considered. We proceed to discuss the instabilities which develop during this interaction, such as micro-bunching, and the coherent emission of radiation which occurs as a result.

## 4.1 Single particle & laser collision

Consider then, one electron of velocity $u_0^\mu$ colliding with a laser pulse, which we model as a plane wave pulse of potential $A^\mu(\varphi) = (0, \boldsymbol{A}(\varphi))$. This potential is

chosen to satisfy the Lorenz gauge

$$(\partial A(\varphi)) = \omega_0 \left(n_0 A'(\varphi)\right) = 0, \tag{4.1}$$

where a prime denotes differentiation with respect to the wave phase, which is defined as

$$\varphi \equiv \omega_0(n_0 x) = \omega_0(t - \boldsymbol{n}_0 \cdot \boldsymbol{x}). \tag{4.2}$$

Here $\omega_0$ is the central frequency, and the laser propagates in a direction defined by the vector $n_0^\mu = (1, \boldsymbol{n}_0)$ which satisfies the null condition $n_0^2 = 0$. We will find it convenient to introduce the Lorentz invariant, normalised amplitude of the laser [49]

$$a_0 \equiv \frac{|e|}{m}\sqrt{\left|A_0^2\right|} = \frac{|e|E_0}{m\omega_0}. \tag{4.3}$$

Where $A_0^\mu \equiv A^\mu(\varphi = 0)$ is the peak value of the potential and $E_0$ is the peak electric field. A modulus is required under the square root, as the potential is a space like four vector $A^2(\varphi) = -\boldsymbol{A}^2(\varphi) < 0$. With this definition, we refer to $a_0 \gtrsim 1$ as a relativistically strong field, so called as it will accelerate one electron to a relativistic velocity within a single cycle. Naturally, we refer to $a_0 \ll 1$ as a relativistically weak laser pulse. To describe the electron with a classical trajectory, we require the fields are sufficiently weak in the rest frame compared to the critical field of QED. To that end, for an electron and laser pulse collision, one typically estimates the maximum value of the quantum parameter with the initial velocity and peak field tensor $F_0^{\mu\nu} \equiv F^{\mu\nu}(\varphi = 0)$,

$$\chi_0 = \frac{\sqrt{\left|(F_0 u_0)^2\right|}}{F_{\text{cr}}}. \tag{4.4}$$

The velocity and field are not necessarily at their respective maxima simultaneously, but it is better to air on the side of caution when defining the classical regime $\chi_0 \ll 1$, which is needed to apply the LL model. In addition, it will be helpful to define a classical parameter for the radiation dominated regime[1] in a plane wave [49, Eq. (26)]

$$R_{\text{C}} = \frac{\chi_0 a_0 r_e}{\lambda_e}, \tag{4.5}$$

[1]The radiation dominated regime was initially considered by Koga et al [55], though we follow the discussion by Di Piazza [33] more closely. In addition, Bulanov et al [56] discuss this regime specifically in the context of plasmas.

written in terms of the classical electron radius $r_e$ and reduced Compton wavelength $\lambda\!\!\!^{-}_e$. Here $R_C$ is essentially the coefficient of the LL self-force in a plane wave. The regime $R_C \gtrsim 1$ indicates that the self-force is comparable to or in excess of the Lorentz force in the rest frame, and is therefore said to dominate the dynamics. It is challenging to see how one can enter this regime while remaining in the domain of classical electrodynamics $\chi_0 \ll 1$. In practice, we will work in the regime $R_C \ll 1$.

To describe the electron trajectory in a plane wave, we suggest to start from the LL equation in Eq. (2.31), which we write again here for convenience

$$m\frac{du^\mu}{d\tau} = eF^{\mu\nu}u_\nu + \frac{2}{3}e^2\Big[\frac{e}{m}(\partial_\alpha F^{\mu\nu})u^\alpha u_\nu + \frac{e^2}{m^2}F^{\mu\nu}F_{\nu\alpha}u^\alpha + \frac{e^2}{m^2}(Fu)^2u^\mu\Big]. \tag{2.31}$$

For brevity, we will omit the dependence of all functions on the wave phase, e.g. for the external field $F^{\mu\nu} = F^{\mu\nu}(\varphi)$, which can be defined from the potential

$$F^{\mu\nu} = \partial^\mu A^\nu - \partial^\nu A^\mu = \omega_0\left[n_0^\mu A'^\nu - n_0^\nu A'^\mu\right]. \tag{4.6}$$

Here a prime denotes a derivative with respect to the wave phase. We will find it convenient to introduce the light cone notation $u_- = (n_0 u) = \gamma - \boldsymbol{n}_0 \cdot \boldsymbol{u}_0$ with respect to the direction along which the plane wave propagates. Contracting the LL equation above with $n_{0,\mu}$, one can identify a differential equation for the light cone coordinate in terms of the wave phase

$$\frac{du_-}{d\tau} = \omega_0 u_- \frac{du_-}{d\varphi}, \tag{4.7}$$

Where the initial value is given by $u_{0,-} = (n_0 u_0)$. However, it is well known that this quantity is conserved[2] when solving the Lorentz equation with a plane wave. In the language of quantum mechanics, this direction is somewhat special as it represents a head-on collision of a particle with photons of the laser pulse, and is therefore indicative when measuring the recoil of the particle from this collision. In the self-force of the LL equation, the following terms can be rewritten with the field tensor shown above (4.6)

[2]To show that the light cone coordinate $u_-$ is conserved, see e.g. Landau & Lifshitz Vol. 2 [8, § 47]. This is also stated more concisely in a review by Di Piazza et al [49, Eqs. (1-3)] with the light cone notation used here.

$$(\partial_\alpha F^{\mu\nu}) u^\alpha u_\nu = \omega_0^2 \left[ (uA')\, n_0^\mu - u_- A'^\mu \right] u_-, \tag{4.8a}$$

$$F^{\mu\nu} F_{\nu\alpha} u^\alpha = -\omega_0^2 u_- (A')^2 n_0^\mu, \tag{4.8b}$$

$$(Fu)^2 u^\mu = \omega_0^2 u_-^2 (A')^2 u^\mu, \tag{4.8c}$$

Upon contraction of the LL equation with $n_{0,\mu}$, the first and second terms of the self-force vanish, in addition to the Lorentz force, by virtue of the transverse property $(n_0 A) = 0$ and null condition $n_0^2 = 0$. Only the friction-like term $(Fu)^2 < 0$, often referred to as the 'radiation reaction', does not vanish. The evolution of the light cone coordinate is then governed by

$$\frac{du_-}{d\varphi} = \omega_0 \tau_e \, u_-^2 \, \frac{e^2}{m^2} \, (A')^2 \, . \tag{4.9}$$

Where we have reintroduced the time scale associated with the classical electron radius $\tau_e = 2r_e/3 = 2e^2/3m$. This can be integrated directly to obtain

$$\int \frac{du_-}{u_-^2} = \omega_0 \tau_e \, \frac{e^2}{m^2} \int (A')^2 \, d\varphi, \tag{4.10a}$$

$$u_-(\varphi) = \frac{u_{0,-}}{1 + \omega_0 \tau_e u_{0,-} \frac{e^2}{m^2} \int_{-\infty}^{\varphi} \left[ \boldsymbol{A}'(\phi) \right]^2 \, d\phi}. \tag{4.10b}$$

Where we have explicitly stated the dependence on the wave phase of all functions, and note the initial condition defined by the limit $u_-(\varphi) \to u_{0,-}$ as $\varphi \to -\infty$. The vector potential is required to vanish asymptotically under the limits $\varphi \to \pm\infty$, for this result to be physically sensible. If one considers an electron and plane wave which are exactly counter-propagating, and the particle is continuously ultra-relativistic throughout the interaction, this equation effectively governs the evolution of the Lorentz factor $u_-(\varphi) \approx 2\gamma(\varphi)$. Finally, we note the approach of Di Piazza [33], who has solved the LL equation *exactly* via iteration, including solutions for the transverse velocity which we have omitted discussion of here. These solutions are in agreement with those derived later, and independently, by Hadad et al [37].

From Eq. (4.10b), one can identify the central impact of radiation reaction in this scenario is to act as a friction-like force, decreasing the Lorentz factor and in particular the longitudinal velocity over time. For ultra-relativistic particles $\gamma \gg 1$ in the presence of extremely strong fields beyond those considered here $a_0 \gg 1$, one can also show radiation reaction will have a non-negligible impact on the transverse velocity [37].

## 4.2 Radiation spectrum from one particle

With the trajectory known, this can be inserted into the Fourier transform of the LW fields to evaluate the spectrum of energy radiated [see Eq. (3.23a)]. To solve these integrals analytically in a plane wave, for one particle let alone many, turns out to be a formidable task when radiation reaction is included. As such, we will develop an analytical understanding of the spectrum obtained with the Lorentz trajectory, and we will rely on numerical solutions for the LL trajectory. For the former to be applicable, we are effectively assuming the impact of radiation reaction on the spectrum is perturbatively small. To evaluate the spectrum, we should first define the vector potential of our laser; consider then, one electron colliding with a laser pulse, modelled as a plane wave pulse of vector potential

$$\frac{|e|}{m}\boldsymbol{A}_L(\varphi) = a_L(\varphi)\,[\delta\cos(\varphi)\hat{\boldsymbol{x}} + \sqrt{1-\delta^2}\sin(\varphi)\hat{\boldsymbol{y}}]. \tag{4.11}$$

Where $\varphi = \omega_0(t+z)$ is the wave phase for a laser propagating along the -$z$ direction with transverse polarisation in the $xy$ plane, central frequency $\omega_0$ and pulse shape $a_L(\varphi)$. Note that the polarisation can vary freely between $\delta = 1$ linear (LP) and $\delta = 1/\sqrt{2}$ circular (CP). For a long pulse, the envelope is approximately constant over one cycle, and we recognise the cycle averaged value is polarisation independent

$$\frac{e^2}{m^2}\boldsymbol{A}_L^2(\varphi) = \frac{1}{2}a_L^2(\varphi)\left[(2\delta^2-1)\cos(2\varphi)+1\right], \tag{4.12a}$$

$$\langle e^2\boldsymbol{A}_L^2(\varphi)/m^2\rangle = \frac{1}{2\pi}\int_{\varphi-\pi}^{\varphi+\pi}\boldsymbol{A}_L^2(\varphi')\,d\varphi' \approx \frac{1}{2}a_L^2(\varphi). \tag{4.12b}$$

Where the oscillatory term provides no contribution when averaged. One can see that by choosing the amplitude of the envelope $a_{L,0} = a_L(\varphi = 0)$, we fix the cycle averaged 'intensity', defined above. However, this implies the laser amplitude $a_0 = |e|E_0/m\omega_0$ will now vary from $a_0 = a_{L,0}$ for LP to $a_0 = a_{L,0}/\sqrt{2}$ for CP. The electric $E_0$ and magnetic $B_0$ field amplitudes, or equivalently the field tensor amplitude $F_0^{\mu\nu}$, will be polarisation dependent in the same way, as will the quantum parameter $\chi_0$.

The spectrum of energy radiated in a monochromatic plane wave ($a_L(\varphi) = a_{L,0}$) was derived by Sarachik & Schappert [65]. Yet, the expressions contained within are cumbersome, and we need not consider a general observation point. As we are considering a counter-propagating particle and plane wave pulse, the velocity will on average lie along $+z$, such that the reflected radiation is of particular interest. This scenario is studied by Kharin et al [66] for a plane wave pulse of generic shape; they utilise the trajectory determined by the Lorentz equation to solve the spectrum via the *stationary phase* method. Strictly speaking, this method only applies in the

asymptotic limit $a_0 \to +\infty$, yet in practice their solutions are accurate[3] providing $a_0^2 \gg 1$. With the vector potential introduced above (4.11), the stationary point(s) $\pm\varphi_*$ determined by Kharin et al [66] are equally distributed about the peak $\varphi = 0$ for a symmetric pulse

$$\omega = \frac{\mathcal{D}\omega_0}{1 + \frac{1}{2}a_L^2(\varphi_*)}. \tag{4.13a}$$

$$\mathcal{D} = \frac{1 + v_{0,\parallel}}{1 - v_{0,\parallel}} \approx 4\gamma_0^2. \tag{4.13b}$$

Where $v_{0,\parallel} = |\boldsymbol{v}_{0,\parallel}|$ is the longitudinal speed and $\mathcal{D}$ is the Doppler reflection. With our vector potential, this result is polarisation independent, and the approximation becomes accurate when the particle is initially relativistic. One can interpret this to mean high frequency radiation tends to be emitted as $\varphi_* \to \pm\infty$, while low frequency radiation is emitted near the pulse peak[4]. Perhaps more intuitively, the longitudinal velocity decreases near the pulse peak due to the magnetic field (for $a_0 \gtrsim 1$), which causes the particle to radiate at lower frequencies. In the monochromatic approximation, one can then write the lowest frequency emitted

$$\omega_s \approx \frac{\mathcal{D}\omega_0}{1 + \frac{1}{2}a_{L,0}^2}. \tag{4.14}$$

Or alternatively, we can write the longest emitted wavelength $\lambda_s = 2\pi/\omega_s$ from the system. The spectrum of energy radiated is usually time integrated, and because emission at a given frequency occurs at two stationary phase points, this will give rise to an interference pattern, even for one particle [66, 68]. Ultimately, we are considering the single particle scenario only to justify our simulation parameters in the next section; with many bodies this interference pattern will be completely altered, and as such is of little interest to us [compare Fig. 4.2(a-d) with Fig. 4.1]. We are, however, interested in the broad characteristics of the spectrum. For CP, one particle will emit a broad spectrum of frequencies on-axis starting from $\omega_s$ up to $\mathcal{D}\omega_0$ in a series of regular harmonics, as shown in Fig. 4.1(a). This is similar in shape to previous results in the literature, for example Fig. (3a) in Ref. [66] or Fig. (7b) in Ref. [68], keeping in mind that we utilise a log scale.

[3] The condition $a_0^2 \gg 1$ was determined by comparing respective terms in the phase of the radiation integral [66, Eq. (5)]. Note that this is independent of the initial velocity. At the other extreme, for $a_0 \ll 1$ the radiation integral simply becomes a Fourier transform of the vector potential.

[4] At the pulse peak / at low frequencies, the stationary points become degenerate and diverge, while the second derivative of the phase of the integral vanishes. In this case, one must expand the phase to third order, to obtain an approximation using Airy functions [67].

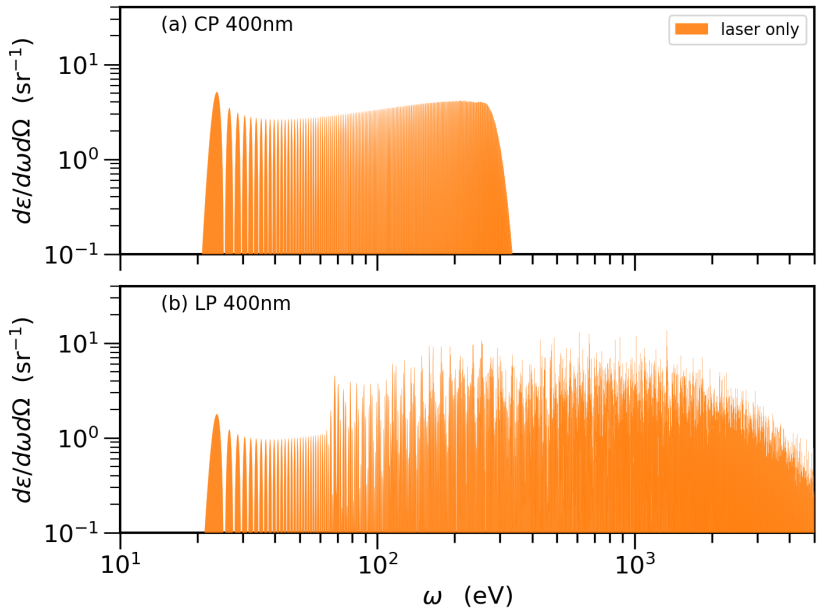


Figure 4.1: Spectrum of radiation reflected on-axis, by a single electron of $\gamma_0 = 5$ colliding with a counter-propagating $\lambda_0 = 400\,\text{nm}$ laser pulse of amplitude $a_{L,0} = 5$, for circular (a) and linear (b) polarisation. Trajectory was obtained by numerically integrating the reduced LL equation of motion, though radiation reaction has virtually no impact for these parameters. Both spectra begin at frequency $\omega_s \approx 23\,\text{eV}$. At $\mathcal{D}\omega_0 \approx 304\,\text{eV}$ the spectrum for CP rapidly converges to zero, while for LP the spectrum peaks here, and converges to zero gradually above $\mathcal{D}a_{L,0}\omega_0 \approx 1500\,\text{eV}$.

For LP, the spectrum does not admit a closed form solution, but can be written in an infinitely long series of Bessel functions $J_n(x)$, of the first kind [65, 66]. As seen in Fig. 4.1(b), for LP the spectrum consists of many overlapping harmonics starting from $\omega_s$, the spectrum peaks around $\mathcal{D}\omega_0$, and will gradually converge to zero above $\sim \mathcal{D}a_{L,0}\omega_0$. The last property results from the asymptotic behaviour of Bessel functions $J_n(x) \sim x^n$. To verify our results against the literature, one can compare Fig. 4.1(b) with Fig. (7c) of Ref. [68].

The characterisation of the reflected radiation given above, does not account for the impact of radiation reaction. When solving the radiation integral with a trajectory obtained from the LL equation [69, 70], one can see the tendency of radiation reaction is to redshift the emitted spectrum [71], and suppress emission at high frequencies by significantly altering the interference pattern [68]. So far, we have considered only a single particle; in the next section, we will use these results to suggest conditions for coherent emission from a small bunch of particles.

## 4.3 Electron-positron bunch & laser properties

Consider then, a relativistic *bunch* of charged particles colliding with a counter propagating laser pulse of amplitude $a_0$, modelled as a plane wave. Our interpretation is that, to see strong collective behaviour we require the emitted radiation to be coherent, and to observe a significant impact from radiation reaction, the particles should be relativistic. We will now see these are competing demands. For a relativistically weak laser pulse $a_{L,0}^2 \ll 1$, the spectrum of radiation reflected on-axis by one particle is simply the Fourier transform of the pulse shape $a_L(\varphi)$, centred on the Doppler shifted frequency $\mathcal{D}\omega_0$. The usual requirement for coherence is that our bunch should then be smaller than the characteristic wavelength emitted $\text{FWHM}_e \ll 2\pi/\mathcal{D}\omega_0$, where FWHM stands for full width at half maximum. Yet, for relativistic particles, which are needed to observe any significant impact from radiation reaction, this quickly leads to an extraordinarily high density. It is challenging then, to see how one could observe both radiation reaction and strong collective behaviour within, say, an electron bunch as suggested previously [19, 20], as this would be highly unstable due to Coulomb repulsion.

Following this logic, we suggest a relativistic and neutral $e^-/e^+$ bunch. At first, positrons are simply introduced to reduce Coulomb repulsion, later we will see their role is instrumental for inducing instabilities within our system[5]. If we instead consider a relativistically strong laser pulse, as described in the previous section, one particle will emit a broad spectrum of frequencies on-axis starting from frequency $\omega_s = \mathcal{D}\omega_0/(1 + a_{L,0}^2/2)$, which corresponds to the longest emitted wavelength $\lambda_s = 2\pi/\omega_s$, which is optimal if we wish to observe coherence. We suggest the laser amplitude should be chosen to concentrate emission at low frequencies $a_{L,0} \sim \gamma_0$, while avoiding back-scattering of the bunch, which occurs for $a_0^2 \gtrapprox \mathcal{D}$ according to the Lorentz equations of motion in a plane wave [49, Eqs. (1-3)], as this would likely be experimentally problematic.

To justify the size of the bunch needed for coherent emission, first consider two co-propagating particles moving with the same velocity, separated by distance $d$ in the direction along which the emitted radiation is observed. From the radiation integral (3.23b), one would expect a destructive fringe at frequency $\pi/d$. This suggests a condition on the size of our bunch $\text{FWHM}_e \lesssim \lambda_s/2$, for many particles to emit coherently, depending on the longest emitted wavelength from the system $\lambda_s$. Any coherence condition on the position should hold during some time interval, which implies only a small initial energy spread can be tolerated. To that end, we have included Appendix A which describes the ballistic expansion of a Gaussian bunch, given an initial position and velocity spread. The key result is Eq. (A.8), which describes the evolution of the standard deviation (in 3D) over time. One can

[5] See simulation results in Fig. 4.2; notice that 'laser & intraspecies' fields produces no micro-bunching, or subsequent coherent amplification of the emitted spectrum, in contrast both of these effects are often present for 'laser & interparticle' fields.

| $e^-/e^+$ bunch | | |
|---|---|---|
| $\mathrm{FWHM}_e$ | 16 | nm |
| $N_{e-}$ | 4000 | |
| $N_{e+}$ | 4000 | |
| $n_0$ | 1.62 | $\times 10^{21}$ particles/cm$^3$ |
| $\gamma_0$ | 5 | |
| $\mathrm{KE}_0$ | 2.044 | MeV |
| $\sigma_{\mathrm{KE}}$ | 0.002 | MeV |
| $\sigma_\vartheta$ | 1 | mrad |

Table 4.1: Initial properties of the neutral electron-positron bunch in the lab frame, as considered in our simulations. By row, one can see the full width at half maximum $\mathrm{FWHM}_e$ (in each dimension) of the Gaussian bunch, number of electrons $N_{e-}$, number of positrons $N_{e+}$, peak density of particles within the bunch $n_0$ including both $e^-$ and $e^+$, average Lorentz factor $\gamma_0$, average kinetic energy of one particle $\mathrm{KE}_0$, the RMS spread in kinetic energy $\sigma_{\mathrm{KE}}$ and RMS angular spread around the z-axis.

insert the kinetic energy spread from Tab. 4.1 into Eq. (A.8) given the length of the laser pulse, to verify the bunch expansion is negligible.

In our simulations, we utilise a laser, modelled as a plane wave pulse of shape $a_L(\varphi) = a_{L,0}\cos^2(\varphi/L)$ and domain $\varphi \in [-\pi L/2, \pi L/2]$, propagating along $-z$ with amplitude $a_{L,0} = 5$. In fact, we actually consider two lasers which differ only by wavelength and intensity. Both lasers have amplitude $a_{L,0} = 5$ and pulse length $\mathrm{FWHM}_L \approx 26.7\,\mathrm{fs}$ (of intensity) as shown in Tab. 4.2. The central wavelengths of the lasers are $\lambda_0 = 400\,\mathrm{nm}$ and $\lambda_0 = 100\,\mathrm{nm}$ respectively; these special wavelengths are chosen because we have fixed $a_0$ to concentrate the spectrum at low frequencies, yet we wish to consider high intensities to induce a strong effect from radiation reaction. The laser pulse collides head-on with a neutral $e^-/e^+$ bunch, which is Gaussian in shape and of size $\mathrm{FWHM}_e = 16\,\mathrm{nm}$ in each dimension. This bunch contains $N_{e-} = 4000$ electrons and $N_{e+} = 4000$ positrons (total particles $N = 8000$), and moves with an average initial Lorentz factor $\gamma_0 = 5$ along $+z$, with a small initial kinetic energy spread as outlined in Tab. 4.1. The bunch remains unchanged throughout all of our simulations.

Notice that the laser in question is sufficiently intense $a_0 \gtrsim 1$ to ionise virtually any atoms or molecules present. Nevertheless, as our model is classical, it is necessary to check the likelihood of forming bound states of $e^-$ and $e^+$ is low (which are known as Positronium). The peak density of a spherically symmetric, Gaussian bunch can be written as (see Eq. (A.2))

$$n_0 = \frac{N}{(2\pi)^{3/2}\,\sigma_e^3}\,, \qquad \sigma_e = \frac{\mathrm{FWHM}_e}{2\sqrt{2\ln 2}}. \tag{4.15}$$

| | *laser 1* | | *laser 2* | | |
|---|---|---|---|---|---|
| | CP | LP | CP | LP | |
| $\lambda_0$ | 400 | 400 | 100 | 100 | nm |
| $a_{L,0}$ | 5 | 5 | 5 | 5 | |
| $a_0$ | $5/\sqrt{2}$ | 5 | $5/\sqrt{2}$ | 5 | |
| $I_0$ | 2.2 | 2.2 | 34.7 | 34.7 | $\times 10^{20}\,\mathrm{W/cm^2}$ |
| $\mathrm{FWHM}_L$ | 26.7 | 26.7 | 26.7 | 26.7 | fs |
| $\chi_0$ | 2.1 | 3.0 | 8.5 | 12.1 | $\times 10^{-4}$ |
| $R_C$ | 5.5 | 11.0 | 22.0 | 44.0 | $\times 10^{-6}$ |

Table 4.2: Properties of the laser(s) considered in our simulations. By row, one can see the central wavelength $\lambda_0$, amplitude of the envelope function $a_{L,0}$, normalised amplitude $a_0$, (cycle averaged) peak intensity $I_0$, full width at half maximum of the laser pulse (in intensity) $\mathrm{FWHM}_L$. Below, one can see the quantum parameter $\chi_0$, and the classical parameter for the radiation dominated regime $R_C$ calculated for $\gamma_0 = 5$ as shown in Tab. 4.1.

With the peak density in Eq. (4.15), we can estimate the minimum interparticle distance in the lab frame $d \sim (1/n_0)^{1/3}$ (in 3D). Due to the spherical symmetry, one can easily identify a corresponding 1D interparticle distance $d/\sqrt{3}$. By considering how each component changes under a Lorentz boost defined by $\gamma_0$, we can evaluate the interparticle distance in the rest frame

$$d^* = d\left(\frac{2+\gamma_0^2}{3}\right)^{1/2}. \tag{4.16}$$

Where an asterisk denotes a rest frame quantity, and clearly $d^* = d$ if the bunch is at rest. This length $d^* \approx 2.55\,\mathrm{nm}$ can be calculated from the peak density of our bunch in Tab. 4.1. In the case of $e^-/e^+$, the relevant length scale for the formation of bound states is the Bohr radius for Positronium $a_{\mathrm{Ps}} = 1/e^2\mu \approx 0.11\mathrm{nm}$, where $\mu = m/2$ is the reduced mass. Comparing these two lengths $d^*/a_{\mathrm{Ps}} \approx 24\mathrm{nm}$, we argue that as the interparticle distance in the rest frame, estimated from the peak density, exceeds the Bohr radius for Positronium by an order of magnitude, the likelihood of bound state formation is small. Finally, we note a small time step $\Delta t \approx d/10 \approx 2.7 \times 10^{-19}\,\mathrm{s}$ is needed to properly resolve the interparticle (LW) fields, and observe the emission of high frequencies via the Nyquist theorem.

## 4.4 Experimental feasibility

It is worth considering the feasibility of our simulation parameters, with regards to what is currently achievable in the laboratory. A variety of lasers operating in the petawatt $I_0 \sim 10^{15}\,\mathrm{W}$ and multi-petawatt $I_0 \gtrsim 10^{16}\,\mathrm{W}$ regimes have become available in recent years [72], including those at the Extreme Light Infrastructure (ELI) [73, 74], Apollon-10 PW [75] and Vulcan-20 PW [76]. These lasers typically operate at optical wavelengths $\lambda_0 = 0.8 - 1\,\mu\mathrm{m}$. For example then, a petawatt laser of central wavelength 800 nm and waist $w_0 = 3\,\mu\mathrm{m}$ focused on a spot of area $\pi w_0^2/2$ would have an intensity in the order of $\sim 10^{21}\,\mathrm{W/cm^2}$; this is comparable to the intensity of the 100 nm laser and exceeds that of the 400 nm laser which we have suggested, in Tab. 4.2. Note, however, that we have chosen two wavelengths that are sub-optical. Frequency doubling an optical laser in a suitable crystal is a common technique even at high intensities [36, 77, 78]. Indeed, parameters exceeding ours, 30 fs pulses at intensity $6.5 \times 10^{21}\,\mathrm{W/cm^2}$, have been obtained previously for 400 nm [79].

A 100 nm laser remains challenging to obtain. This would require repeated doubling of an optical laser, for which it is difficult to maintain a efficiency, and conventional optics tend to become transparent as one approaches the extreme ultraviolet (EUV) regime. We note that significant progress has been made towards developing a 100 nm laser by four-wave mixing [80], and both high harmonic generation from laser-plasma interactions [61] and free electron lasers (FEL) operate at these wavelengths. However, to our knowledge none of these techniques have yet reached the intensity discussed here. In short, the 400 nm laser suggested in Tab. 4.2 is readily obtainable, while the 100 nm laser is more speculative.

Now we discuss the feasibility of producing an $e^-/e^+$ bunch of the kind described in Tab. 4.1. Beams of $e^-/e^+$ pairs are typically[6] generated in the laboratory as energetic, charged particles propagate through a high-Z target emitting bremsstrahlung radiation, which in turn creates $e^-/e^+$ pairs via the Bethe-Heitler process, thus generating a cascade [62, 83, 84]. To obtain a $e^-/e^+$ beam with a low energy spread, it seems logical to first start from a high quality electron beam. Near mono-energetic beams of electrons ($\sigma_{\mathrm{KE}} \sim 0.1\,\%$) with low angular spread ($\sigma_\vartheta \sim 1\,\mathrm{mrad}$) can be created via plasma based particle accelerators [85, 86]. As these electrons pass through a high-Z target, one can create an $e^-/e^+$ beam containing $\sim 1\,\mathrm{pC}$ of $e^+$ concentrated at the MeV-energies of interest here [60, 62–64]. This is several orders of magnitude above our bunch, which contains $6.4 \times 10^{-4}\,\mathrm{pC}$ of $e^+$. We suggest a quasi-monogenetic $e^-/e^+$ bunch could then be fabricated by selecting the desired

[6] For completeness, we mention a few additional schemes for generating $e^-/e^+$ pairs in the laboratory. An ultra-relativistic electron colliding with an intense laser pulse can emit a photon by non-linear Compton scattering, which in turn can create an $e^-/e^+$ pair upon interacting with the background laser field [49]. Tiny numbers of $e^+$ were created via this method at SLAC [78]. Alternatively, with two colliding lasers operating at higher intensities $\gtrsim 10^{24}\,\mathrm{W/cm^2}$, one could accelerate electrons directly with the laser(s), avoiding the need for a conventional accelerator [81, 82].

energies in a magnetic chicane compressor, without loss of charge or current posing a problem.

## 4.5 Results & discussion

With the simulations complete, we can review the results as shown in Fig. 4.2. Here the laser wavelength and polarisation vary in each column, in order of increasing energy radiated by the particles, from left to right. The first [Fig. 4.2 (a-d)] and second rows [Fig. 4.2 (e-h)] describe the spectrum of total and incoherent energy radiated respectively, onto a small $1\,\mathrm{cm}^2$ detector at 1m along the $+z$ axis. Correspondingly, Fig. 4.2 (i-l) are histograms of the final particle energies. In the last row [Fig. 4.2 (m-p)] we have drawn a schematic of the transverse $e^-/e^+$ dynamics at the laser pulse peak, without interparticle fields, which illustrates the charge separation. Immediately, one notices the inclusion of interparticle fields when solving the (reduced) LL equation tends to coherently amplify the emitted spectrum, across a broad range of frequencies in the soft X-ray domain $0.1 - 1\,\mathrm{keV}$, which would otherwise be incoherent. This amplification happens to be both polarisation and wavelength (or intensity) dependent, which we discuss in detail below.

By comparing the total and incoherent spectra, one can identify frequencies at which the energy radiated scales coherently with the total number of particles $N \sim 10^4$. When solving the LL equation with the 'laser only', for the 400 nm laser we see coherence below approx. 90 eV, while for 100 nm the spectrum is always incoherent. For the 'laser only', each particle observes the same field and collisions do not occur, and so we expect the bunch to remain stable in size (except for the small impact of the initial momentum spread); the transition from coherent to incoherent then occurs approximately at the frequency $2\pi/\mathrm{FWHM}_e \approx 78\,\mathrm{eV}$ corresponding to the bunch size. This transition cannot be seen in the 100 nm case as the spectrum begins above this frequency at $\omega_s \approx 90\,\mathrm{eV}$, while for 400 nm the spectrum begins at $\omega_s \approx 23\,\mathrm{eV}$. This explains why, with the 'laser only', all spectra exhibit similar degrees of coherence at the same absolute frequency (in eV). For the incoherent spectra, all cases for the fields are overlapping and effectively indistinguishable, and the spectrum closely resembles that of a single particle seen in Fig. 4.1. This suggests the underlying trajectories are only altered perturbatively, but that the particles are spatially reorganised in such a way that they tend to emit coherently.

The inclusion of interparticle fields when solving the LL equation coherently amplifies a broad range of frequencies, from approximately 70 eV to 300 eV in all cases except for the 400 nm laser with CP, where little amplification occurs. An apparent explanation is offered by the schematics. While the $e^-/e^+$ occupy the same volume initially, for the 400 nm laser both species separate transversely due to the electric field, inducing a charge separation. For CP, the $e^-/e^+$ orbit a common guiding centre and remain separated at the pulse peak, for LP, the $e^-/e^+$ periodically re-collide as the field is oscillating. Hence for CP we expect Coulomb repulsion to play a large role expanding the bunch and reducing coherence, which is confirmed by comparing 'laser and interparticle' with 'laser & intraspecies'; these cases are nearly identical, confirming that the $e^-/e^+$ interaction is negligible.

For the 100 nm laser, the $e^-/e^+$ are continuously interacting, and so the spectra and final particle energies exhibit a weaker dependence on polarisation. For both the 100 nm laser, and 400 nm laser with LP, 'laser & intraspecies' fields acts as an intermediate case, inducing a weaker coherent amplification confined to low frequencies, which is reflected in the final particle energies. This highlights the importance of the $e^-/e^+$ interaction when inducing coherent emission, and particularly the role of the re-collision process seen with LP. As such, we are very sceptical at the notion that similar results can be obtained with only electrons. It would be interesting, however, to check if similar behaviour can be reproduced with an electron-ion system, in future.

Correspondingly, one can observe a broad and inhomogeneous loss of energy by particles within the bunch in Fig. 4.2 (i-l). This appears to confirm that our results are consistent. However, a fair comparison of the radiation spectra and final particle energies is difficult for several reasons, for example: (i) we only consider radiation emitted close to the axis in the spectra, (ii) the role of the potential energy is recorded here, and is not necessarily negligible as a charge separation (effectively a dipole) is induced, and (iii) for LP we have truncated the spectra around 2 keV as all cases become incoherent at very high frequencies, such that it is difficult to identify the total energy radiated. Recall from the introduction, that we discussed a model suggested by several authors [19, 20], that one can treat a 'small' bunch of $N$ particles as a single *point* particle, which would experience a coherently enhanced self-force, which is proportional to the effective classical electron radius $Nr_e$. Yet, if we used this approach to determine the final Lorentz factor(s) via Eq. (4.10b), we can clearly see this would not account for the inhomogeneous loss of energy in our simulations. This highlights the fact that each particle will observe a different electromagnetic field, and subsequently will lose a distinct amount of energy and momentum depending on its position within the bunch.

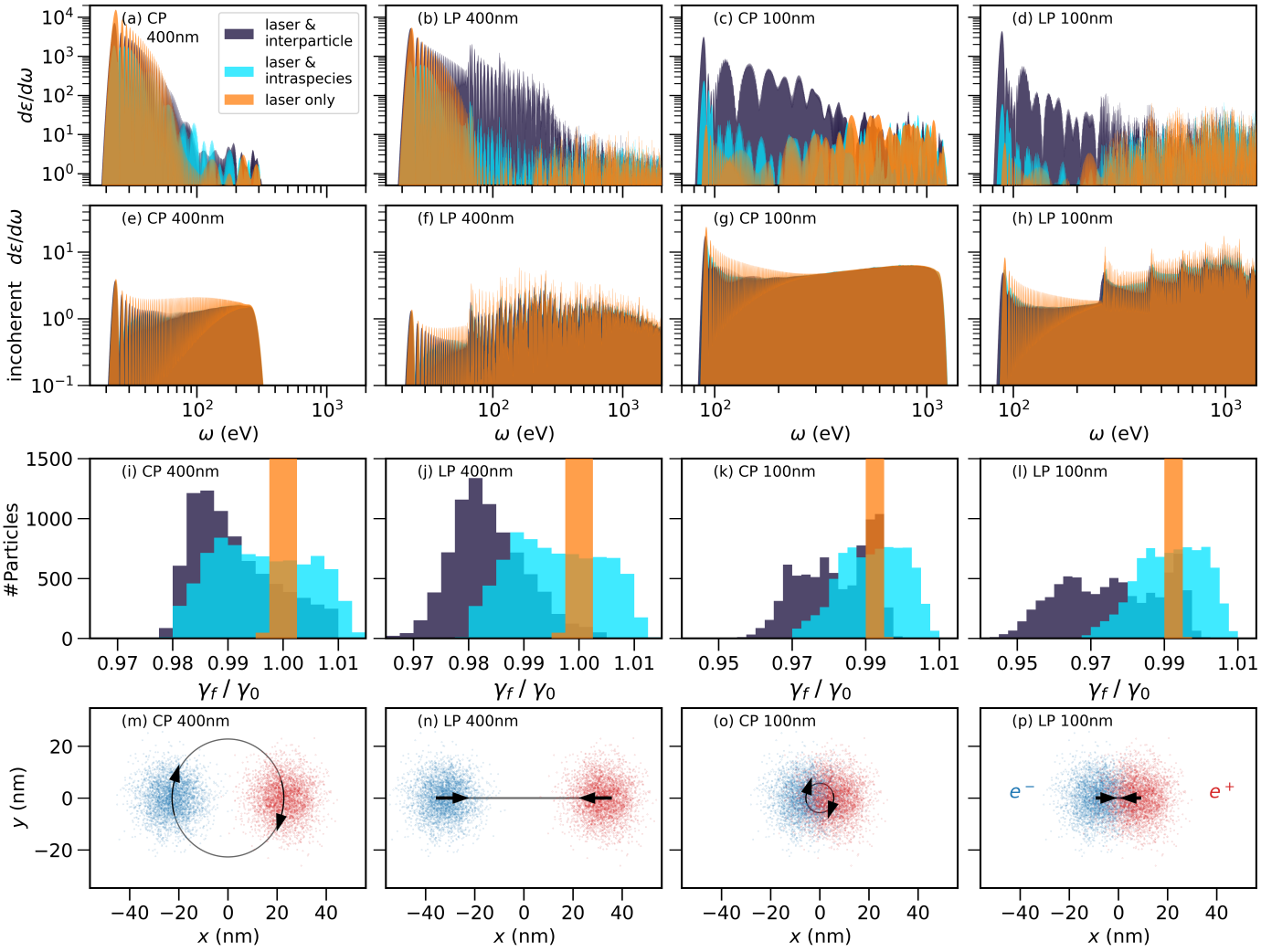


Figure 4.2: Inclusion of interparticle fields when solving the LL equation. Legend in (a) applies to plots (a-l). Spectrum of total energy radiated (a-d) and incoherent energy (e-h) reflected onto a small detector, and final particle energies (i-l). Laser varies between circular (CP) and linear (LP) polarisation, wavelengths 400 nm and 100 nm, in each column. Schematics (m-p) show the transverse $e^-/e^+$ dynamics at the laser pulse peak, without interparticle fields. In (a-d), different cases for the fields are overlapping except at frequencies where interparticle fields cause additional radiation to be emitted. For the incoherent spectra (e-h), 'laser & interparticle fields' and 'laser & intraspecies fields' (no $e^-/e^+$ interaction) are indistinguishable and overlapping with 'laser only'. For the 400 nm laser, the incoherent spectra are virtually identical in shape to the one electron spectrum shown earlier in Fig. 4.1; one cannot easily compare the energy radiated on the y-axis, as here we have integrated over the solid angle. Figure was created by the author and can also be found in a corresponding paper [1].

## 4.6 Coherent emission via micro-bunching

To explain this coherent amplification, consider the longitudinal profile of the $e^-/e^+$ bunch at the laser pulse peak, as shown in Fig. 4.3. Why have we chosen this specific time, and what is so important about the longitudinal direction? To the first point, we expect emission to be strongest at the maximum value of the fields, near the pulse peak. To the second question, we expect coherent emission at low frequencies to drive any collective behaviour, and from the stationary phase approximation described earlier [see Eq. (4.13a)], low frequencies tend to be emitted on-axis close to the pulse peak (all be it, over a large radiation cone subtended by angle $a_0/\gamma_0 \sim 1$, from the ratio of the transverse to longitudinal momentum). With the 'laser only', the initial shape of the bunch appears to be preserved in all cases. With interparticle fields, for the 400 nm laser with CP the bunch appears to be skewed along $z$ in the opposite direction to the velocity, which corresponds to a small amount of energy emitted as seen in Fig.4.2 (a,i). For LP, a single, sharp peak of FWHM $\approx$ 4.4 nm can be seen, which is about one-quarter the size of the initial bunch. This accounts for coherent emission up to approx. $2\pi/\text{FWHM} \approx 280$ eV, as seen in Fig. 4.2 (b).

For the 100 nm laser a triple peak structure emerges for both polarisations, which occurs on the scale of the longest emitted wavelength $\lambda_s = 2\pi/\omega_s$ (or lowest emitted frequency), at which much of the energy radiated is concentrated in Fig. 4.3 (a-d). For CP, no single peak is dominant and a measurement of the peak width is difficult to perform accurately. However, any estimate would likely be smaller than the initial bunch. For LP, the left-most peak is somewhat dominant and has a FWHM $\approx$ 4.7 nm which accounts for coherent amplification up to approximately 260 eV. It should be clear that these frequencies are estimates, particularly for LP as the bunch has expanded to the scale of one wavelength at the pulse peak, and consequently these structures begin to oscillate with the fields, making an accurate measurement challenging. Finally, we note that as no micro-bunching effect or broad coherent amplification of the spectra can be seen for 'laser & intraspecies' fields[7], their longitudinal profile has not been plotted in Fig. 4.3.

The full, time dependent dynamics in position space can be seen with *videos* in the supplementary material [87–90]. These compare the two most important cases, 'laser only' and 'laser & interparticle' fields, side by side over time. A snapshot from these videos is provided at the laser pulse peak in Fig. 4.4. For the 100 nm laser, one can see a transverse focusing of the bunch at the laser pulse peak, in addition to the longitudinal modulations described before. For the 400 nm laser, with CP we simply observe a rapid expansion due to Coulomb repulsion, while with LP the respective species form a pair of coherently emitting 'discs', which experience no transverse compression.

[7]The longitudinal profile for 'laser & intraspecies' fields' loosely resembles Fig. 4.3 (a), and contains no interesting structures.

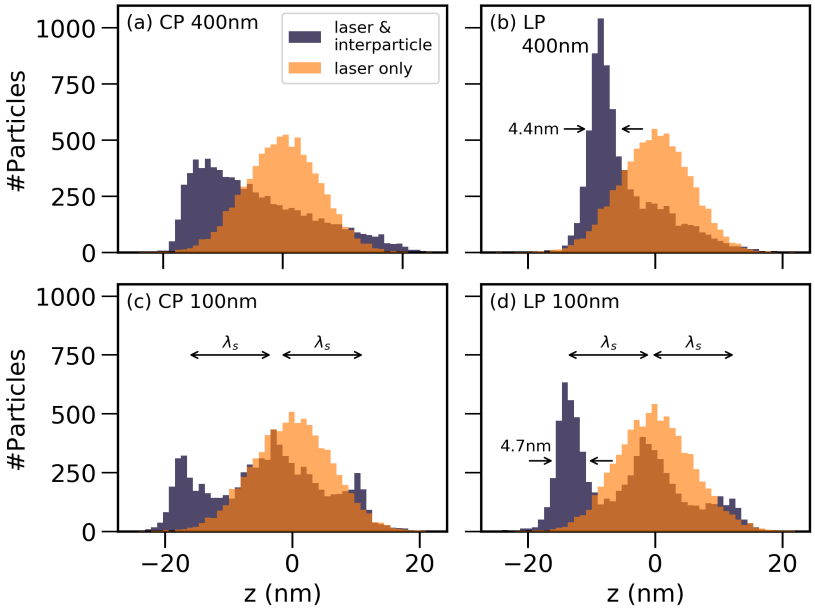


Figure 4.3: Longitudinal profile of the $e^-/e^+$ bunch at the laser pulse peak. Legend in (a) applies to all panels. Here $\lambda_s$ refers to the longest emitted wavelength from the system, while the distance between the twin arrows in (b) and (d) is the full width at half maximum of the dominant peak. Figure was created by the author and can also be found in a corresponding paper [1].

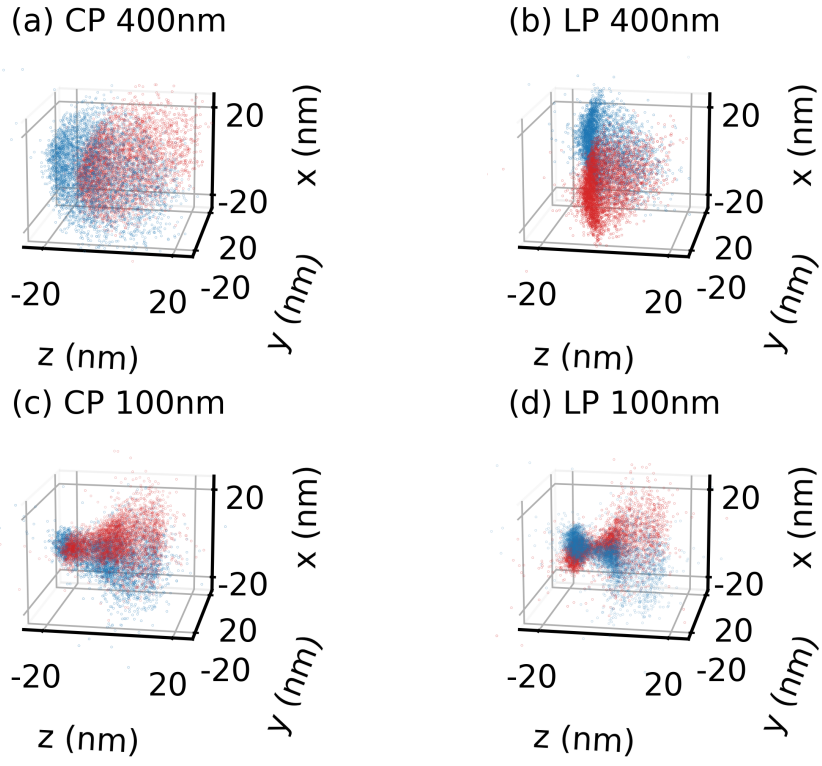


Figure 4.4: Distribution of $e^-$ (blue dot) and $e^+$ (red dot) in 3D at the laser pulse peak, congruent with Fig. 4.3. For the 100 nm laser, we can transverse focusing in addition to the longitudinal modulation.

In short, the emitted radiation drives a micro-bunching effect in the longitudinal direction, on the scale of the longest emitted wavelength, which tends to scale coherently. These compressions induce coherent emission in the spectrum at frequencies where none would typically be expected (with 'laser only'); note that for the 100 nm laser coherent emission only occurs when interparticle fields are included. The collective behaviour which takes place at the laser pulse peak is complex and time dependent, and in particular we do not have a satisfactory explanation for any transverse focusing which has occurred with the 100 nm laser. However, as can be seen in the videos [87–90], or alternatively with the final particle energies in Fig. 4.2 (i-l), the $e^-/e^+$ bunch expands in phase space when interparticle fields are included by the *end* of the simulation, for all wavelengths and polarisations. The explanation appears to be that if each particle experiences a different electromagnetic field, energy losses within the bunch will be inhomogeneous, which leads to a phase space expansion that impedes coherent emission, and subsequently the collective behaviour studied here must be transient. This contrasts with a previous theorem for the Vlasov equation, which shows a phase space contraction and decrease in entropy, demonstrated for an external and self-consistent mean field [42, 91]. The discrepancy is likely due to collisions, which we have taken into account exactly here.

## 4.7 Role of radiation reaction

Note that when we justified the size and initial energy-momentum spread of the $e^-/e^+$ bunch which was necessary for coherent emission, we utilised the single particle spectrum, which was derived from the Lorentz equation, or trajectory. Given that the spectra in Fig. 4.2 have been interpreted using the frequency $\omega_s$ and wavelength $\lambda_s$ which do not dependent on the length scale associated with radiation reaction, specifically the classical electron radius; it is natural then, to ask exactly what is the role of radiation reaction in these simulations? This is most clearly seen by referring to Fig. 4.5, where we have repeated the simulations in Fig. 4.2 using the Lorentz equation instead of the LL equation.

By comparing the top (Lorentz) and bottom (LL) rows, one can see that the self-force is negligible in practice for the 400 nm laser. The formation of a coherently radiating disc, as observed with LP in Fig. 4.4, must arise due to the inclusion of interparticle fields within the Lorentz force alone. However, for the 100 nm, some contribution from radiation reaction is clear; one can see the entire distribution is somewhat shifted, or skewed to lower particle energies. In practice, the micro-bunching phenomena and broad coherent emission appear to arise regardless of the equation of motion utilised. As such, we have decided not to replot the information already contained in Fig. 4.2 again here.

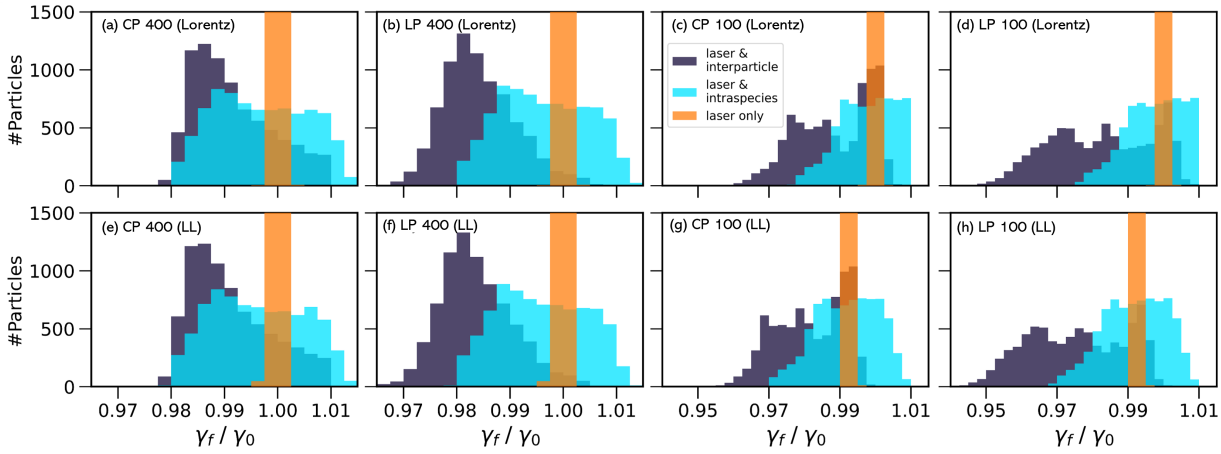


Figure 4.5: Histograms of final particle Lorentz factors when solving the Lorentz equation (a-d) and LL equation (e-h) for the collision of an $e^-/e^+$ bunch and laser pulse. The central laser wavelength varies from 400 nm to 100 nm, from CP to LP, in each column.

# Chapter 5

## Electron-positron beam in a constant & uniform magnetic field

> *"With the advent of big new telescopes, I hope we will be able to clarify what is producing things like fast radio bursts and tidal disruption events, and study the mergers now being detected by gravitational wave detectors such as LIGO"*
>
> — J. Bell Burnell, discussing pulsars as an opportunity to test fundamental physics [92]

In the previous chapter, we considered the interplay of radiation reaction and collective behaviour within an $e^-/e^+$ bunch and laser pulse collision, with an interest towards laboratory experiments. We seek to extend our discussion to scenarios which are analogous to an astrophysical environment. Relativistic pair plasmas are thought to be created in the presence of extremely strong electromagnetic fields, near black holes [93] and pulsars [94]. It is the strong magnetic field found in the latter which is of interest here.

We take a moment to summarise the usual model for $e^-/e^+$ pair creation in the pulsar magnetosphere. One often models the electromagnetic field emanating from a pulsar as a rotating magnetic dipole [95, 96]. Charged particles propagating along the open magnetic field lines near the poles are unable to return; this creates a charge depleted region with a strong electric field known as a gap, from the neutron star surface to the magnetosphere [97]. In close proximity to the surface these fields can be in the order of, and even exceed, the critical field of QED. High energy photons are absorbed by such a field to create an $e^-/e^+$ pair. These charged particles are rapidly accelerated by the electric field (in opposite directions), propagating along the magnetic field; the electromagnetic radiation emitted is thought to generate secondary $e^-/e^+$ pairs, of lower energy and moving at greater angles relative to the magnetic field, which will result in a distinctly different trajectory. This will have a significant impact on the frequency and polarisation of the emitted radiation. The production of $e^-/e^+$ pairs is expected to eventually screen the electric field, preventing further acceleration.

Consider that we approximate a curved magnetic field line as a circular arc of radius $\rho$. A charged particle propagates along this line, with pitch angle $\alpha$ between

the field and velocity at some instant. One then argues as $\rho \to \infty$, the trajectory becomes helical and the spectrum is that of *synchrotron* radiation, with a characteristic frequency [18]

$$\omega_{\rm sc} = \frac{3}{2}\gamma^2 |\omega_B| \sin(\alpha). \tag{5.1}$$

Here the particle is assumed to be relativistic and $\omega_B = eB/m$ is the frequency associated with the magnetic field, including the sign on the charge. The initial frequency of rotation is then $|\omega_B|/\gamma_0$. Alternatively, as $\alpha \to 0$ the characteristic frequency is that of *curvature* radiation [23, Ch. 14.6]

$$\omega_{\rm cv} = \frac{3}{2}\frac{\gamma^3}{\rho}. \tag{5.2}$$

One expects the primary charged particles ejected from the gap are ultra-relativistic and emit *curvature* radiation. Given that we observe GeV gamma rays from pulsars [98], likely from the inner magnetosphere where the fields are strongest, one infers by Eq. (5.2) that some particles are accelerated to extreme Lorentz factors $\gamma \lesssim 10^9$ [17]. For rest frame fields beyond the classical regime, a particle would rapidly cascade down through the Landau levels (quantised orbits in a strong magnetic field). At the opposite end of the electromagnetic spectrum, coherent curvature radiation from charge bunches is one of many mechanisms proposed to explain pulsar radio emission [97, 99]. For secondary $e^-/e^+$ pairs at lower energies and larger pitch angles, one expects *synchrotron* emission to play a more important role. The transition between curvature and synchrotron remains unclear; both Cheng & Zhang [100] and Kelner et al [101] have attempted to define these regimes as asymptotic limits of a unified synchro-curvature theory, the latter in particular includes classical radiation reaction. It is well known the emission spectrum of the Crab nebulae is accurately characterised by synchrotron, from radio to UV wavelengths. It is also thought that secondary $e^-/e^+$ pairs are responsible for the emission of crossed fan beams[1] of X rays and gamma rays [103], differing from those emitted in curvature radiation.

We seek to proceed as in the previous chapter, by identifying a regime in which coherent emission and collective behaviour occurs, where radiation reaction ideally also plays a role. Yet, the range of parameters that can be resolved with our numerical approach is extremely limited. Our code must operate for a length of time which is long enough for an instability to develop, with a time step small enough to properly resolve the LW fields between particles. Similar difficulties are often remarked upon when attempting to identify sites for gamma ray emission [17] or

[1] The term 'crossed fan beam' as opposed to 'pencil' or 'conal' beam of radiation, is unfamiliar to us but appears occasionally in the literature. The distinction appears to be the angle at which the radiation propagates relative to the magnetic field; see Fig. 1 of Ref. [102].

acceleration regions [104] within the magnetosphere; this requires reconciling vast differences in scales, from the neutron star radius[2] $\sim$ 10km over which the pulsar fields will vary significantly, to the Larmor radius over which the trajectory varies, which is often *many* orders of magnitude smaller. To that end, we consider the simplified case of weakly relativistic particles propagating in a constant and uniform magnetic field (i.e. the *synchrotron* regime). The parameters utilised will be comparable to those in the previous chapter concerning lasers; it is unclear if our results can relate directly to the astrophysical scenarios described above, or if rescaling is needed (or possible). The above conversation about astrophysics is then provided as a motivation to study this problem in detail. As before, it will be instructive to start from the single particle case.

## 5.1 Trajectory in a constant & uniform magnetic field

In the presence of a constant and uniform magnetic field, the LL equation (2.31) can be separated into transverse and longitudinal components

$$\frac{d\gamma}{d\tau} = -\omega_d \gamma^3 \boldsymbol{v}_\perp^2, \tag{5.3}$$

$$\frac{d\boldsymbol{v}_\perp}{d\tau} = \frac{e}{m}(\boldsymbol{v}_\perp \times \boldsymbol{B}) - \omega_d \boldsymbol{v}_\perp, \tag{5.4}$$

$$\frac{dv_\parallel}{d\tau} = 0. \tag{5.5}$$

Where $\tau_e = 2r_e/3 \sim 10^{-23}$ s is the small time interval associated with the classical electron radius. One can already identify the friction-like behaviour of radiation reaction from the decay of the Lorentz factor, over some interval of proper time. This occurs on a time scale associated with the damping frequency $\omega_d = \omega_B^2 \tau_e > 0$. As with the Lorentz equation, no force is exerted parallel to the magnetic field, such that the longitudinal velocity is conserved $v_\parallel = v_{0,\parallel}$. This is why we have chosen to work with the velocity $\boldsymbol{v} = \boldsymbol{u}/\gamma$ instead of $\boldsymbol{u}$, as oddly enough the longitudinal component $\boldsymbol{v}_\parallel$ is conserved, yet $\boldsymbol{u}_\parallel$ is not. It will prove convenient to define a Lorentz factor associated with this velocity

$$\gamma_{0,\parallel} = \frac{1}{\sqrt{1 - v_{0,\parallel}^2}}. \tag{5.6}$$

This indicates that we could perform a Lorentz boost along $v_{0,\parallel}$ before solving. However, this extra step is unnecessary as the problem is sufficiently simple in

[2] A typical estimate for the neutron star radius, for a young pulsar of rotational period $\sim$ 0.1 sec. To define 'young', see e.g. Fig. (1) of the second Fermi-LAT catalogue [98].

the current frame of reference. Taking the scalar product of Eq. (5.4) with $\boldsymbol{v}_\perp$ and integrating, we can observe the exponential decay of the transverse velocity due to radiation reaction

$$\int \frac{d(\boldsymbol{v}_\perp^2)}{\boldsymbol{v}_\perp^2} = -2\omega_d \int d\tau, \tag{5.7a}$$

$$\boldsymbol{v}_\perp^2(\tau) = \boldsymbol{v}_{0,\perp}^2\, e^{-2\omega_d \tau}. \tag{5.7b}$$

Where we have applied the initial condition $\boldsymbol{v}_\perp(\tau = 0) = \boldsymbol{v}_{0,\perp}$. With the speed known, we can perform another integration for the particle's Lorentz factor

$$\int \frac{d\gamma}{\gamma^3} = -\omega_d^2 \int \boldsymbol{v}_\perp^2(\tau)\, d\tau, \tag{5.8a}$$

$$\gamma(\tau) = \frac{\gamma_{0,\parallel}}{\sqrt{1 - \gamma_{0,\parallel}^2 \boldsymbol{v}_{0,\perp}^2\, e^{-2\omega_d \tau}}}. \tag{5.8b}$$

Here the Lorentz factor satisfies the initial condition $\gamma(\tau = 0) = \gamma_0$ and asymptotic limit $\gamma(\tau \to \infty) = \gamma_{0,\parallel}$, where the latter reflects conservation of the longitudinal velocity. Notice that for $\tau > 0$ the solutions are always real and therefore physical, as the coefficient of the exponential term is always between zero and one by the on-shell condition

$$\gamma_{0,\parallel}^2 \boldsymbol{v}_{0,\perp}^2 = \gamma_{0,\parallel}^2 (\boldsymbol{v}_0^2 - v_{0,\parallel}^2) = 1 - \frac{\gamma_{0,\parallel}^2}{\gamma_0^2} < 1. \tag{5.9}$$

As with the Lorentz equation, we expect the transverse velocity to be oscillatory. Yet without conservation of angular momentum the period of oscillation will not be constant. For simplicity, if we define the magnetic field along $\boldsymbol{B} = B\,\hat{\boldsymbol{z}}$ and the initial transverse velocity as $\boldsymbol{v}_{0,\perp} = v_{0,\perp}\,\hat{\boldsymbol{y}}$, one can identify the following solution

$$\boldsymbol{v}_\perp(\tau) = v_{0,\perp}\, e^{-\omega_d \tau} \left[ \sin(\omega_B \tau)\,\hat{\boldsymbol{x}} + \cos(\omega_B \tau)\,\hat{\boldsymbol{y}} \right], \tag{5.10}$$

which can be verified by substitution into Eq. (5.4). This constitutes an exact solution to the LL equation for the velocity. Recall, however, that the LL equation is typically derived as a perturbative expansion of the LAD equation. The exact solutions derived above agree with the solutions of the LAD equation to first order, when solved with a perturbative series in terms of the small quantity $\omega_d \tau_e$ [44, 105]. Even at the critical magnetic field $B_{\text{cr}} \sim 10^9$ T of QED, well beyond the regime of validity for the LL and LAD equations, this quantity is still remarkably small

$\omega_d \tau_e \sim 10^{-5}$ which suggests the LAD and LL equations will be in excellent agreement.

With the equations for the three vector velocity and Lorentz factor above, one can construct the four vector velocity $u^\mu = \gamma(\tau)(1, \boldsymbol{v}(\tau))$. Then, from the definition of $u^\mu$ as the derivative of position with respect to proper time, we can write

$$x^\mu(\tau) - x_0^\mu = \int_0^\tau u^\mu(\tau')\, d\tau'. \tag{5.11}$$

As before, the position satisfies the initial condition $x_0^\mu = x^\mu(\tau = 0)$. It will prove convenient, once again, to resolve into components with respect to the magnetic field. As the longitudinal velocity is conserved, determining the position parallel to the magnetic field is trivial $x_\parallel(t) = x_{0,\parallel} + v_{0,\parallel}\, t$, as a function of the coordinate time $t$. One can then relate the coordinate and proper time by integrating the $\mu = 0$ component of the integral above. Earlier in Eq. (3.22b), we performed the inverse procedure by finding the proper time as a function of the coordinate time, which allowed the analytical results found here to be used as a benchmark of our numerical integrator for the (reduced) LL equation. The integral for the transverse position is more complex

$$\boldsymbol{x}_\perp(\tau) - \boldsymbol{x}_{0,\perp} = v_{0,\perp} \int_0^\tau \gamma(\tau')\, e^{-\omega_d \tau'} \left[ \sin(\omega_B \tau')\, \hat{\boldsymbol{x}} + \cos(\omega_B \tau')\, \hat{\boldsymbol{y}} \right] d\tau'. \tag{5.12}$$

As the timescale associated with radiative damping tends to be far larger than that of the magnetic field $\omega_d \ll \omega_B$, we suggest to account for radiation reaction perturbatively, first by integrating over the oscillating terms with parts

$$\begin{aligned} \Rightarrow \frac{v_{0,\perp}}{\omega_B} \Big[ \gamma(\tau') e^{-\omega_d \tau'} \left( -\cos(\omega_B \tau')\, \hat{\boldsymbol{x}} + \sin(\omega_B \tau')\, \hat{\boldsymbol{y}} \right) \Big]_0^\tau \\ - \frac{v_{0,\perp}}{\omega_B} \int_0^\tau \frac{d}{d\tau'} \left\{ \gamma(\tau') e^{-\omega_d \tau'} \right\} \left[ -\cos(\omega_B \tau')\, \hat{\boldsymbol{x}} + \sin(\omega_B \tau')\, \hat{\boldsymbol{y}} \right] d\tau'. \end{aligned} \tag{5.13}$$

One can see the first term will provide the leading order behaviour, while the second term will be suppressed by the damping frequency, incurred when differentiating both the Lorentz factor and exponential term. The approximate solution is then

$$\begin{aligned} \boldsymbol{x}_\perp(\tau) - \boldsymbol{x}_{0,\perp} \approx \frac{u_{0,\perp}}{\omega_B} \Bigg[ \left( 1 - \frac{\gamma(\tau)}{\gamma_0} e^{-\omega_d \tau} \cos(\omega_B \tau) \right) \hat{\boldsymbol{x}} \\ + \frac{\gamma(\tau)}{\gamma_0} e^{-\omega_d \tau} \sin(\omega_B \tau) \hat{\boldsymbol{y}} \Bigg]. \end{aligned} \tag{5.14}$$

Where one can identify the initial Larmor radius $R_0 = |\boldsymbol{u}_{0,\perp}/\omega_B| = |u_{0,\perp}/\omega_B|$. The oscillations in the transverse position are then exponentially damped over time, as with the transverse velocity.

## 5.2 Spectrum of radiation from one particle

Traditionally in astrophysics, the main source of information about distant objects is the electromagnetic radiation they emit. Having considered the impact of radiation reaction on the trajectory, according to the LL equation, it seems natural to determine the subsequent impact on the radiation spectrum, which can be written as [23, Ch. 14.5, Eq. (14.67)]

$$\frac{d\mathcal{E}}{d\omega d\Omega} = \frac{e^2}{4\pi^2}\,|\boldsymbol{\mathcal{I}}|^2\,, \tag{5.15a}$$

$$\boldsymbol{\mathcal{I}} = \omega \int_{-\infty}^{+\infty} \boldsymbol{n}\times(\boldsymbol{n}\times\boldsymbol{u})\, e^{i\omega(nx)}\, d\tau, \tag{5.15b}$$

$$\omega(nx) = \omega[t - \boldsymbol{n}\cdot\boldsymbol{x}]. \tag{5.15c}$$

Where $\omega$ is the frequency seen by a distant observer, in the direction of the four vector $n^\mu = (1, \boldsymbol{n})$ which satisfies $n^2 = 0$, and is approximately constant. Note that the integration is performed over the proper time, which can easily be exchanged with the coordinate time via $dt/d\tau = \gamma$. For brevity, any dependence on the proper time will be implicit in this section, for example $\gamma = \gamma(\tau)$. If we are considering charged particles propagating almost parallel with the magnetic field, we suggest to observe directly along the field line $\boldsymbol{n} = \boldsymbol{B}/B$, in which case the integrand will simplify significantly

$$\boldsymbol{n}\times(\boldsymbol{n}\times\boldsymbol{u}) = -\gamma\boldsymbol{v}_\perp, \tag{5.16a}$$

$$\omega(nx) = -\omega x_{0,\parallel} + \omega(1 - v_{0,\parallel})\, t. \tag{5.16b}$$

Here we have used the ballistic motion of the particle parallel to the field line as shown in the previous section. In practice, the initial position will vanish under the square modulus, and can therefore be thrown away (this is only true for a single particle). At this point, we would prepare to insert the transverse velocity shown earlier in Eq. (5.10). Decomposing each sinusoid with Euler's formula, one can see there are two contributions, from $e^{+i|\omega_B|}$ and $e^{-i|\omega_B|}$, regardless of the sign on the charge which appears in $\omega_B$. Following this logic, we separate our integral into positive and negative contributions

$$|\mathcal{I}|^2 = \frac{1}{2}|\mathcal{I}_-|^2 + \frac{1}{2}|\mathcal{I}_+|^2 . \tag{5.17}$$

Where the negative contribution to the integral can be written as

$$\mathcal{I}_- = \omega v_{0,\perp} \int_0^{+\infty} \gamma\, e^{-\omega_d \tau}\, e^{i\Phi}\, d\tau \tag{5.18a}$$

$$\Phi = -|\omega_B|\tau + \omega(1 - v_{0,\parallel})\, t. \tag{5.18b}$$

The positive contribution $\mathcal{I}_+$ is identical to $\mathcal{I}_-$, except that the sign on the frequency associated with the magnetic field is $+|\omega_B|$ in the phase of the integral $\Phi$, instead of $-|\omega_B|$ as shown above. The leading order behaviour of $\mathcal{I}_+$ is discussed in Appendix B, to justify why it can be neglected compared to the negative contribution $|\mathcal{I}_+|^2 \ll |\mathcal{I}_-|^2$. Notice that we have truncated the limits of integration to finite interval. Strictly speaking[3], this is only valid if the acceleration is zero outside the range of integration, for $\tau < 0$, which is problematic when considering constant fields. Often one avoids this problem in special cases where the boundary terms vanish, such as circular motion as described by the *Lorentz* equation in a constant and uniform magnetic field [106], or motion in a plane wave [65], where the initial and final velocity are identical. The latter is a consequence of the Lawson–Woodward theorem. We will assume the boundary terms can be neglected, and this will be proven later by comparison with numerical solutions [via the integral in Eq. (3.23b)].

To solve the integral $\mathcal{I}_-$, we should carefully inspect its oscillatory behaviour. If the observed frequency tends to zero $\omega \to 0$, the integral simply becomes a Fourier transform of the Lorentz factor and decaying amplitude of the transverse velocity. At the other extreme $\omega \to +\infty$, one can solve by the *stationary phase* approximation. This technique is found in any standard textbook on asymptotic analysis. The general idea is, that under the high frequency limit the integral oscillates rapidly, such that one only needs to make a small expansion around the stationary point of $\Phi$ for good approximation. To see when this is appropriate, we can rewrite the exponent

$$\Phi = |\omega_B| \int_0^{\tau} \left[ -1 + \varpi \frac{\gamma(\tau')}{\gamma_{0,\parallel}} \right] d\tau'. \tag{5.19}$$

One can see an asymptotic approach $\omega \to +\infty$ will tend to be valid when the second

[3]The radiation integral in Eq. (5.15b) is usually obtained via an integration by parts, of the Fourier transform, of the LW fields [23, Ch. 14.5]. The boundary terms which arise do not vanish identically for zero acceleration; Jackson argues one should insert a 'convergence factor', which forces the integral to vanish at the end points of integration.

term under the integral dominates. Here $\varpi = D\omega/|\omega_B|$ is the observed frequency in units of the longitudinal Doppler shift

$$D = \sqrt{\frac{1 - v_{0,\parallel}}{1 + v_{0,\parallel}}} \approx \frac{1}{2\gamma_{0,\parallel}}. \tag{5.20}$$

Asymptotic methods usually proceed by identifying one or more stationary point(s) $\tau_*$ in the exponent. One argues that higher order oscillatory terms tend to oscillate rapidly and therefore cancel, such that only the leading order term is required. The first derivative can be written

$$\Phi'_* \equiv \Phi'(\tau_*) = 0, \tag{5.21a}$$

$$\varpi\gamma_* \equiv \varpi\gamma(\tau_*) = \gamma_{0,\parallel}. \tag{5.21b}$$

Where derivatives with respect to proper time are denoted by a prime. The frequencies for which a stationary point exists can already be identified $\varpi \in [\gamma_{0,\parallel}/\gamma_0, 1]$, and in practice, the integral will be exponentially suppressed outside of this domain (see Appendix B). Note the information conveyed above; high frequencies $\varpi = 1$ are emitted in the limit $\tau_* \to +\infty$, while low frequencies $\varpi = \gamma_{0,\parallel}/\gamma$ are emitted in the limit $\tau_* \to 0$. We can interpret this for a relativistic particle, moving at angle $\alpha$ relative to the magnetic field. Initially, the cone (of instantaneous angle $\sim 1/\gamma$) into which radiation is emitted by the particle is not aligned with the magnetic field. Usually with synchrotron radiation, we expect high frequency radiation will be confined to the plane in which the circular motion takes place. Therefore, we expect low frequency radiation to be observed along the magnetic field, around the initial time. However, at advanced times the transverse velocity decays exponentially due to radiation reaction, such that the velocity aligns with the magnetic field. Then, we tend to see the Doppler shifted peak at $\omega_\parallel \approx 2\gamma_{0,\parallel}|\omega_B|$, which occurs due to conservation of the longitudinal velocity.

Recalling the expression derived earlier for the Lorentz factor, in (5.8b), we can proceed to find the *single* stationary point

$$e^{-\omega_d \tau_*} = \frac{1}{\gamma_{0,\parallel} v_{0,\perp}} \sqrt{1 - \varpi^2}\,, \tag{5.22a}$$

$$\tau_* = \frac{1}{2\omega_d} \ln\left(\frac{1 - \frac{\gamma_0^2}{\gamma_{0,\parallel}^2}}{1 - \varpi^2}\right). \tag{5.22b}$$

To simplify, we have also utilised the on-shell condition Eq. (5.9) to remove any dependence on $v_{0,\perp}$. Differentiating the exponent again, one can identify the second derivative, evaluated at the stationary point

$$\Phi''_* \equiv \Phi''(\tau_*) = -|\omega_B|\omega_d\left(\frac{1}{\varpi^2} - 1\right). \tag{5.23}$$

To derive this expression, one is required to differentiate the Lorentz factor from Eq. (5.8b), and evaluate using the steps shown above Eqs. (5.22a) and (5.21b). Higher order derivates are suppressed by increasing powers of the small quantity $|\omega_B|\tau_e$ which appears in the damping frequency $\omega_d$. We can then write the phase of the integral as a small expansion around the stationary point

$$\Phi \approx \Phi_* + \frac{\Phi''_*}{2}(\tau - \tau_*)^2. \tag{5.24}$$

In practice, we will not need to calculate $\Phi_*$ as it vanishes under the square modulus. With this expansion in hand, we can attempt to solve the radiation integral

$$\mathcal{I}_- \approx \omega v_{0,\perp}\int_0^{+\infty} \gamma\, e^{-\omega_d \tau}\, e^{\frac{i}{2}\Phi''_*(\tau-\tau_*)^2}\, d\tau. \tag{5.25}$$

One then argues that the Lorentz factor and exponentially decaying term can be treated as approximately constant, compared with the oscillating part of the integral. A similar, perturbative approach was used earlier in Eq. (5.14), to define the transverse trajectory position while including corrections from radiation reaction. After taking the slowly varying terms outside the integral, they can be evaluated at the stationary point according to the results derived above

$$\mathcal{I}_- \approx \frac{\omega}{\varpi}(1-\varpi^2)^{\frac{1}{2}}\,\mathcal{J}, \tag{5.26a}$$

$$\mathcal{J} = \int_{-\tau_*}^{+\infty} e^{\frac{i}{2}\Phi''_*(\tau-\tau_*)^2}\, d\tau. \tag{5.26b}$$

The key problem remaining involves the purely oscillatory integral $\mathcal{J}$ , and specifically the finite, lower limit. We suggest to separate this into two parts, one which can be solved exactly, and another which can be evaluated numerically

$$\int_{-\tau_*}^{+\infty} \equiv \int_0^{+\infty} + \int_{-\tau_*}^{0} = \int_0^{+\infty} + \int_0^{\tau_*}. \tag{5.27}$$

Where we have employed a schematic notation, omitting the integrand for convenience. The last equation requires changing the sign on the subject of integration.

As the second derivative is always negative $\Phi''_* < 0$, we will write the minus sign explicitly from now on $\Phi''_* = -|\Phi''_*|$. The first integral is a standard Gaussian. We can therefore write

$$\mathcal{J} = \frac{1}{2}\left(\frac{2\pi}{|\Phi''_*|}\right)^{\frac{1}{2}} \left[e^{-i\frac{\pi}{4}} + \sqrt{2}\,C + \sqrt{2}\,e^{-i\frac{\pi}{2}}\,S\right], \tag{5.28a}$$

$$C \equiv C\left(\left(\frac{|\Phi''_*|}{\pi}\right)^{\frac{1}{2}} |\omega_B|\tau_*\right), \tag{5.28b}$$

$$S \equiv S\left(\left(\frac{|\Phi''_*|}{\pi}\right)^{\frac{1}{2}} |\omega_B|\tau_*\right). \tag{5.28c}$$

Here $C$ and $S$ are the cosine and sine like Fresnel integrals, respectively, which can be written as

$$C(x) = \int_0^x \cos\left(\frac{\pi}{2}\tau^2\right) d\tau, \tag{5.29a}$$

$$S(x) = \int_0^x \sin\left(\frac{\pi}{2}\tau^2\right) d\tau,. \tag{5.29b}$$

To obtain the spectrum of energy radiated, we require only the square modulus, which can be easily carried out as the Fresnel integrals are always real

$$|\mathcal{J}|^2 = \frac{\pi\,\varpi^2}{2|\omega_B|\omega_d(1-\varpi^2)}\left[1 + 2(C+S) + 2(C^2+S^2)\right]. \tag{5.30}$$

With the oscillatory part of our integral known, this can be inserted into our equation for the radiation integral $\mathrm{I}_-$ (5.26a). One can then simplify using the second derivative $\Phi''_*$ at the stationary point defined previously, to obtain

$$|\mathcal{I}_-|^2 = \frac{\pi\,\omega^2}{2|\omega_B|\omega_d}\left[1 + 2(C+S) + 2(C^2+S^2)\right]. \tag{5.31}$$

In practice, only the negative contribution to the exponent $\mathcal{I}_-$ is significant. For the positive contribution $\mathcal{I}_+$, no stationary points exist and the integral is exponentially suppressed, as is demonstrated in Appendix B. As a result, we can write the spectrum of energy radiated along the magnetic field line, in terms of the Fresnel integrals

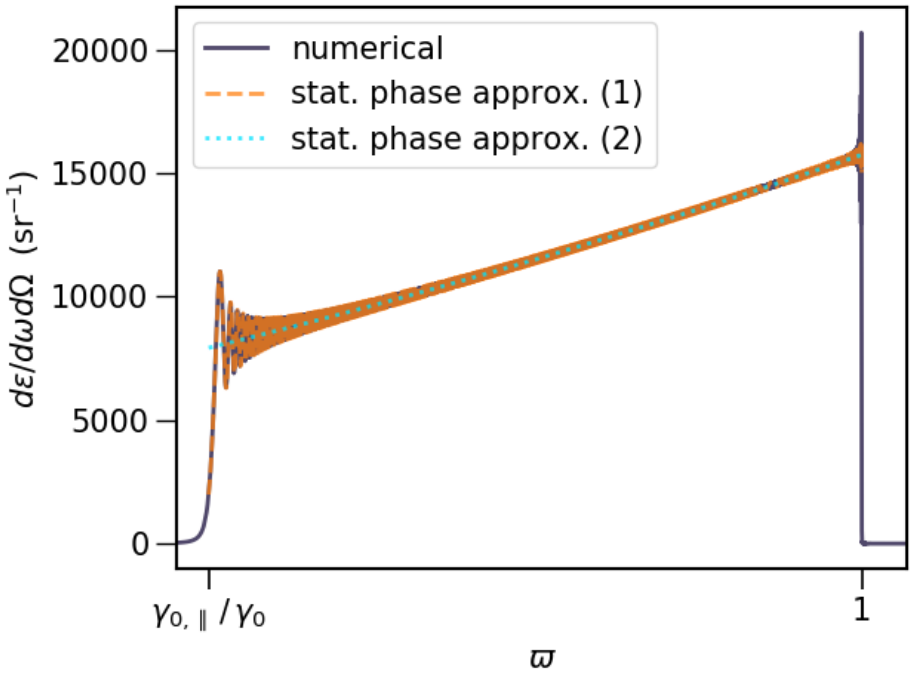


Figure 5.1: Spectrum of energy radiated by one electron, observed along the magnetic field, and integrated over all time. Plot shows solutions obtained by numerically integrating the reduced LL equation and emitted spectrum of radiation (as described in Chapter 3), and approximate analytical solutions (1) in Eq. (5.32) and (2) in Eq. (5.33) to the spectrum, obtained via the stationary phase method.

$$\left.\frac{d\varepsilon}{d\omega d\Omega}\right|_{\parallel} \approx \frac{e^2}{4\pi}\,\frac{\pi\omega^2}{4|\omega_B|\omega_d}\left[1+2(C+S)+2(C^2+S^2)\right]. \tag{5.32}$$

This result is plotted in Fig. 5.1 (1), where the Fresnel integrals are evaluated numerically. To perform this simulation, we have chosen a strong magnetic field $B = 10^7$ T, relativistic particle $\gamma_0 = 10$, with an initial pitch angle $\alpha = 0.1$. This scenario remains inside the classical regime $\chi_0 \approx 2.3 \times 10^{-3}$ [see (5.35)].

One notices a convenient approximation which applies as $\tau_* \to +\infty$. This occurs as the frequency tends to its maximum value $\varpi \to 1$. At this point the Fresnel integrals tend to their asymptotic values, $S \to 1/2$ and $C \to 1/2$, and we can write

$$\lim_{\tau_*\to+\infty}\left.\frac{d\varepsilon}{d\omega d\Omega}\right|_{\parallel} \approx \frac{e^2}{4\pi}\,\frac{\pi\omega^2}{|\omega_B|\omega_d}. \tag{5.33}$$

In practice, this approximation is excellent as shown in Fig. 5.1 (2), because a very large number of oscillations are required for the transverse velocity to vanish, and

so the spectrum tends to oscillate rapidly; it is well approximated by an average. Notice, however, the stationary phase approximation breaks down at $\varpi = 1$, which is a result of the second derivative (5.23) vanishing at this point. To gain a more accurate approximation in this region, one would need to include the third order derivative in Eq. (5.24), and represent the spectrum with Airy functions [67].

The spectra derived in this section are of little use unless the velocity is at least partially along the magnetic field. We see no reason why this method could not be generalised to include additional observation directions. In this case, the exponent of Eq. (5.15c) would depend on the transverse coordinates (5.14), which are oscillatory. We expect these could be taken out of the integral using the generating function for Bessel functions $J(x)$ of the first kind [107, Ch. 9]

$$e^{ix\sin\phi} = \sum_{n=-\infty}^{+\infty} J_n(x)\, e^{in\phi}. \tag{5.34}$$

As the Bessel functions depend only on the slowly varying terms like the Lorentz factor, these could similarly be taken outside of the integral. This scenario would likely not admit a simple closed form, as we have obtained here.

## 5.3 Properties of the beam and B-field

In the previous chapter, we considered a Gaussian bunch of $e^-/e^+$ colliding with a laser pulse. The key difficulty was to explain how such a bunch might be created in the laboratory; we suggested one could pass an $e^-/e^+$ beam through magnetic spectrometer, select a desired range of energies and compressing in space before the $e^-$ and $e^+$ were recombined. To create the $e^-/e^+$ beam, we suggested to pass a quasi-monoenergetic electron beam obtained from a plasma-based accelerator through a high-Z target [60, 62]. Here the problem is inverted; it is universally accepted that $e^-/e^+$ plasmas populate the pulsar magnetosphere, yet to our knowledge, little is known about their distribution.

We suggest to consider a uniformly dense cylinder of $e^-/e^+$, with a length $L$ exceeding its radius $R$, along the magnetic field line. Clearly this is a crude approximation to what might exist in nature. The cylindrical shape itself is not unreasonable, and reflects the topology; if charged particles propagate close to (and radiate along) the magnetic field, we expect recoil from photon emission to create a variation in energy and momentum, which induces a spatial spread over time along the field line. To justify the choice of uniform density, consider the alternative of a localised $e^-/e^+$ bunch. Often $e^-/e^+$ solitons[4] are proposed, at far lower densities than what will be considered here, to account for pulsar radio emission via the

[4]Soliton, here meaning a self-reinforcing wavepacket of $e^-/e^+$ which remains stable.

coherent curvature mechanism [97, 108]. Yet this model is criticised because of short lived nature of these bunches [109]. Similarly with the laser pulse, we saw such a bunch exhibit collective behaviour, emit coherently and self-destruct in the process (in vacuum). A uniform density then avoids these difficulties. Note that the tiny bunch employed with the laser actually expanded globally as the micro-bunches responsible for coherent emission were formed [see Fig. 4.3, note the initial $\mathrm{FWHM}_e = 16\,\mathrm{nm}$]. The choice of uniform density would then compliment our previous results, allowing any instability to form naturally, instead of being dramatically influenced by the initial parameters of the bunch.

How could we design an instability comparable to that seen with the laser field? At first glance, we notice that the transverse motion of $e^-/e^+$ in a monochromatic, circularly polarised wave is comparable to a constant magnetic field [see Figs. 4.2 (m,o)]. For a constant magnetic field, no longitudinal force exists which allows us to control the spectrum of energy radiated. Instead, we expect emission at the characteristic frequency of synchrotron radiation $\omega_{\mathrm{sc}} = \frac{3}{2}\gamma^2|\omega_B|\sin\alpha$ from Eq. (5.1). As described in chapter 4 with the laser pulse in the weak field regime $a_0 \ll 1$, the dependence on $\gamma_0^2$ quickly leads to an extreme density of particles necessary for coherent emission. However, from the previous section, we saw that radiation emitted along the magnetic field lines tends to be concentrated at a lower frequency $\omega_\parallel \approx 2\gamma_{0,\parallel}|\omega_B|$ for relativistic particles.

Consider then a magnetic field of strength $B = 10^6\,\mathrm{T}$ along the $z$ axis with associated frequency $|\omega_B| \approx 0.12\,\mathrm{keV}$. We initialise the electrons and positrons with average Lorentz factor $\gamma_0 = 5$, and a small, RMS spread in the kinetic energy $\sigma_{\mathrm{KE}} = 0.1\%$ as seen with the laser-bunch collision in Tab. 4.1. The average pitch angle between the initial velocity and magnetic field is $\alpha = 0.5\,\mathrm{rad}$, and we include a RMS spread in angle around the initial velocity $\sigma_\vartheta = 1\,\mathrm{mrad}$. As the field is constant, to initialise the simulation, one must numerically integrate the trajectories of all particles backwards in time with only the external magnetic field. This step is necessary to calculate the LW fields at the initial time. At this point, we must check the rest frame fields are not so strong as to render a classical description inappropriate $\chi_0 \approx 5.4 \times 10^{-4}$, where the quantum parameter in a constant magnetic field is defined as

$$\chi_0 = \frac{\gamma_0 B}{B_{\mathrm{cr}}}\sin(\alpha). \tag{5.35}$$

With the velocity distribution and magnetic field defined above, we create a neutral cylinder containing 5000 electrons and 5000 positrons ($N = 10^4$ total particles) *parallel to the magnetic field*, as opposed to being parallel to the initial velocity, with length $L = 10\lambda_\parallel$ and radius $R = 2R_0$, where $\lambda_\parallel = 2\pi/\omega_\parallel$. The cylinder radius is chosen to be comparable to the Larmor value such that the $e^-/e^+$ are continuously interacting in a re-collision process, which previously produced strong collective behaviour in a laser pulse. It is less clear how the cylinder length

should be chosen, yet we expect any instability to occur on the scale of the emitted wavelengths $\lambda_\parallel$ within this cylinder. For the parameters listed here, $R_0 \approx 4.0\,\text{nm}$ is the initial Larmor radius and $\lambda_\parallel = 2\pi/\omega_\parallel \approx 29.4\,\text{nm}$ the typical wavelength emitted parallel to the magnetic field. The cylindrical beam is of uniform density $n_0 \approx 1.7 \times 10^{21}\,\text{particles/cm}^3$, such that the average interparticle distance in this frame of reference is $d \sim (1/n_0)^{1/3} \approx 0.84\,\text{nm}$. As the density and Lorentz factor are nearly identical to those used previously [see Tab. 4.1], the same argument applies that our simulations can be considered reliable if the interparticle distance in the rest frame exceeds the Bohr radius for Positronium by an order of magnitude or more [see Eq. (4.16)]. To resolve the LW fields between neighbouring particles, we choose a small time step $\Delta t = d/15 \approx 1.9 \times 10^{-19}\,\text{sec}$, and the simulation runs for $150\,T_0$ cycles, where $T_0 = 2\pi\gamma_0/|\omega_B|$ is the initial period of oscillation.

When solving the reduced LL equation of motion numerically (2.32), we consider either the external magnetic field only ('B-field only'), or the external and interparticle fields ('B-field & interparticle' fields). Having demonstrated the unfavourable results obtained with only one species of particles in the previous chapter, we see little reason to include the 'intraspecies fields' case here.

Finally, we briefly mention the applicability of our simulation parameters to astrophysical regimes. It is clear that one could easily find a magnetic field of this strength, perhaps in the inner magnetosphere of a pulsar. It is somewhat more challenging to find regions where the $e^-/e^+$ are co-propagating. Primary $e^-/e^+$ pairs are ejected from the gaps (e.g. at the poles) and tend to be accelerated rapidly by the electric field in opposite directions. Therefore, we suggest to consider the secondary $e^-/e^+$ pairs, which are more likely to be co-propagating and radiating in the synchrotron regime, which Cheng & Zhang [100] define as $\sin\alpha \gg R_0/\rho_0$. For our parameters, one can see this condition will be satisfied for any reasonable estimate of the radius of curvature, which will be many kilometres long. As before with the laser pulse, the most severe condition is the low energy and momentum spread; there is no clear reason why this should be respected in nature.

## 5.4 Simulation results

The simulation results are presented in Fig. 5.2, and we will attempt to interpret them here. First, consider how the total kinetic energy of the cylindrical beam varies over time, in Fig. 5.2 (d). With only the external 'B-field', the beam loses energy incoherently. The time scale is not long enough to see the exponential decay described earlier (5.8b), here we observe only a tangent. With the Lorentz factor written as a function of the coordinate time, derived earlier in Eq. (3.21), we can show the kinetic energy of one particle will be 0.993% of its initial value at $150\,T_0$, which provides excellent agreement with Fig. 5.2 (d), validating our numerical integrator for the (reduced) LL equation. When interparticle fields are included, we

initially see a rapid, coherently amplified loss of energy until $t = 50T_0$. After this initial stage, the gradient of both curves tends to converge. With the results of the previous chapter in mind, we interpret this to mean a rapid coherent emission occurs, followed by an expansion in phase space which kills the coherence, and subsequently the particles radiate only incoherently (as determined by the external field).

This behaviour is reflected by the final particle energies shown in Fig. 5.2 (b). With interparticle fields, one observes an additional energy loss up to approximately 2% greater than what would be predicted with only the external magnetic field. As seen with the laser in Fig. 4.2 (i-l), this energy loss is inhomogeneous as the electromagnetic field observed differs from one particle to another, leading to the phase space expansion alluded to above.

To check our interpretation is consistent, we can consult the spectrum of energy radiated along the magnetic field (per unit frequency, per unit solid angle). Here Fig. 5.2 (a) shows the total energy radiated while Fig. 5.2 (c) shows only the incoherent emission, a comparison then allows us to identify the degree of coherent amplification at a given frequency. Indeed, we observe partial coherent amplification of about one order of magnitude around frequency $10^{-1}\omega_{\parallel} \approx 42\,\mathrm{eV}$, when comparing the total energy radiated (with interparticle fields) to the incoherent case. With only the external magnetic field, significant destructive interference occurs at low frequencies around $10^{-2}\omega_{\parallel}$ in the total energy radiated; compared with this, the introduction of interparticle fields dramatically increases emission by around two orders of magnitude, at low frequencies from $10^{-1} - 10^{-2}\omega_{\parallel}$.

As expected, we observe a strong peak in spectrum of emitted radiation, yet this does not occur at the Doppler shift from the longitudinal velocity $\omega_{\parallel}$. Instead, the peak is red-shifted and appears at frequency $\omega_{\mathrm{pk}} \approx 0.43\omega_{\parallel}$. The explanation for this is not entirely clear, so we shall list a few possibilities. Our estimate for $\omega_{\parallel}$ depends only on the initial, longitudinal velocity which is conserved in the single particle picture (even when radiation reaction is accounted for). It could be that the inclusion of interparticle fields breaks this assumption, and provides a force parallel to the external magnetic field. If true, this would be difficult to account for, as one would expect the longitudinal velocity and frequency of this peak to vary over time, yet the results presented here are time integrated (which is necessary as the LW fields are not simultaneously defined). Alternatively, perhaps we have neglected some important role of the geometry, such as the pitch angle $\alpha$, in the re-collision process.

We can calculate a wavelength $\lambda_{\mathrm{pk}} = 2\pi/\omega_{\mathrm{pk}} \approx 6.8\,\mathrm{nm}$ corresponding to the frequency of the peak in Fig. 5.2 (a). Now, consider the spatial distribution of the $e^-/e^+$ at time $t = 37.5T_0$ shown in Fig. 5.3, which is optimal for observing any instability as it occurs during the period of coherent emission [see $t < 50T_0$ in Fig. 5.2 (d)]. One can see the development of micro-bunches within the cylindrical beam in Fig. 5.3 (a). This appears to generalise the behaviour previously seen

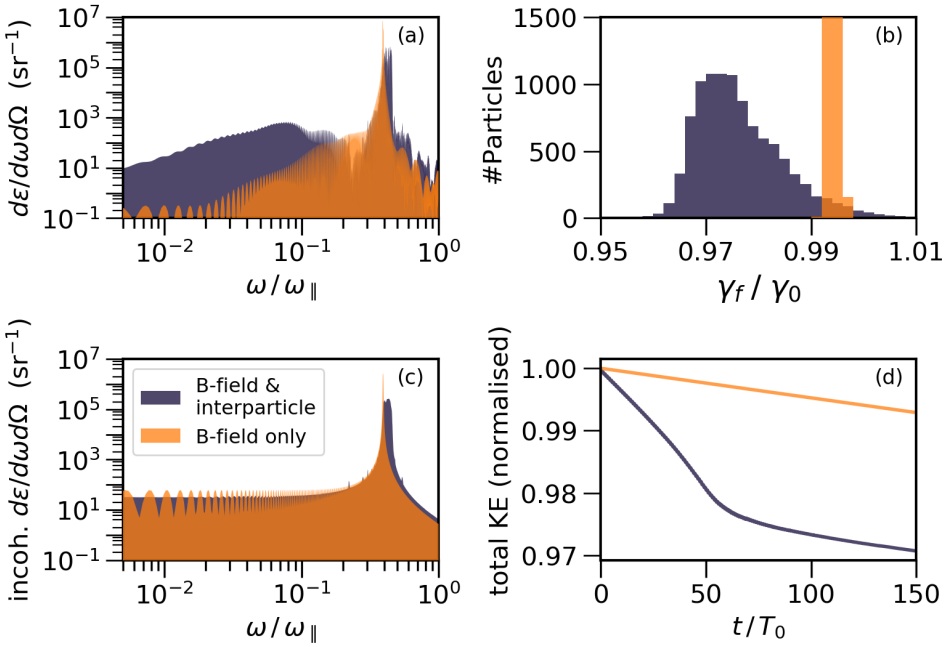


Figure 5.2: Simulation results for a neutral, relativistic and cylindrical $e^-/e^+$ beam propagating in a constant and uniform magnetic field, with various cases for the fields utilised when solving the (reduced) LL equation. Legend in (c) applies to all plots (a-d). The total (a) and incoherent (c) spectrum of energy radiated along the magnetic field is shown, together with a histogram of the final Lorentz factors of all particles in (b), while (d) shows how the total kinetic energy varies over time.

with the laser pulse in Fig. 4.3. By demonstrating that micro-bunching of this type can self-generate within a uniform beam of $e^-/e^+$, one could perhaps relax the stringent requirements on the position and momentum needed for coherence. One could imagine such strict conditions are necessary to maintain a localised, coherently emitting bunch, but may not as strict in the case of a uniformly dense beam. The longitudinal profile of the cylindrical beam is shown in Fig. 5.3 (b). With only the external magnetic field, the beam remains uniformly dense, as expected. Yet, if interparticle fields are included when solving the LL equation, one can see a weak micro-bunching effect. The two left-most peaks are separated by a distance similar to the peak wavelength $\lambda_{\text{pk}}$, suggesting these results are at least consistent with the spectrum of radiation emitted. The puzzle of why $\lambda_{\text{pk}}$, which was measured from the spectrum and not predicted from theory, is favoured over $\lambda_\parallel \approx 2.9\,\text{nm}$ remains unanswered. However, we do note the two right-most peaks are closer together than $\lambda_\parallel$, and have almost merged. With the laser, we could identify the FWHM of the peaks and relate this to the coherent amplification of the spectrum. It challenging to perform any such measurement here, as no single peak is dominant or easily distinguishable from the rest and so any attempt would likely be inaccurate.

This system becomes yet more complex when we recall the time dependence. The

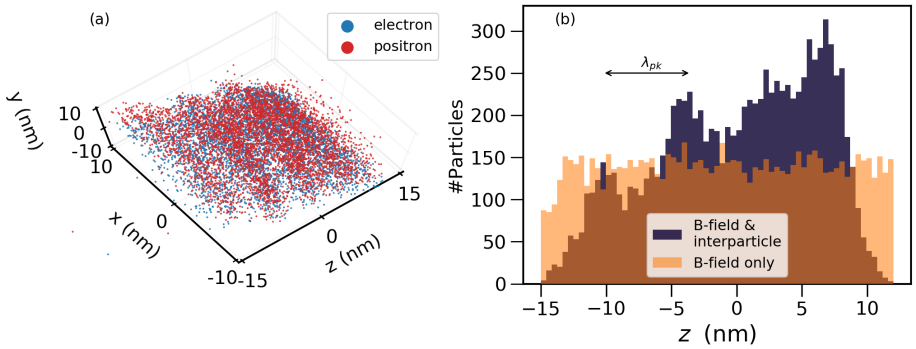


Figure 5.3: Illustration of the weak, longitudinal micro-bunching which occurs along the magnetic field axis ($z$), in 3D (a) and 2D (b), at time $t = 37.5\,T_0$.

full time evolution of the beam can be seen with a *video* in the supplementary material [110]. As with the laser pulse, we can compare side-by-side solutions of the LL equation with the external magnetic field only, and solutions including interparticle fields in addition to the external field. Each frame is centred on the average $z$ coordinate of the beam, at that instant of time. Here, one notices the development of the instability described above at around 30-35 s, which seems to have collapsed by around 1 min, and is followed by a gradual expansion in phase space, particularly in the longitudinal direction. In short, it appears the beam self-modulates, emits coherently, expands and begins to emit incoherently; and so the effect is transient as we saw with the laser pulse. We point out that this is consistent with the inhomogeneous loss of energy, and phase space expansion observed in Fig. 5.2 (b).

# Conclusion and outlook

The central, motivating idea behind this thesis was the extension of the classical radiation reaction formalism, specifically the Landau-Lifshitz equation of motion, to systems of many point particles. The original derivations of the self-force in the early $20^{\text{th}}$ were imposed by *consistency* with the principle of energy-momentum conservation. At this time, radiation reaction was merely a theoretical curiosity; an apparently irrelevant problem of little importance given the available experimental equipment of the day, or the limited knowledge of exotic, compact astrophysical objects. Over half a century passed before the status quo began to change. We have proceeded in much the same way, arguing by *consistency*, that one cannot in principle treat charged particles independently in an external field without violating energy-momentum conservation.

Following this logic, we set out to find regimes in which the inclusion of fields from neighbouring point particles (interparticle fields) would play a significant role in the dynamics, and therefore spectra of radiation emitted from the system in question. To that end, in chpater 3 we developed a code optimised for the GPU, capable of numerically integrating the equations of motion and radiation spectra in a self-consistent manner. This was tested against exact solutions in the case of a constant and uniform magnetic field.

The first scenario we considered was the collision of a counter-propagating laser pulse, and $e^-/e^+$ bunch, in chapter 4. To begin, we characterised the trajectory and spectrum of radiation reflected along the wave propagation axis, by a single particle. From the properties of the emitted radiation, we suggested how to tune the laser amplitude and bunch size to observe coherent emission. In running numerical simulations with these parameters, we observed a plethora of interesting behaviour. The coherent emission at low frequencies, along the propagation axis, induced a micro-bunching effect on the sub-nanometre scale. This in turn lead to coherent amplification of the radiation spectrum, across a broad range of frequencies in the soft X-ray domain. The $e^-/e^+$ re-collision process in the presence of a linearly polarised laser, was particularly conducive to coherent emission, and highlighted the importance of considering both species of particles. One might expect this mechanism was self-reinforcing, however, in the process of coherent emission each particle experienced a distinct electromagnetic field, which lead to an inhomogeneous energy loss and therefore expansion in phase space, which eventually suppressed coherent emission. At least in vacuum, the behaviour studied here was therefore transient. In the process, we demonstrated the previously suggested model of treating a bunch of $N$ particles as one particle with effective classical electron radius $Nr_e$, was unable to describe the inhomogeneous energy loss.

While the instabilities and coherent emission outlined above are particularly interesting, the key difficulty remains the experimental feasibility of the parameters suggested. The peak density of electrons and positrons utilised in our simulations is high $\sim 10^{21}$ particles/cm$^3$. This is still well below solid density, and previous suggestions for collective radiation reaction have considered even higher densities [19, 20], yet this is clearly challenging to obtain with current experimental methods. For reference, Sarri et al achieved a density in the order of $10^{17}$ particles/cm$^3$. While the angular spread was a reasonable 1 mrad, the tiny energy spread imposes an even more restrictive condition than the density. We attempted to resolve this problem by suggesting the use of a magnetic chicane compressor, arguing that a loss of charge and current imposed by selecting a tiny range of energies was not a problem, as we required only a miniscule number of particles $\sim 10^4$.

Ultimately, the difficulty here lies in disentangling the physical requirements for observing this collective behaviour from the limitations of our numerical approach. As the reduced Landau-Lifshitz equation has, to our knowledge, never been solved for many point particles, we chose to proceed from first principles using the Liénard–Wiechert fields. In doing so, we hoped to instil a certain amount of confidence that our results would be physically correct. All behaviour mediated by classical electromagnetism, including instabilities as seen in plasma physics and collisions, would be automatically included. However, this severely constrained the number of bodies we could consider, and the time scales we could simulate (as the computational cost per time step scales with $O(N^2)$). It is difficult then, to state whether the microscopic instability studied here could occur on a larger scale, in a macroscopic plasma. It is tempting to suggest that we should utilise a Particle-in-Cell code to simulate a macroscopic system, but it is far from self-evident that these codes can (even if the resources are unlimited) include the full interplay of coherent emission, radiation reaction and crucially, phase space expansion on a microscopic level, likely due to collisions. If the latter is neglected, the results could be misleadingly optimistic.

As a final note about the parameters considered in chapter 4, we refer to the properties of the laser pulse in Tab. 4.2. We considered two lasers, of central wavelength 400 nm and 100 nm. The former is readily available in the laboratory, and even in this case we saw strong collective behaviour and coherent emission, from a disc-like structure [see Fig. 4.3 (b)]. Yet, in this case there was only a tiny impact from the self-force. With the 100 nm laser, we saw stronger energy losses and coherent emission including a significant role from the self-force, however this wavelength and intensity are more speculative given current technology. In short, we seem to be in a better position than the theorists who studied radiation reaction near a century ago, which we alluded to at the beginning of this conclusion; we have studied a variety of interesting collective behaviours, some of these regimes are readily accessible (400 nm laser) and some are a remote prospect (100 nm laser).

In the interests of demonstrating that this 'collective radiation reaction' can apply to a general, external electromagnetic field, we sought to reproduce similar results in a constant and uniform magnetic field. The field strength $B \sim 10^6$ T discussed in chapter 5 is far beyond what can be achieved in the laboratory, yet this is thought to be easily accessible in the presence of compact, astrophysical objects such as a pulsar. We argued that primary $e^-/e^+$ pairs ejected from polar gaps tend to be too relativistic to be of relevance, and in any case, these particles would be accelerated in opposite directions by the electric field, yet we require almost co-propagating particles. Instead, we argued weakly relativistic, secondary $e^-/e^+$ pairs offer a better candidate as an application for our results.

For the magnetic field, we began as with the laser pulse, by evaluating the trajectory and spectrum of radiation emitted by a single particle. In particular, we identified the relatively low frequency radiation emitted along the magnetic field lines as being of particular interest, in the synchrotron regime. From our simulations, we observed a magnetic field induced instability with subsequent signs of coherent emission along the magnetic field. This effect was weaker than that observed in a laser pulse. In this regime, both collective behaviour and a strong impact from the self-force were evident [see Fig. 5.2]. As it stands, our argument that these results would have relevance towards the dynamics of the pulsar magnetosphere is incomplete. We see a couple of methods to proceed: (i) one could argue that a plasma similar to that which we have modelled might exist in the inner magnetosphere. It seems unlikely that plasmas with a density in the order of $\sim 10^{21}$ particles/cm$^3$ might exist there; this is about ten orders of magnitude larger than the Goldreich-Julian density typical of a young pulsar. The more important problem remains the initial energy spread; there is no reason to believe why such a restrictive condition would be satisfied in nature. Yet, this requirement was imposed to maintain a localised bunch of $e^-/e^+$ in chapter 4, and so we are optimistic that this condition can be relaxed in a uniformly dense plasma (assuming this resembles what one might see in nature). Alternatively (ii), we could rescale our simulation results to lower densities and weaker magnetic fields, which would become more applicable to nature. The instability may well survive this procedure, however the impact from radiation reaction is intrinsically scale dependent (on the classical electron radius), and so would likely be negligible at weaker fields.

# Appendix A

## Ballistic expansion of a Gaussian bunch

> *"...vether it's worth while goin' through so much, to learn so little,*
> *as the charity boy said ven he got to the end of the alphabet,*
> *is a matter o' taste"*
>
> — Charles Dickens, *The Pickwick Papers* (Ch. 27)

This appendix has been included to demonstrate how the standard deviation of a Gaussian bunch of particles will evolve over time, providing the trajectory of each particle is ballistic.

Consider a bunch of $N$ particles at time $t = 0$ described by a distribution function $f(\boldsymbol{x}, \boldsymbol{u})$, which represents the density of particles per unit of phase space, and is normalisable

$$N = \iint_{-\infty}^{+\infty} f(\boldsymbol{x}, \boldsymbol{u})\, d^3\boldsymbol{x} d^3\boldsymbol{u}. \tag{A.1}$$

We would like to consider how the distribution in space varies over time given some initial position and velocity spread, specifically for a bunch of particles as one might produce in the laboratory. Consider then, a cold bunch of particles centred at the origin. We will find it convenient to separate the distribution function into parts $f(\boldsymbol{x}, \boldsymbol{u}) = f_{\boldsymbol{x}}(\boldsymbol{x})\, f_{\boldsymbol{u}}(\boldsymbol{u})$. If the bunch is a spherically symmetric Gaussian in position space, with standard deviation $\sigma_e$ in each dimension at $t = 0$, we can write the number density of particles as

$$f_{\boldsymbol{x}}(\boldsymbol{x}) = \frac{N}{(2\pi)^{3/2}\sigma_e^3}\, e^{-\frac{1}{2\sigma_e^2}\boldsymbol{x}^2}. \tag{A.2}$$

We can also adopt a Gaussian distribution for the velocity with no particular symmetry

$$f_{\boldsymbol{v}}(\boldsymbol{v}) = \frac{1}{(2\pi)^{3/2}\sigma_{v_x}\sigma_{v_y}\sigma_{v_z}}\, e^{-\frac{1}{2\sigma_{v_x}^2}(v_x - v_{0,x})^2 - \frac{1}{2\sigma_{v_y}^2}(v_y - v_{0,y})^2 - \frac{1}{2\sigma_{v_z}^2}(v_z - v_{0,z})^2}. \tag{A.3}$$

When multiplied and integrated over all phase space, these functions satisfy the

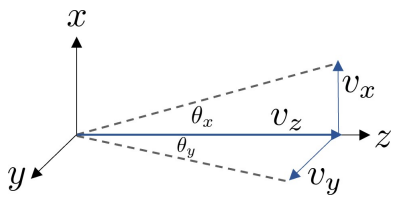


Figure A.1: Velocity distribution for small angles around z-axis

normalisation defined in Eq. (A.1). However, in the laboratory, one usually considers a small momentum spread around a given axis (in our case, the z-axis, as can be seen in Fig. A.1), and so it is customary to use polar coordinates:

$$v_x = v_0 \tan\theta_x \approx v_0\theta_x, \tag{A.4a}$$

$$v_y = v_0 \tan\theta_y \approx v_0\theta_y, \tag{A.4b}$$

$$v_z = \frac{v_0}{\sqrt{1 + \tan^2\theta_x + \tan^2\theta_y}} \approx v_0. \tag{A.4c}$$

Where $v_0 = \sqrt{v_{0,x}^2 + v_{0,y}^2 + v_{0,z}^2}$ is the mean speed at $t = 0$, separated into Cartesian coordinates. The approximation indicates only terms up to first order in the angular spread are considered. This corresponds to the following, approximate probability density in velocity space

$$f_{\boldsymbol{v}}(\boldsymbol{v}) \approx \frac{1}{(2\pi)^{3/2}\, v_0^2 \sigma_\vartheta^2 \sigma_v}\, e^{-\frac{1}{2\sigma_v^2}(v-v_0)^2 - \frac{1}{2\sigma_\vartheta^2}\vartheta^2}. \tag{A.5}$$

Here we have imposed cylindrical symmetry $\sigma_{\theta_x} = \sigma_{\theta_y} \equiv \sigma_\vartheta$, and defined $\vartheta = \sqrt{\theta_x^2 + \theta_y^2}$ providing the angular spread is small in both dimensions, $x$ and $y$. With Cartesian coordinates, the Gaussian vanishes at the limits of integration and is exactly normalisable. For polar coordinates this is no longer the case. Therefore, function $f_{\boldsymbol{v}}(\boldsymbol{v})$ can only be interpreted as an approximate probability density, providing the angular spread is far smaller than the sphere's surface $\sigma_\vartheta \ll 4\pi$, and the velocity never approaches zero, $v_0 > 0$ and $\sigma_v \ll v_0$, at which the distribution function would diverge and not be normalisable. This problem would not emerge if one was considering a thermal energy spread, described by a Maxwell-Boltzmann distribution, as this function would correctly converge to zero as $v_0 \to 0$. Yet, it would have other undesirable properties, such as restricting our ability to vary the mean velocity and velocity spread independently. From the equations above, we can generate a bunch of particles propagating along the z-axis. Now we consider how the bunch expands over time. At first approximation, we neglect interparticle

fields and assume particles within the bunch move ballistically $\boldsymbol{x}(t) = \boldsymbol{x}_0 + \boldsymbol{v}t$. Then we can find the expected values of the position and its square, to determine the variance of the position (in 3D)

$$\langle \boldsymbol{x}(t) \rangle = \langle \boldsymbol{x}_0 \rangle + \langle \boldsymbol{v} \rangle t, \tag{A.6a}$$

$$\langle \boldsymbol{x}^2(t) \rangle = \langle \boldsymbol{x}_0^2 \rangle + 2\langle \boldsymbol{x}_0 \rangle \cdot \langle \boldsymbol{v} \rangle + \langle \boldsymbol{v}^2 \rangle t^2, \tag{A.6b}$$

$$\sigma_{\boldsymbol{x}}^2(t) = \langle \boldsymbol{x}^2(t) \rangle - \langle \boldsymbol{x}(t) \rangle^2 \Rightarrow \sigma_{\boldsymbol{x}_0}^2 + \sigma_{\boldsymbol{v}}^2 t^2. \tag{A.6c}$$

Where the expectation values are defined by integrating over phase space, e.g.

$$\langle \boldsymbol{x} \rangle = \int_{-\infty}^{+\infty} \boldsymbol{x}\, f(\boldsymbol{x}) \left\{ \int_{-\infty}^{+\infty} f(\boldsymbol{v})\, d^3\boldsymbol{v} \right\} d^3\boldsymbol{x} = \int_{-\infty}^{+\infty} \boldsymbol{x}\, f(\boldsymbol{x})\, d^3\boldsymbol{x}, \tag{A.7a}$$

$$\langle \boldsymbol{v} \rangle = \int_{-\infty}^{+\infty} f(\boldsymbol{x}) \left\{ \int_{-\infty}^{+\infty} \boldsymbol{v}\, f(\boldsymbol{v})\, d^3\boldsymbol{v} \right\} d^3\boldsymbol{x} = N \int_{-\infty}^{+\infty} \boldsymbol{v}\, f(\boldsymbol{v})\, d^3\boldsymbol{v}, \tag{A.7b}$$

and similar integrals apply for $\langle \boldsymbol{x}^2 \rangle$ and $\langle \boldsymbol{v}^2 \rangle$. The variance of the initial position $\sigma_{\boldsymbol{x}_0}^2 = 3\sigma_e^2$ and velocity $\sigma_{\boldsymbol{v}}^2 \approx 2v_0^2\sigma_\vartheta^2 + \sigma_v^2$ can be separated into their respective Cartesian components, which add by quadrature. Separating the variance of the position at time $t$ into its components $\sigma_{\boldsymbol{x}}^2(t) = \sigma_x^2(t) + \sigma_y^2(t) + \sigma_z^2(t)$, we recognise the bunch will not have spherical symmetry at $t > 0$ if the initial velocity distribution is anisotropic, as is the case here. Following this logic, we can rewrite the standard deviation at time $t$ from Eq. (A.6c)

$$\sigma_{\boldsymbol{x}}(t) \approx \sqrt{3\sigma_e^2 + (\sigma_v^2 + 2v_0^2\sigma_\vartheta^2)\, t^2}. \tag{A.8}$$

Instead of referring to a spread in the initial speed $\sigma_v$, it is customary to refer to a variation in the initial kinetic energy $\mathrm{KE}_0 = m_e(\gamma_0 - 1)$ where $\gamma_0 = 1/\sqrt{1 - v_0^2}$. Yet we can easily exchange between speed and kinetic energy with a first-order Taylor expansion, providing the variance is small

$$\sigma_v \approx \frac{\gamma_0 - 1}{\gamma_0^3 v_0} \frac{\sigma_{\mathrm{KE}}}{\mathrm{KE}_0}. \tag{A.9}$$

In summary, providing one knows the initial spread in position and momentum space of a Gaussian bunch, we can determine the spread in position at a later time, providing the particles within the bunch propagate ballistically.

# Appendix B

## Stationary phase approximation: exponentially suppressed terms

The purpose of this appendix is to demonstrate why the statement $|\mathcal{I}_+|^2 \ll |\mathcal{I}_-|^2$ is justified, when using the stationary phase method. The integral $\mathcal{I}_+$ can be written in the following way, from Eq. (5.17)

$$\mathcal{I}_+ = \omega v_{0,\perp} \int_0^{+\infty} \gamma\, e^{-\omega_d \tau}\, e^{i\Phi}\, d\tau \tag{B.1a}$$

$$\Phi = +|\omega_B|\tau + \omega(1 - v_{0,\parallel})\, t. \tag{B.1b}$$

The first derivative of the integral phase is given by

$$\Phi' = |\omega_B|\left(1 + \varpi \frac{\gamma}{\gamma_{0,\parallel}}\right). \tag{B.2}$$

For positive frequencies $\omega > 0$, there are no, real stationary points $\varphi_*$ which satisfy $\Phi'_* = \Phi'(\varphi_*) = 0$. In this case, the leading order behaviour can be identified with an integration by parts

$$\mathcal{I}_+ = \omega v_{0,\perp} \int_0^{+\infty} \frac{\gamma}{i\Phi'}\, e^{-\omega_d \tau}\, d\left(e^{i\Phi}\right) \tag{B.3a}$$

$$\Rightarrow \omega v_{0,\perp} \left[\frac{\gamma}{i\Phi'}\, e^{-\omega_d \tau}\, e^{i\Phi}\right]_0^{+\infty} - \omega v_{0,\perp} \int_0^{+\infty} \frac{d}{d\tau}\left(\frac{\gamma}{i\Phi'}\, e^{-\omega_d \tau}\right) e^{i\Phi}\, d\tau. \tag{B.3b}$$

Differentiation will incur additional powers of the damping frequency, and therefore the small quantity $|\omega_B|\tau_e$. When applying the stationary phase approximation, one considers the limit $\omega \to +\infty$, for which the oscillatory terms begin to oscillate rapidly. Intuitively, we expect the integral of a rapidly oscillating function will tend to zero more quickly than the function itself (more formally, one can apply the Riemann-Lebesgue lemma). The boundary terms then provide the leading order behaviour. The term at the upper limit vanishes, leaving only the lower limit

$$\mathcal{I}_+ \approx \frac{i\omega}{|\omega_B|\left(\varpi + \frac{\gamma_{0,\parallel}}{\gamma_0}\right)} \sqrt{1 - \frac{\gamma_{0,\parallel}^2}{\gamma_0^2}}\,. \tag{B.4}$$

Where we have used the on-shell condition to simplify [see Eq. (5.9)]. The approximation indicates that higher order terms we have neglected, from the integration by parts above. In practice, it is the square modulus that we must evaluate

$$|\mathcal{I}_+|^2 \approx \frac{\omega^2\left(1 - \frac{\gamma_{0,\parallel}^2}{\gamma_0^2}\right)}{\omega_B^2\left(\varpi + \frac{\gamma_{0,\parallel}}{\gamma_0}\right)^2} \sim \frac{\omega^2}{\omega_B^2}. \tag{B.5}$$

The last order of magnitude estimate essentially recognises the terms inside the brackets are typically in the order of unity, or less. Comparing this with our equation for $|\mathcal{I}_-|^2$ [utilised in deriving (5.33)], where we can also neglect terms in the order of unity, one can see

$$|\mathcal{I}_-|^2 \sim \frac{\omega^2}{|\omega_B|\omega_d}, \tag{B.6}$$

one can take the ratio of these integrals to find

$$\frac{|\mathcal{I}_+|^2}{|\mathcal{I}_-|^2} \sim \frac{\omega_d}{|\omega_B|} \equiv |\omega_B|\tau_e. \tag{B.7}$$

As discussed earlier in chapter 5, this quantity is always small in the classical regime, and so the approximation $|\mathcal{I}_+|^2 \ll |\mathcal{I}_-|^2$ is justified. Even at the critical field of QED this quantity is tiny

$$|\omega_B|\tau_e \sim 10^{-5}.$$

# Bibliography


[1] M. J. Quin, A. D. Piazza, C. H. Keitel, and M. Tamburini, Interparticle-fields amplified radiation reaction (2023), arXiv:2306.17832 [physics.plasm-ph] .

[2] S. Bohlen, Z. Gong, M. J. Quin, M. Tamburini, and K. Põder, Colliding pulse injection of polarized electron bunches in a laser-plasma accelerator (2023), arXiv:2304.02922 [physics.acc-ph] .

[3] Z. Gong, M. J. Quin, S. Bohlen, C. H. Keitel, K. Põder, and M. Tamburini, Spin-polarized electron beam generation in the colliding-pulse injection scheme (2023), arXiv:2303.16966 [physics.acc-ph] .

[4] M. Abraham, *Theorie der Elektrizität Vol. II Elektromagnetische Theorie der Strahlung* (B.G. Teubner, 1905).

[5] P. A. M. Dirac, Proc. Roy. Soc. Lond. A **167**, 148 (1938).

[6] F. Rohrlich, *Classical Charged Particles*, 3rd ed. (World Scientific, 2007).

[7] F. Rohrlich, Physics Letters A **283**, 276 (2001).

[8] L. D. Landau and E. M. Lifshitz, *The Classical Theory of Fields*, 2nd ed. (Elsevier, Oxford, 1975).

[9] R. T. Hammond, Phys. Rev. A **81**, 062104 (2010).

[10] D. Gromes, (2015), arXiv:1507.05736 [physics.class-ph] .

[11] D. Strickland and G. Mourou, Optics Communications **56**, 219 (1985).

[12] K. Poder, M. Tamburini, G. Sarri, A. Di Piazza, S. Kuschel, C. D. Baird, K. Behm, S. Bohlen, J. M. Cole, D. J. Corvan, M. Duff, E. Gerstmayr, C. H. Keitel, K. Krushelnick, S. P. D. Mangles, P. McKenna, C. D. Murphy, Z. Najmudin, C. P. Ridgers, G. M. Samarin, D. R. Symes, A. G. R. Thomas, J. Warwick, and M. Zepf, Phys. Rev. X **8**, 031004 (2018).

[13] J. M. Cole, K. T. Behm, E. Gerstmayr, T. G. Blackburn, J. C. Wood, C. D. Baird, M. J. Duff, C. Harvey, A. Ilderton, A. S. Joglekar, K. Krushelnick, S. Kuschel, M. Marklund, P. McKenna, C. D. Murphy, K. Poder, C. P. Ridgers, G. M. Samarin, G. Sarri, D. R. Symes, A. G. R. Thomas, J. Warwick, M. Zepf, Z. Najmudin, and S. P. D. Mangles, Phys. Rev. X **8**, 011020 (2018).

[14] C. F. Nielsen, J. B. Justesen, A. H. Sørensen, U. I. Uggerhøj, and R. Holtzapple (CERN NA63), New Journal of Physics **23**, 085001 (2021).

[15] C. F. Nielsen, J. B. Justesen, A. H. Sørensen, U. I. Uggerhøj, and R. Holtzapple (CERN NA63), Phys. Rev. D **102**, 052004 (2020).

[16] A. Di Piazza, T. N. Wistisen, and U. I. Uggerhøj, Physics Letters B **765**, 1 (2017).

[17] J. Pétri, Monthly Notices of the Royal Astronomical Society **484**, 5669 (2019).

[18] J. Pétri, Astronomy and Astrophysics **666** (2022).

[19] A. E. Kaplan and P. L. Shkolnikov, Phys. Rev. Lett. **88**, 074801 (2002).

[20] P. Smorenburg, L. Kamp, G. Geloni, and O. Luiten, Laser and Particle Beams **28**, 553–562 (2010).

[21] I. Kimel and L. R. Elias, Phys. Rev. Lett. **75**, 4210 (1995).

[22] J. Schwinger, Foundations of Physics **13**, 373 (1983).

[23] J. D. Jackson, *Classical Electrodynamics*, 3rd ed. (John Wiley and Sons, Inc., 1998).

[24] C. Teitelboim, Phys. Rev. D **1**, 1572 (1970).

[25] C. Teitelboim, Phys. Rev. D **3**, 297 (1971).

[26] C. Teitelboim, Phys. Rev. D **4**, 345 (1971).

[27] T. Erber, Fortschritte der Physik **9**, 343 (1961).

[28] C. J. Eliezer, Rev. Mod. Phys. **19**, 147 (1947).

[29] H. Spohn, Europhysics Letters **50**, 287 (2000).

[30] R. Ekman, T. Heinzl, and A. Ilderton, New Journal of Physics **23**, 055001 (2021).

[31] T. N. Wistisen, A. Di Piazza, H. V. Knudsen, and U. I. Uggerhøj, Nature Communications **9**, 795 (2018).

[32] T. N. Wistisen, A. Di Piazza, C. F. Nielsen, A. H. Sørensen, and U. I. Uggerhøj (CERN NA63), Phys. Rev. Res. **1**, 033014 (2019).

[33] A. Di Piazza, Lett. Math. Phys. **83**, 305 (2008).

[34] A. I. Nikishov and V. I. Ritus, Sov. Phys. JETP **19**, 529 (1964).

[35] A. I. Nikishov and V. I. Ritus, Sov. Phys. JETP **19**, 1191 (1964).

[36] C. Bula, K. T. McDonald, E. J. Prebys, C. Bamber, S. Boege, T. Kotseroglou, A. C. Melissinos, D. D. Meyerhofer, W. Ragg, D. L. Burke, R. C. Field, G. Horton-Smith, A. C. Odian, J. E. Spencer, D. Walz, S. C. Berridge, W. M. Bugg, K. Shmakov, and A. W. Weidemann, Phys. Rev. Lett. **76**, 3116 (1996).

[37] Y. Hadad, L. Labun, J. Rafelski, N. Elkina, C. Klier, and H. Ruhl, Phys. Rev. D **82**, 096012 (2010).

[38] A. Hosak and A. Di Piazza, European Physical Journal D **76**, 200 (2022).

[39] S. G. Rajeev, Annals of Physics **323**, 2654 (2008).

[40] H. Heintzmann and E. Schrüfer, Physics Letters A **43**, 287 (1973).

[41] M. Tamburini, F. Pegoraro, A. Di Piazza, C. H. Keitel, and A. Macchi, New J. Phys. **12**, 123005 (2010).

[42] M. Tamburini, *Radiation reaction effects in superintense laser-plasma interaction*, PhD thesis, University of Pisa (2011).

[43] M. Vranic, J. Martins, R. Fonseca, and L. Silva, Computer Physics Communications **204**, 141 (2016).

[44] A. V. Borisov and Y. V. Grats, Soviet Physics Journal **15**, 377 (1972).

[45] J. Derouillat, A. Beck, F. Pérez, T. Vinci, M. Chiaramello, A. Grassi, M. Flé, G. Bouchard, I. Plotnikov, N. Aunai, J. Dargent, C. Riconda, and M. Grech, Computer Physics Communications **222**, 351 (2018).

[46] T. D. Arber, K. Bennett, C. S. Brady, A. Lawrence-Douglas, M. G. Ramsay, N. J. Sircombe, P. Gillies, R. G. Evans, H. Schmitz, A. R. Bell, and C. P. Ridgers, Plasma Physics and Controlled Fusion **57**, 113001 (2015).

[47] C. K. Birdsall and A. B. Langdon, *Plasma Physics via Computer Simulation* (Taylor and Francis, 1991).

[48] R. W. Hockney and J. W. Eastwood, *Computer Simulation Using Particles* (CRC Press, 1981).

[49] A. Di Piazza, C. Müller, K. Z. Hatsagortsyan, and C. H. Keitel, Rev. Mod. Phys. **84**, 1177 (2012).

[50] A. Gonoskov, T. G. Blackburn, M. Marklund, and S. S. Bulanov, Rev. Mod. Phys. **94**, 045001 (2022).

[51] A. Fedotov, A. Ilderton, F. Karbstein, B. King, D. Seipt, H. Taya, and G. Torgrimsson, Physics Reports **1010**, 1 (2023).

[52] J. Barnes and P. Hut, Nature **324**, 446 (1986).

[53] J. P. Boris, *Proceedings of the Fourth Conference on Numerical Simulation of Plasmas* (Naval Research Laboratory, Washington D.C., 1970) p. 3.

[54] H. Qin, S. Zhang, J. Xiao, J. Liu, Y. Sun, and W. M. Tang, Physics of Plasmas **20**, 084503 (2013).

[55] J. Koga, T. Z. Esirkepov, and S. V. Bulanov, Physics of Plasmas **12**, 093106 (2005).

[56] S. V. Bulanov, T. Z. Esirkepov, J. Koga, and T. Tajima, Plasma Physics Reports **30**, 196 (2004).

[57] J. W. Cooley and J. W. Tukey, Math. Comput. **19**, 297 (1965).

[58] J. Keiner, S. Kunis, and D. Potts, ACM Trans. Math. Softw. **36** (2009).

[59] G. Sarri, W. Schumaker, A. Di Piazza, M. Vargas, B. Dromey, M. E. Dieckmann, V. Chvykov, A. Maksimchuk, V. Yanovsky, Z. H. He, B. X. Hou, J. A. Nees, A. G. R. Thomas, C. H. Keitel, M. Zepf, and K. Krushelnick, Phys. Rev. Lett. **110**, 255002 (2013).

[60] G. Sarri, K. Poder, J. M. Cole, W. Schumaker, A. di Piazza, B. Reville, T. Dzelzainis, D. Doria, L. A. Gizzi, G. Grittani, S. Kar, C. H. Keitel, K. Krushelnick, S. Kuschel, S. P. D. Mangles, Z. Najmudin, N. Shukla, L. O. Silva, D. Symes, A. G. R. Thomas, M. Vargas, J. Vieira, and M. Zepf, Nature Communications **6**, 6747 (2015).

[61] B. Dromey, M. Zepf, A. Gopal, K. Lancaster, M. S. Wei, K. Krushelnick, M. Tatarakis, N. Vakakis, S. Moustaizis, R. Kodama, M. Tampo, C. Stoeckl, R. Clarke, H. Habara, D. Neely, S. Karsch, and P. Norreys, Nature Physics **2**, 456 (2006).

[62] H. Chen, S. C. Wilks, J. D. Bonlie, S. N. Chen, K. V. Cone, L. N. Elberson, G. Gregori, D. D. Meyerhofer, J. Myatt, D. F. Price, M. B. Schneider, R. Shepherd, D. C. Stafford, R. Tommasini, R. Van Maren, and P. Beiersdorfer, Physics of Plasmas **16**, 122702 (2009).

[63] H. Chen, F. Fiuza, A. Link, A. Hazi, M. Hill, D. Hoarty, S. James, S. Kerr, D. D. Meyerhofer, J. Myatt, J. Park, Y. Sentoku, and G. J. Williams, Phys. Rev. Lett. **114**, 215001 (2015).

[64] H. Chen and F. Fiuza, Physics of Plasmas **30** (2023).

[65] E. S. Sarachik and G. T. Schappert, Phys. Rev. D **1**, 2738 (1970).

[66] V. Y. Kharin, D. Seipt, and S. G. Rykovanov, Phys. Rev. A **93**, 063801 (2016).

[67] N. B. Narozhnyi and M. S. Fofanov, Sov. Phys. JETP **83**, 14 (1996).

[68] M. Ruijter, V. Y. Kharin, and S. G. Rykovanov, Journal of Physics B Atomic Molecular Physics **51**, 225701 (2018).

[69] A. Di Piazza and G. Audagnotto, Phys. Rev. D **104**, 016007 (2021).

[70] A. Di Piazza, Physics Letters B **782**, 559 (2018).

[71] B. King, Classical radiation reaction in red-shifted harmonics (2023), arXiv:2305.14429 [hep-ph] .

[72] C. N. Danson, C. Haefner, J. Bromage, T. Butcher, J.-C. F. Chanteloup, E. A. Chowdhury, A. Galvanauskas, L. A. Gizzi, J. Hein, D. I. Hillier, N. W. Hopps, Y. Kato, E. A. Khazanov, R. Kodama, G. Korn, R. Li, Y. Li, J. Limpert, J. Ma, C. H. Nam, D. Neely, D. Papadopoulos, R. R. Penman, L. Qian, J. J. Rocca, A. A. Shaykin, C. W. Siders, C. Spindloe, S. Szatmári, R. M. G. M. Trines, J. Zhu, P. Zhu, and J. D. Zuegel, High Power Laser Science and Engineering **7** (2019).

[73] Extreme light infrastructure (ELI) whitebook (2011).

[74] S. Gales, K. A. Tanaka, D. L. Balabanski, F. Negoita, D. Stutman, O. Tesileanu, C. A. Ur, D. Ursescu, I. Andrei, S. Ataman, M. O. Cernaianu, L. D'Alessi, I. Dancus, B. Diaconescu, N. Djourelov, D. Filipescu, P. Ghenuche, D. G. Ghita, C. Matei, K. Seto, M. Zeng, and N. V. Zamfir, Reports on Progress in Physics **81**, 094301 (2018).

[75] D. Papadopoulos, J. Zou, C. Le Blanc, G. Chériaux, P. Georges, F. Druon, G. Mennerat, P. Ramirez, L. Martin, A. Fréneaux, and et al., High Power Laser Science and Engineering **4**, e34 (2016).

[76] Central laser facility (CLF) website: Vulcan laser (2023).

[77] S. Y. Mironov, V. N. Ginzburg, V. V. Lozhkarev, G. A. Luchinin, A. V. Kirsanov, I. V. Yakovlev, E. A. Khazanov, and A. A. Shaykin, Quantum Electronics **41**, 963 (2011).

[78] D. L. Burke, R. C. Field, G. Horton-Smith, J. E. Spencer, D. Walz, S. C. Berridge, W. M. Bugg, K. Shmakov, A. W. Weidemann, C. Bula, K. T. McDonald, E. J. Prebys, C. Bamber, S. J. Boege, T. Koffas, T. Kotseroglou, A. C. Melissinos, D. D. Meyerhofer, D. A. Reis, and W. Ragg, Phys. Rev. Lett. **79**, 1626 (1997).

[79] Y. Wang, S. Wang, A. Rockwood, B. M. Luther, R. Hollinger, A. Curtis, C. Calvi, C. S. Menoni, and J. J. Rocca, Opt. Lett. **42**, 3828 (2017).

[80] L. Drescher, O. Kornilov, T. Witting, V. Shokeen, M. J. J. Vrakking, and B. Schütte, Nature Photonics **15**, 263 (2021).

[81] A. R. Bell and J. G. Kirk, Phys. Rev. Lett. **101**, 200403 (2008).

[82] J. G. Kirk, A. R. Bell, and I. Arka, Plasma Physics and Controlled Fusion **51**, 085008 (2009).

[83] J. W. Shearer, J. Garrison, J. Wong, and J. E. Swain, Phys. Rev. A **8**, 1582 (1973).

[84] C. D. Arrowsmith, N. Shukla, N. Charitonidis, R. Boni, H. Chen, T. Davenne, A. Dyson, D. H. Froula, J. T. Gudmundsson, B. T. Huffman, Y. Kadi, B. Reville, S. Richardson, S. Sarkar, J. L. Shaw, L. O. Silva, P. Simon, R. M. G. M. Trines, R. Bingham, and G. Gregori, Phys. Rev. Res. **3**, 023103 (2021).

[85] W. T. Wang, W. T. Li, J. S. Liu, Z. J. Zhang, R. Qi, C. H. Yu, J. Q. Liu, M. Fang, Z. Y. Qin, C. Wang, Y. Xu, F. X. Wu, Y. X. Leng, R. X. Li, and Z. Z. Xu, Phys. Rev. Lett. **117**, 124801 (2016).

[86] C. S. Hue, Y. Wan, E. Y. Levine, and V. Malka, Matter and Radiation at Extremes **8**, 024401 (2023).

[87] Video of the electron-positron bunch dynamics in a $\lambda_0 = 400\,\mathrm{nm}$ laser with circular polarisation (CP) (2023).

[88] Video of the electron-positron bunch dynamics in a $\lambda_0 = 400\,\mathrm{nm}$ laser with linear polarisation (LP) (2023).

[89] Video of the electron-positron bunch dynamics in a $\lambda_0 = 100\,\mathrm{nm}$ laser with circular polarisation (CP) (2023).

[90] Video of the electron-positron bunch dynamics in a $\lambda_0 = 100\,\mathrm{nm}$ laser with linear polarisation (LP) (2023).

[91] M. Tamburini, F. Pegoraro, A. Di Piazza, C. Keitel, T. Liseykina, and A. Macchi, Nuclear Instruments and Methods in Physics Research Section A: Accelerators, Spectrometers, Detectors and Associated Equipment **653**, 181 (2011), superstrong 2010.

[92] J. Bell Burnell, Nature Astronomy **1**, 831 (2017).

[93] R. D. Blandford and R. L. Znajek, Monthly Notices of the Royal Astronomical Society **179**, 433 (1977).

[94] P. Goldreich and W. H. Julian, Astrophysical Journal **157**, 869 (1969).

[95] A. J. Deutsch, Annales d'Astrophysique **18**, 1 (1955).

[96] V. Radhakrishnan and D. J. Cooke, Astrophysical Letters **3**, 225 (1969).

[97] M. A. Ruderman and P. G. Sutherland, Astrophysical Journal **196**, 51 (1975).

[98] A. A. Abdo, M. Ajello, A. Allafort, L. Baldini, J. Ballet, G. Barbiellini, M. G. Baring, D. Bastieri, A. Belfiore, and R. Bellazzini et al, The American Astronomical Society **208**, 17 (2013).

[99] D. Mitra, J. Gil, and G. I. Melikidze, The Astrophysical Journal **696**, L141 (2009).

[100] K. S. Cheng and J. L. Zhang, Astrophysical Journal **463**, 271 (1996).

[101] S. R. Kelner, A. Y. Prosekin, and F. A. Aharonian, The Astronomical Journal **149**, 33 (2015).

[102] G. Schönherr, J. Wilms, P. Kretschmar, I. Kreykenbohm, A. Santangelo, R. E. Rothschild, W. Coburn, and R. Staubert, Astronomy and Astrophysics **472**, 353 (2007).

[103] K. S. Cheng, C. Ho, and M. Ruderman, Astrophysical Journal **300**, 522 (1986).

[104] B. Cerutti, A. Philippov, K. Parfrey, and A. Spitkovsky, Monthly Notices of the Royal Astronomical Society **448**, 606 (2015).

[105] A. A. Sokolov, I. M. Ternov, and C. W. Kilmister, *Radiation from Relativistic Electrons* (American Institute of Physics, 1986).

[106] J. Schwinger, Phys. Rev. **75**, 1912 (1949).

[107] M. Abramowitz and I. Stegun, *Handbook of Mathematical Functions with Formulas, Graphs, and Mathematical Tables* (1968).

[108] G. I. Melikidze, J. A. Gil, and A. D. Pataraya, The Astrophysical Journal **544**, 1081 (2000).

[109] D. B. Melrose, Reviews of Modern Plasma Physics **1**, 5 (2017).

[110] Video of the electron-positron beam in a constant and uniform magnetic field (2023).

# Acknowledgments

Remarkably, when I defend this thesis in October 2023 it will have been four years since I moved to Heidelberg, to pursue a PhD in physics. It seems appropriate to reflect on the contributions of those who supported me on this journey.

First and foremost, to my supervisors Dr. Matteo Tamburini and Prof. Dr. Antonino Di Piazza. Without their guidance, and near endless patience, this project would simply have not been possible. To the former, I owe thanks for accepting me as a PhD student and encouraging me to pursue my wildest, physics-related ideas. To the latter, I owe almost my entire (all be it limited) knowledge of quantum electrodynamics thanks to Antonino's excellent lectures at Heidelberg university.

In addition, none of this work would have been possible without the support of the Max Planck Institute for Nuclear Physics, specifically from Hon. Prof. Dr. Christoph H. Keitel. I would also like to thank apl. Prof. Dr. John G. Kirk for agreeing to act as my referee, and for stimulating conversations about environs of pulsars.

Many thanks to Konstantin Beyer, who assisted in the translation of my abstract into German starting from my initial draft, which was, truly awful.

To my various friends and colleagues at MPIK; thanks to A. Boitsov, I. Valuev and K. Dzikowski for the jokes and friendly office environment. To the 'gruppo italiano': G. Audagnotto, S. Montefiori and L. Monteforte for always knowing how to make me laugh. To previous students D. Bakucz Canário, H. Cakir, P. Andrejic and A. Sampath who I appreciate meeting up with when time permits. To N. Oreshkina and various members of the Hinton division, for persuading me to start bouldering. Finally, thanks to B. Reville and N. Kumar for ever interesting discussions about astrophysical plasmas and shocks.

Many thanks to my friends in Heidelberg, specifically J. Schultheiss, R. Krauter and M. Haus for meeting up every week during the pandemic to chat. A similar thanks is owed to my closest friends at home in Portadown, Armagh and Belfast: P. Sinton, A. Hamilton, J. Cunningham, S. Coughlin and P. Agnew.

Above all, I owe thanks to my family at home, in particular my parents Robin and Karen, and sister Emma. I would not have been able to endure the last four years, particularly the pandemic, without your continuous support in the form of our weekly conversations. A similar thanks is owed to my wonderful grandparents Harold, Myrtle, Noel and Jeanette for their encouragement, as well as my extended family, and the congregants of Mahon Methodist church who, having known me almost since birth, effectively function as extended family.